Auxiliary Proteins and Allosteric Control of the Mitochondrial Branch of B$_{12}$ Trafficking, Assembly, and Reactivity.

by

Michael W. Lofgren

A dissertation submitted in partial fulfillment
of the requirements for the degree of
Doctor of Philosophy
(Biological Chemistry)
in The University of Michigan
2013

Dissertation Committee:

Professor Ruma V. Banerjee, Chair
Professor David P. Ballou
Professor Paul F. Hollenberg
Professor E. Neil Marsh
Professor Stephen Ragsdale

ACKNOWLEDGEMENTS

I have not done this alone. At every turn in the time since I arrived at the University of Michigan, I have been received with love, care, support, compassion, fellowship and friendship.

First and foremost, I must acknowledge my wonderful, intelligent, loving and supportive partner in crime and life, Elizabeth (Liz) Townsend (Ph.D.). I would be remiss if I did not also express a sincere debt of gratitude toward Beth Goodwin for assigning Liz to be my student host during my interview weekend at the University of Michigan! Liz and her family originiate from Boston, MA and when she announced her decision to pursue her graduate studies at the University of Michigan, a close Townsend family friend warned her that if she was not careful she would find herself "… settling down with a corn fed beauty of a farm boy from the Midwest." While I do indeed hail from the Midwest (St. Paul, Minnesota) and enjoy summer corn as much as any Midwesterner, I have never stepped foot on a farm. When Liz and I first met on March 8, 2007, my 24th birthday, neither she nor I could have envisioned that 6 years later, after sharing our lives with one another for the majority of that time, we would be leaving Ann Arbor together to embark on the next chapter in our lives together. The loving partner and friend that I received on March 8, 2007 was a birthday gift that cannot be topped! This dissertation will be recognized as my own, but it would have not been possible if not for the support of my rock, my best friend, and the love of my life, Liz Townsend. Any and all praise for the work presented in this dissertation belongs as much to her as it does to me. I could not be happier, more excited, or grateful than I am to be moving forward in my life with her by my side. Liz, my love, thank you! I could never have done this without you!

I would also like the express sincere gratitude toward Dr. Ruma Banerjee (Ruma) for being my graduate mentor. She has challenged me, and compelled me to strive for what I did not think I could achieve. She has offered support beyond that which any graduate could (or should) reasonably expect! She has instilled in me a strong appreciation for the special relationship shared between a mentor and their student. Whether she realizes it or not, I have learned from her a curiousity about the world that extends past lab bench and the scientific journals. She took me into her lab at a time when I needed strong and effective mentoring, and it would be an understatement to say that she delivered on both fronts. What I have appreciated most, from a professional standpoint, and have tried to cultivate in my own attitudes toward science is her inate curiousity and passion for science. To the best that one can, she has always seemed willing to let new discoveries direct the path of her research and to gracefully follow that path, substituting trepidation with vim and verve while embarking on areas of study outside of ones primary field of expertise. Her example has always been one in which the researcher need not limit themselves to a particular niche in science. She has demonstrated to me how to be a teachable student and to follow the research wherever it may lead. With every resource at my command, I could not have selected nor designed a better mentor! I am eternally grateful to have had Ruma as my graduate mentor. She is a treasure to the Department of Biological Chemistry and to the University of Michigan! It is my sincere hope that our relationship continues on well past my time in Ann Arbor, MI.

In all honesty, my decision to matriculate at the University of Michigan was based on random chance – literally. Tails (the University of Wisconsin – Madison) lost to heads in two of three flips of a quarter. In retrospect both institutions would have provided me with excellent graduate training, but today, I am very proud to be a Michigan Wolverine and alumnus of a top

tier academic institution. Furthermore, the Department of Biological Chemistry at Michigan is among a select few remaining temples of structural and mechanistic enzymology. Any success I have experienced in this field can at least be partially attributed to the vibrant community of structural and mechanistic enzymologists that I am fortunate enough to call my colleagues.

Graduate school has instilled in me a disdain for mundane administrative work. If I had been left to my own abilities and desires, I would have long ago been dismissed from the University of Michigan on account of overdue library books, the accumulation of fees for late registration, and the unintential non-compliance with course enrollment and thesis progress requirements. Saving me from this miserable fate was a kind woman of true character and parental commitment to the graduate students of the Department of Biological Chemistry. Of course, I am speaking Beth Goodwin, Graduate Program Manager in the Department of Biological Chemistry. Beth is a wonderful woman and she has helped me in more ways than I can count! I am quite serious when I proclaim that I would not be completing my Ph.D. without Beth's unwavering commitment to the graduate students in Biological Chemistry. Thank you Beth!

I would also like to extend my thanks to the department of biological chemistry in helping me in a time of need. In late July of 2008, my father was involved in an accident that later claimed his life. The administrative staff, particularly Beth Goodwin, Sharon Hoffman, Prasanna Baragi, and Julie Woodruff all helped in some fashion to arrange for the advance payment and booking of the soonest flight back home to see my father in his last days. I am forever grateful for that!

I have been fortunate to work closely with a number of talented researchers in and around Dr. Banerjee's lab. I wish to extend a sincere thank you to members of the Banerjee lab, past and present, for supporting an intellectually stimulating and internally collaborative working

received. He saw something in me that I was blinded from at the time, and I am eternally thankful for his wisdom and friendship. Dad, I love you and you are missed dearly. I am so thankful for the time that we spent together and I am certain you would be proud of me today. My mother has been a pillar of strength for me and for our family. Her love, her faith in me, and her support has never waivered even in her darkest of hours. She has helped to carry me in times when I could not manage on my own. What you have achieved in being the wonderful parent and friend that you are makes me proud to call you my mother. Finally, I would like to recognize my siblings, their significant others, and their beautiful children whom I love dearly and who can always lift my spirits. In particular, I would like to thank my friend and brother-in-law John Brady for disabusing me of the notion that the practice of medicine is science and for stearing me toward the path I am walking today.

TABLE OF CONTENTS

LIST OF FIGURES

LIST OF TABLES

LIST OF ABBREVIATIONS

AdoCbl, coenzyme-B_{12}, 5'-deoxy-5'-adenosylcobalamin, adenosylcobalamin

AdoHcy, Adenosylhomocysteine

AdoMet/SAM, *S*-adenosylmethionine

AMPPCP, 5'-adenylyl-(β-,γ-methylene)diphosphonate

ATR, ATP-dependent Cob(I)alamin adenosyltransferase;

CNCbl, cyanocobalamin;

CoA, coenzymeA;

Cob(III), Cob(III)alamin

Cob(II), Cob(II)alamin

Cob(I), Cob(I)alamin

DMB, dimethylbenzimidazole

EPR, Electron paramagnetic resonance

FMN, flavin mononucleotide

FAD, Flavin adenine dinucleotide

GAP, **G**TPase **a**ctivating **p**rotein

GDP, Guanosine-5'-disphospahte

GEF, **g**uanine nucleotide **e**xchange **f**actor;

GMPPNP, guanosine 5'-(β,γ-imido)triphosphate;

GSH, Glutathione

GTP, Guanosine-5'-triphosphate

HC, Haptocorin

HPLC, high performance liquid chromatography;

ICM, isobutyryl-CoA mutase;

IcmF, **i**sobutyryl-**C**oA **m**utase **f**used;

IF, Intrinsic factor

IPTG, isopropyl-1-thio-β-D-galactopyranoside;

ITC, Isothermal Titration Calorimetry

LIC, ligase independent cloning;

M-CoA/MCoA, methylmalonyl-CoA

MCM, methylmalonyl-CoA mutase

MCS, Malonyl-CoA synthetase

MMAA, Methylmalonic acidemia type A

MMACHC, methylmalonic aciduria type C and homocystinuria

MMADHC, methylmalonic aciduria type D and homocystinuria

MMAHC, methylmalonic aciduria and homocystinuria

MMA, methylmalonic aciduria

MeCbl, methylcobalamin

MMAA, for methymalonic aciduria linked to the cblA complementation group

MRP1, Mutlidr23ug-resistance protein 1

MS, Methionine synthease

MSR, Methionine synthase reductase

MTHF, Methylene tetrahydrofolate

NADH, reduced Nicotinamide adenine dinucleotide

NADPH, reduced Nicotinamde adenine dinucleotide phosphate

OH_2Cbl/H_2OCbl, aquacobalamin

OHCbl, hydroxocobalamin

PCR, polymerase chain reaction

RGS, Regulator of G-protein signaling

S-CoA/SCoA, Succinyl-CoA

SIMIBI, Signal recognition particle MinD and BioD

TC, Transcobalamin

TCR, Transcobalamin Receptor

TCEP, Tris(2-carboxyethyl)phosphine hydrochloride

THF, Tetratahydrofolate

TIM, triosephosphate isomerase

UV-vis, ultraviolet visible

ABSTRACT

The presence of cofactors in enzymes broadens the range of chemical transformations catalyzed in Nature. Adenosylcobalamin (AdoCbl) or coenzyme-B_{12}, is a biologically active derivative of vitamin B_{12} and an organometallic enzyme cofactor that is rare and reactive by virtue of having a labile organocobalt bond. To cope with the low cellular abundance and high reactivity of active B_{12} derivatives, Nature uses auxiliary proteins that support absorption, assimilation, trafficking and targeting of B_{12} precursors to B_{12}-dependent enzymes. In humans, methylmalonyl-CoA mutase (MCM) is a mitochondrial protein and the only known AdoCbl-dependent enzyme. Genetic disruption of the gene encoding MCM, or to genes encoding the auxiliary proteins, lead to a rare genetic disorder known as methylmalonic acidemia. In humans, two mitochondrial proteins, an adenosyltransferase (ATR) and a GTPase (G-protein) chaperone of MCM, CblA, perform the final steps in AdoCbl synthesis and delivery to the MCM active site. ATR is a bifunctional enzyme with ATP-dependent cob(I)alamin adenosyltranserase and ATP-dependent AdoCbl transfer activities. Much of our understanding of the mammalian mitochondrial B_{12}-trafficking pathway is derived from clinical genetic studies on patients with cobalamin disorders and detailed enzymological studies of closely related bacterial orthologs particularly from *Methylbacterium extorquens*.

The findings reported in this dissertation demonstrate the critical role of allosteric communication in mediating the AdoCbl trafficking from its point of synthesis on ATR to its delivery to MCM. Using *M. extorquens* ATR to mimic a C-terminal truncation mutation reported

in human ATR that is associated with methylmalonic academia provided new insights into the biochemical basis for the pathogeneticity. The study revealed that intersubunit allosteric communication involving the C-terminus of ATR, which is homotrimeric, is important in transferring AdoCbl from ATR to MCM.

Previous work in our group demonstrated that MeaB, the bacterial ortholog of CblA, functions as nucleotide-dependent molecular chaperone of MCM function that mediates AdoCbl transfer from ATR, protects MCM from inactivation and reactivates terminally inactivated MCM. In turn, MCM accelerates the intrinsically slow GTPase activity of MeaB, thus functioning as a GTPase activating protein (GAP). In collaboration with our crystallographer colleague Dr. Markos Koutmos, we have provided the first insights into a novel mechanism for bidirectional signaling in the MCM:MeaB complex. We demonstrate that MeaB employs an unusual and conformationally flexible switch III motif for enabling its chaperone and MCM's GAP functions. We further demonstrate that signaling in the MCM:MeaB complex depends on the canonical signaling motifs, switch II and I. Switch II appears to serve an auto-inhibitory function to minimize the GTPase activity of uncomplexed MeaB and is important for switch III-dependent signal transmission. Finally, we demonstrate that switch I supplies the MeaB active site with catalytic residues in the activated conformation found in the MCM:MeaB complex. Together these studies provide detailed insights into how flexible switch regions in MeaB are used for orchestrating its complex chaperone functions and for communication with MCM.

CHAPTER 1

Navigating the B$_{12}$ Road: Assimilation, Delivery and Disorders of Cobalamin[1,2]

1.1 Abstract

The reactivity of the cobalt-carbon bond in cobalamins is the key to their chemical versatility, supporting both methyltransfer and isomerization reactions. During evolution of higher eukaryotes that utilize B$_{12}$, the high-reactivity of the cofactor, coupled with its low abundance, pressured development of an efficient system for uptake, assimilation and delivery of the cofactor to client B$_{12}$-dependent enzymes. While most proteins suspected to be involved in B$_{12}$ trafficking were discovered by 2009, the recent identification of a new protein reveals that the quest for elucidating the intracellular B$_{12}$ highway is still not complete. Herein, we review the biochemistry of cobalamin trafficking.

1.2 Introduction

Cofactors are variously deployed in Nature to stabilize macromolecular structures, expand catalytic functionality, transport gases, transduce signals and function as sensors. Due to their

---

relative rarity and/or reactivity, cells have evolved strategies for sequestering and regulating the movement of cofactors from their point of entry into the cell to their point of docking in target proteins (1). A subset of cofactors, i.e., the vitamins, is obtained in a precursor form from the diet. Reactions catalyzing the assimilation of inactive cofactors into their active forms are integral to their trafficking pathways. Similarly, elaboration of metals into clusters often occurs on chaperones that subsequently transfer the cofactor to target proteins. The inter-protein transfer of metals can occur via ligand exchange reactions that are driven by differences in metal coordination geometry and affinity between the donor and acceptor proteins (*2, 3*). Seclusion of cofactors in chaperones during assembly/processing into their active forms minimizes unwanted side reactions while guided delivery averts dilution and promotes specificity of cofactor docking.

In contrast to our understanding of cellular strategies used for trafficking metals (4-6) and metal clusters (7), significantly less is known about strategies for shepherding organic and organometallic cofactors to target proteins. This picture has however been changing with the convergence of clinical genetics and biochemical approaches that are beginning to illuminate an elaborate pathway for assimilation and delivery of dietary B_{12} or cobalt-containing cobalmin, a complex organometallic cofactor (8-10). Much less is known about how the tetrapyrrolic cousins of B_{12}, e.g., iron-protoporphyrin (heme), nickel-corphin (F_{430}) or magnesium-chlorin (chlorophyll) are guided to specific destinations.

In this mini-review, we describe a model for mammalian cobalamin trafficking, which includes strategies for conversion of inactive precursors to the active cofactor forms, methylcobalamin (MeCbl) and 5′-deoxyadenosylcobalamin (AdoCbl or coenzyme B_{12}), and discuss the human diseases that result from impairments along the trafficking highway. We posit that the navigation strategy for B_{12} in which a rare, reactive and high-value cofactor is

sequestered and targeted to client proteins, might represent a general archetype for the trafficking of other essential but scarce organic and organometallic cofactors.

1.3 B$_{12}$ Chemistry and Catalysis

Cobalamin, discovered as the anti-pernicious anemia factor (*11*), was first crystallized in the cyanocobalamin (CNCbl) form (*12*), which is technically vitamin B$_{12}$. The biologically active alkylcobalamins, MeCbl and AdoCbl, serve as cofactors for the methyltransferase and isomerase family of B$_{12}$ enzymes respectively (*13*). While mammals have only two B$_{12}$-dependent enzymes, methionine synthase and methylmalonyl-CoA mutase (MCM), there are many "handlers" that tailor dietary B$_{12}$ and deliver it to its target enzymes (*8, 9*). The existence of the B$_{12}$ trafficking pathway was suggested by careful clinical genetics studies spanning several decades on patients with inborn errors of cobalamin metabolism (10).

Chemically, cobalamins comprise a central cobalt atom that is coordinated by four equatorial nitrogen atoms donated by the tetrapyrrolic corrin ring (Fig. 1.1a). A bulky base, 5,6-dimethylbenzimidazole (DMB), extends from one edge of the corrin ring and coordinates the cobalt at the lower or α-axial position. The identity of the upper or β-axial ligand varies and includes cyano, aquo, methyl, and 5′-deoxyadenosyl groups. Ironically, six decades after its discovery, the origin and biological relevance of the cyano group remains unknown, although we have recently described a decyanase activity in the processing pathway (*14*), which allows utilization of CNCbl used in vitamin supplements. As the cobalt oxidation state decreases from $3^+ \rightarrow 2^+ \rightarrow 1^+$, the coordination number typically decreases from $6 \rightarrow 5 \rightarrow 4$. In solution, alkylcobalamins preferentially exist in the six-coordinate "base-on" state, which is in contrast to the "base-off/His-on" state found in the active site of both mammalian B$_{12}$ enzymes (*15, 16*)

(Fig. 1.1b). Since the pK$_a$ for the "base-on" to "base-off" transition ranges from -2.13 to 3.17 depending on the identity of the upper axial ligand (*17*), the "base-on" conformation predominates at physiological pH.

a
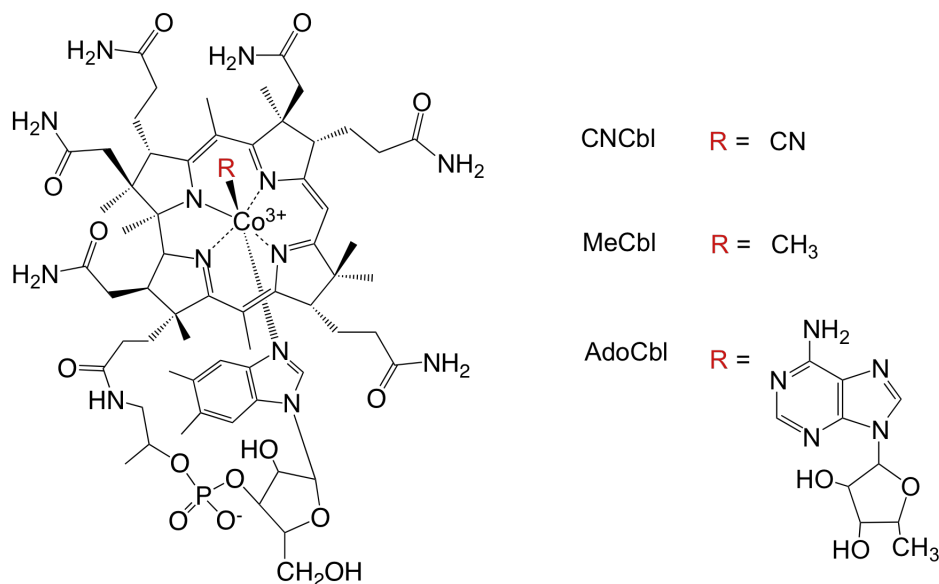
b
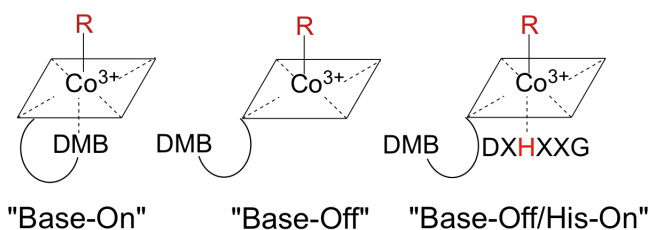
Figure 1.1: Cobalamin structure and conformations. (a) Cobalamin is shown in the "base-on" conformation with DMB coordinating cobalt from the lower axial face of the corrin ring. The variable upper ligands are denoted as R on the right. (b) Alternative conformations of cobalamins differing with respect to the lower or α-axial ligation site.

The cobalt-carbon bond in alkylcobalamins is inherently weak and holds the key to the reactivity of this cofactor. The bond-dissociation energies for "base-on" AdoCbl and MeCbl are 30 kcal/mol and 37 kcal/mol, respectively (*18, 19*). Methyltransferases utilize MeCbl, and the cobalt-carbon bond is cleaved heterolytically during nucleophilic displacement of the methyl

group from MeCbl to an acceptor. In contrast, the isomerases cleave the cobalt-carbon bond homolytically to generate a radical pair: 5´-deoxyadenosyl radical and cob(II)alamin. The former is the "working" radical, which abstracts a hydrogen atom from the substrate to initiate a radical-based isomerization reaction. The cobalt-carbon bond is reformed at the end of each catalytic cycle.

1.4 Absorption, Transport and Storage of Cobalamin

The recommended dietary allowance for cobalamin is 1-5 µg/day. A multistep process delivers the cofactor from the mouth into circulation and thereon to cells (Fig. 1.2) (*20*). Cobalamin released from food is first bound by haptocorrin, a salivary glycoprotein with broad specificity and high affinity for B_{12} at both neutral and acidic pH (*21*). In the duodenum, pancreatic proteases release cobalamin from the haptocorrin•B_{12} complex and from other proteins containing bound B_{12} that have been ingested. Subsequent binding of cobalamin to a second glycoprotein, intrinsic factor, facilitates its uptake by intestinal cells via cubilin/AMN receptor-mediated endocytosis (*22*). Intrinsic factor is highly selective for the physiologically relevant precursors of cobalamin containing an intact lower axial DMB ligand (*23*). Following internalization into enterocytes, intrinsic factor is degraded in the lysosome and cobalamin is released into the blood stream. An ATP-dependent transporter ABCC1 (also known as multidrug resistance protein 1; MRP1) present in the basolateral membrane of intestinal epithelial and other cells, exports cobalamin bound to transcobalamin out of the cell (*24*). MRP1 knock out mice accumulate cobalamin in the distal part of the intestine and exhibit low plasma, liver and kidney cobalamin (*24*).

In the bloodstream, cobalamin is associated with two carriers, transcobalamin and haptocorrin. It is estimated that ~20% of the circulating cobalamin is bound to transcobalamin while the remainder including incomplete B_{12} derivatives, is bound to haptocorrin (*25, 26*).
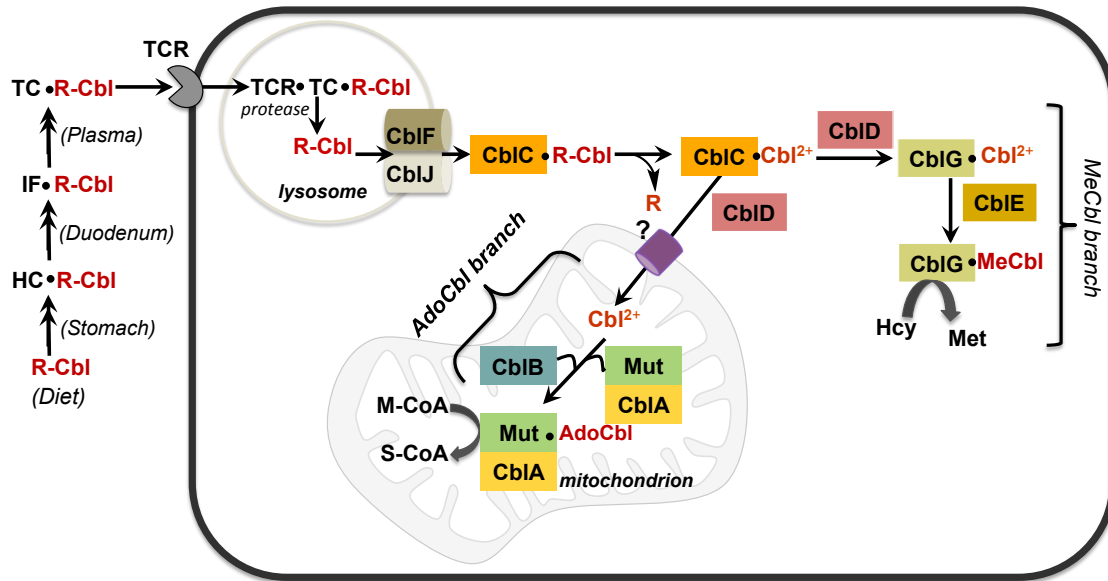
Figure 1.2. A model for cobalamin utilization and intracellular trafficking in mammals. Dietary cobalamin (R-Cbl) is bound by a series of proteins found in saliva and stomach (haptocorrin, HC), in the duodenum (intrinsic factor, IF) and in blood (transcobalamin, TC). The details of these early trafficking steps are not shown in this figure. TC is recognized by the transcobalamin receptor (TCR) found on cell surfaces and endocytosed into the lysosome where R-Cbl is released following proteolytic digestion of TC. R-Cbl exits the lysosome in a process that requires the products of the *cbl*J and *cbl*F loci. In the cytoplasm, CblC converts R-Cbl (and CNCbl) to cob(II)alamin (Cbl^{2+}). Cbl^{2+} is partitioned to (i) the MeCbl pathway in the cytoplasm, which involves CblG (methionine synthase), CblE (methionine synthase reductase), and CblD and (ii) the AdoCbl pathway in the mitochondrion, which requires CblD, CblB (adenosyltransferase or ATR), and CblA (the G-protein or MeaB in bacteria) in addition to MCM (Mut). The question mark by the mitochondrial cobalamin transporter denotes that it is unidentified. Hcy, Met, M-CoA and S-CoA denote homocysteine, methionine, methylmalonyl-CoA and succinyl-CoA respectively.

Transcobalamin preferentially binds the intact cobalamin cofactor, representing a second level of molecular sieving out of degraded derivatives that could potentially compete with and inhibit B_{12}-dependent enzymes (*21, 27*). Transcobalamin binds B_{12} avidly and mediates its transport across cells following complexation with the transcobalamin receptor, which is internalized into

the lysosome (*28*). Lysosomal degradation of transcoblamin by resident hydrolases releases cobalamin that is retained and further processed intracellularly.

Despite their low sequence identity (~25%), the human cobalamin-binding proteins share a common evolutionary origin with transcobalamin being the oldest, followed by intrinsic factor and haptocorrin (*29*). Biochemical studies with native or recombinant proteins indicate that all three proteins bind a single equivalent of B_{12} with high affinity (K_d <1 pM), albeit with different specificities (*21*). Both transcobalamin and intrinsic factor bind cobalamin in a "base-on" conformation while the binding mode for haptocorrin depends on the lower axial ligand. In addition to cobalamins, haptocorrin can bind cobinamides, which are B_{12} analogs lacking the DMB moiety and cannot be converted to the active cofactor forms by mammals. Cobinamides account for ~40% of the total plasma corrins (*30*). While a definitive role for haptocorrin remains to be established, its suggested functions include a role in B_{12} storage and in removal of inhibitory corrinoid derivatives.

1.5 Lysosomal Egress of Cobalamin

Transport of cobalamin across the lysosomal membrane requires two membrane proteins with apparently distinct functions: CblF and CblJ (*31, 32*) (Fig. 1.2). Defects in the genes encoding these two transporters result in accumulation of B_{12} in the lysosome, and are classified as *cbl*F (LMBD1) and the recently discovered *cbl*J (ABCD4) complementation groups (*32, 33*). Subcellular localization studies indicate that both LMBD1 and ABCD4 co-localize with other lysosomal proteins such as LAMP1; however, the precise role of each protein to the lysosomal export of cobalamin is unclear. Transport of free cobalamin into prokaryotes and the export of cobalamin from mammalian cells are fuelled by ATP hydrolysis (*24, 34*). ABCD4 is an ATP-

binding cassette transporter, which might be the true lysosomal cobalamin transporter that is assisted by LMBD1. Alternatively, LMBD1, a putative transmembrane protein might facilitate passive transport of cobalamin across the lysosomal membrane. In this model, ABCD4 could be involved in an ATPase-driven loading of B_{12} from the lysosome onto LMBD1 and/or in releasing the cobalamin cargo from LMBD1. Functional studies using fibroblasts from patients with *cbl*F and *cbl*J defects indicate that the two transporters can only partially complement each other and therefore it is likely that they act synergistically. Clearly, biochemical studies are needed to decipher their function in the lysosomal egress of cobalamin. We have previously suggested that the release of cobalamin in the acidic environment of the lysosome favors formation of the "base-off" conformation of the cofactor and that once cobalamin exits this compartment, it retains this conformation by being protein-bound (9).

1.6 Early Steps in the Cytosolic Processing of Cobalamin

Upon arrival in the cytosol, cobalamins with various upper axial ligands must be processed to a common intermediate that can be allocated to the MeCbl and AdoCbl synthesis pathways to meet cellular needs. The protein that is postulated to accept the cobalamin cargo exiting the lysosomal compartment is MMACHC (for methylmalonic aciduria type C and homocystinuria), the product of the *cbl*C locus and hereafter referred to as CblC (9) (Fig. 1.3). Mutations in CblC impair both AdoCbl and MeCbl synthesis and are the most common cause of inherited cobalamin disorders (*35*).

Human CblC is a soluble protein in which the C-terminal ~40 amino acid residues appear to be a recent evolutionary addition and are predicted to be highly disordered (*36*). Two CblC variants, a full length (32 kDa) and a truncated form (26 kDa), have been reported in human

fibroblasts and in murine tissue (*36, 37*). The formation of the truncated CblC form is attributed to a predicted splicing variant (*36*). While the prevalence of the truncated CblC form is not known, the presence of the C-terminal domain diminishes the stability of human CblC and is not required for its function (*36*). The crystal structures of the truncated variant of human CblC do not reveal the presence of a C-terminally located bacterial TonB-like domain as predicted previously (*36, 38*).
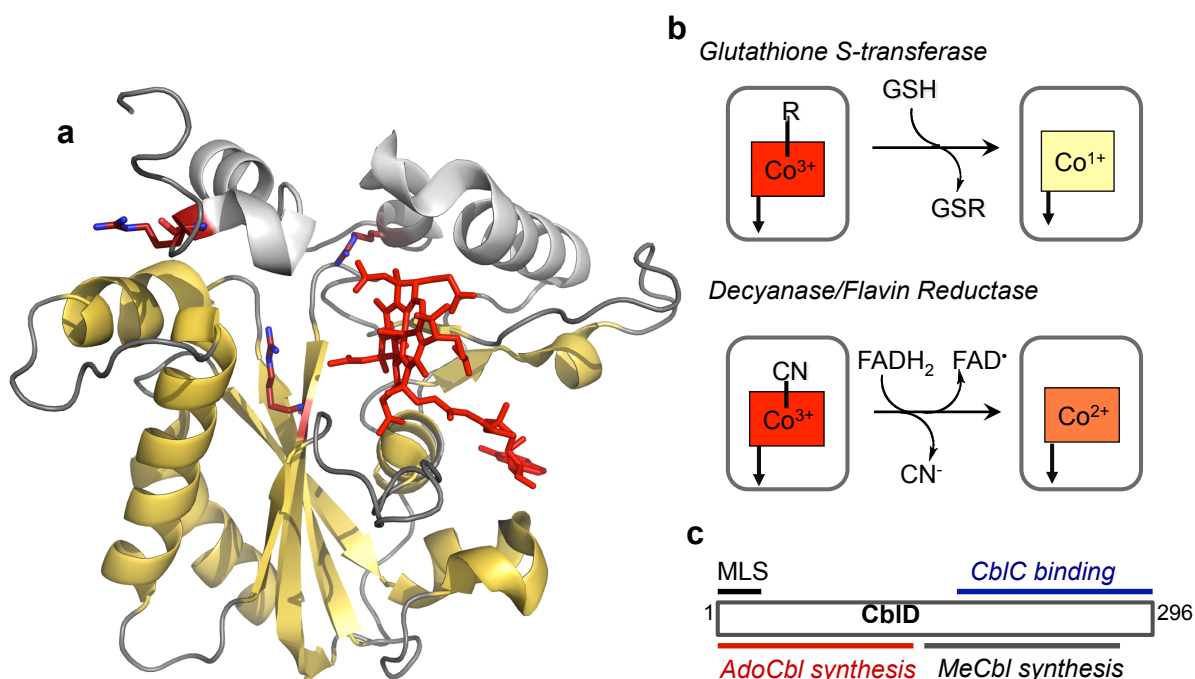
Figure 1.3. Biochemical functions of CblC and CblD. (a) The structure of human CblC with MeCbl (PDB 3SC0). MeCbl (red) is bound in a "base-off" conformation with the DMB tail being located in a side pocket. The flavin reductase domain is shown in yellow. The arginine residues that are mutated in patients are shown in stick representation. (b) Reactions catalyzed by CblC. (c) Localization of mutations in CblD that lead to impaired AdoCbl or MeCbl synthesis and the minimal length required for binding to CblC. MLS denotes mitochondrial leader sequence.

CblC binds B_{12} stoichiometrically and exhibits a broad tolerance for the β-axial ligand accommodating C1-C6 alkyl, adenosyl, cyano and hydroxyl groups. Cobalamin is bound to CblC in a five-coordinate "base-off" conformation where the DMB tail is dissociated from the cobalt.

9

In the structure of MeCbl-bound CblC, the cobalamin tail is secured away from the corrin ring in a pocket dominated by hydrophobic interactions (Fig. 1.3a) (*36*). CblC exhibits remarkable chemical versatility by its ability to cleave cobalt-carbon bonds via both homolytic and heterolytic mechanisms, depending on the nature of the upper axial ligand (Fig. 1.3b). Thus, when an alkylcobalamin is bound to the active site, CblC catalyzes a nucleophilic displacement reaction in the presence of glutathione (Fig. 1.3b) (*39*). Mechanistically, the dealkylation reaction resembles the first half reaction catalyzed by methionine synthase in which the thiolate of homocysteine displaces the methyl group in MeCbl to form the thioether methionine and cob(I)alamin (Fig. 1.4a). Similarly, in the CblC-catalyzed dealkylation reaction, the glutathione thioether and cob(I)alamin form upon transfer of the alkyl group. When CNCbl is in the active site, electrons provided by free or protein-bound reduced flavin promote reductive homolytic cleavage leading to cyanide elimination (*14, 36*). Based on UV-visible and EPR spectroscopy, "base-off" cob(II)alamin has been identified as the other product of the reductive elimination, consistent with a homolytic cleavage reaction mechanism. The modest decyanation and dealkylation rates exhibited by CblC are apparently sufficient to handle the flux through the cobalamin-processing pathway to meet cellular needs. Fibroblasts derived from *cbl*C patients confirm that CblC is required for processing alkyl- and cyano-cobalamins for apportioning dietary B_{12} into MeCbl and AdoCbl, respectively (*40*).

Unexpectedly, the crystal structure of CblC revealed a flavin reductase fold (Fig. 1.3a) (*36*). Flavin binds at the dimer interface in two structurally related flavin reductases, BluB and iodotyrosine deiodinase. However, solution studies indicate that CblC exists predominantly as a monomer (*14, 38*). Unlike the structure of apo- and MeCbl-bound CblC, a dimeric crystal structure has been reported for AdoCbl-bound CblC, where the dimer interface is stabilized by

interactions between residues belonging to a highly conserved "PNRRP" loop (*38*). The increase

in the proportion of dimeric CblC in the presence of AdoCbl and FMN to ~50% of the total
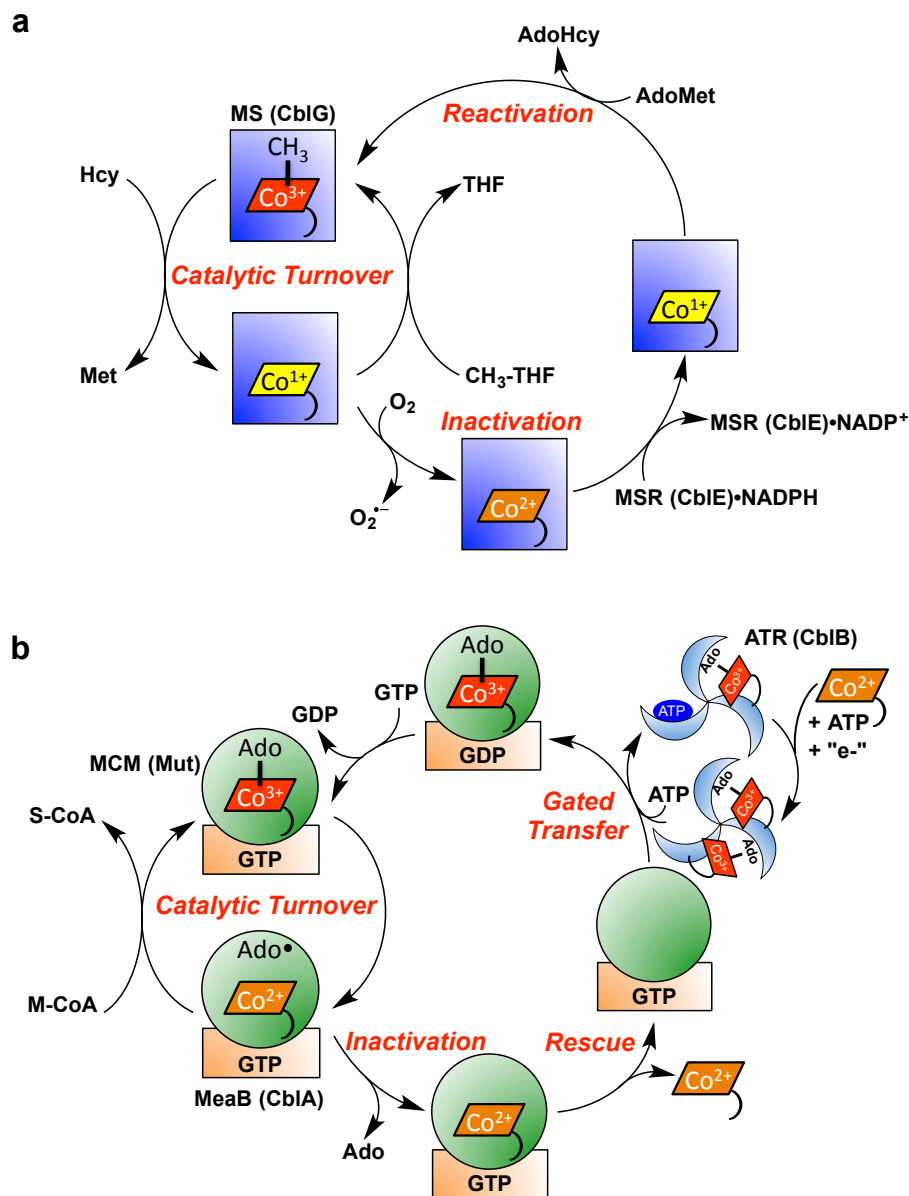
Figure 1.4. Cofactor loading, activity and repair of the mammalian cobalamin-dependent enzymes. (a) Methionine synthase (MS or CblG, blue square) catalyzes the overall transfer of a methyl group from N^5-methyl-tetrahydrofolate (CH_3-THF) to homocysteine (Hcy) to give methionine (Met) and tetrahydrofolate (THF). Occasional oxidative escape of the cob(I)alamin intermediate during the catalytic cycle leads to the inactive cob(II)alamin species. The latter is rescued to MeCbl in a reductive methylation reaction needing NADPH, methionine synthase reductase (MSR or CblE) and AdoMet. This repair reaction is also likely to represent the route for formation of MeCbl following transfer of cob(II)alamin to apo-methionine synthase. The mechanism for cob(II)alamin transfer during methionine synthase reconstitution is not known.

(b) ATR (or CblB, blue wheel) converts ATP and cob(II)alamin in the presence of a reductant to AdoCbl. Two equivalents of AdoCbl are bound at one time and binding of ATP to the vacant site triggers transfer of one AdoCbl to MCM (Mut, green circle) active site in a reaction that is gated by GTP hydrolysis in the G-protein chaperone (MeaB or CblA, orange rectangle). The GTP-bound state of MeaB blocks transfer of cob(II)alamin from ATR to the MCM:G-protein complex. During catalysis, the cobalt-carbon bond is cleaved homolytically to initiate a radical-based mechanism for the conversion of methylmalonyl-CoA (M-CoA) to succinyl-CoA (S-CoA). Occasional loss of 5′-deoxyadenosine from the active site precludes reformation of AdoCbl at the end of the catalytic cycle and leads to inactive mutase. In this situation, the GTP-containing chaperone promotes dissociation of cob(II)alamin, permitting reconstitution of the mutase with active cofactor.

Studies on the ΔN11 (lacking the mitochondrial leader sequence) and the ΔN61 (starting at the second methionine initiation codon) CblD variants identified disordered regions in the N-terminus of the protein that decrease its stability (*37*). Studies on fibroblasts derived from *cbl*D patients that express shorter CblD variants reveal that the N-terminal 115 amino acids are not required for MeCbl synthesis (*43*). They are also not required for binding to CblC (*44*). The structural determinants needed for AdoCbl synthesis are harbored within a stretch of residues extending from 62-116 (*43*).

Despite the presence of a predicted B_{12} binding sequence, CblD does not bind B_{12} suggesting that its involvement in intracellular B_{12} delivery might be exerted indirectly (*37*). The ability of CblC and CblD to form a complex that is stabilized in the presence of alkylcobalamin and glutathione (*44*), indicates that CblD might assist in the delivery of cobalamin from CblC to downstream targets

1.7 MeCbl synthesis

Methionine synthase, encoded by the *cbl*G locus in humans (*45-47*), catalyzes the methyl transfer from N^5-methyl-tetrahydrofate to homocysteine in two half-reactions (*48*) (Fig. 1.4a). First, the methyl group is transferred from MeCbl to homocysteine to give methionine and

cob(I)alamin. Second, the supernucleophilic cob(I)alamin removes the methyl group from N^5-methyl-tetrahydrofate to give tetrahydrofolate and re-forms MeCbl. Occasional oxidation of the bound cob(I)alamin to the inactive cob(II)alamin state necessitates repair via a reductive methylation reaction in which the methyl group of S-adenosylmethionine (AdoMet) is transferred to cobalamin in the presence of the electron donor, NADPH and the diflavin oxidoreductase, methionine synthase reductase, encoded by the *cbl*E locus (Fig. 1.2).

Mutations in *cbl*G and *cbl*E loci result in isolated hyperhomocysteinemia, i.e., without methylmalonic aciduria (*49*). Human methionine synthase is an ~140 kDa monomeric protein that is predicted to be modular like its better-studied bacterial counterpart. The four modules in bacterial methionine synthase bind homocysteine, N^5-methyl-tetrahydrofolate, cobalamin and AdoMet, respectively (*50*). Methionine synthase reductase shuttles electrons derived from NADPH to methionine synthase-bound cobalamin (*51, 52*). The reduction of cob(II)alamin to cob(I)alamin by methionine synthase reductase is thermodynamically unfavorable (*53, 54*) and driven by kinetic coupling to the exothermic methyl group transfer reaction (*55*). The coupled reactions convert cob(II)alamin to MeCbl. Hence, in addition to rescuing inactive enzyme generated during the catalytic turnover cycle, it also represents a mechanism for the in situ synthesis of MeCbl from cob(II)alamin, loaded into the active site of apo-methionine synthase. It is unclear how cob(II)alamin bound to CblC is transferred to the methionine synthase and what role CblD plays in this process. Methionine synthase reductase has been postulated to assist in the cofactor docking process (*56*). However, while the interaction between these proteins appears to stimulate cofactor docking to methionine synthase *in vitro*, a compulsory role for methionine synthase reductase *in vivo* is unlikely as fibroblasts derived from patients with the *cbl*E defect have 84-100% holo-methionine synthase (*57*).

1.8 Tailoring of AdoCbl in the Mitochondrion

ATP-dependent cob(I)alamin adenosyl- transferase (ATR) catalyzes the synthesis of AdoCbl and is encoded by the *cbl*B locus (*58, 59*). ATR is a bifunctional mitochondrial enzyme that catalyzes the formation of AdoCbl and subsequently transfers the cofactor to the lone AdoCbl-utilizing enzyme, methylmalonyl-CoA mutase (*60*) (Fig. 1.4b). UV-visible, magnetic circular dichroism and EPR spectroscopy studies have established that cob(II)alamin is bound to ATR in a "base-off" 4-coordinate state (*61-63*). The "base-off" state makes reduction of cob(II)alamin to cob(I)alamin, which precedes the adenosyl transfer step, more facile. In solution, the redox potential of the cob(I)alamin/cob(II)alamin is -610 mV versus ~-500 mV for the "base-on" versus "base-off" states (*64*). It is not known if a dedicated reductase couples to the ATR. In vitro studies have demonstrated that flavoprotein oxidoreductases such a methionine synthase reductase, ferredoxin, and flavodoxin can couple to ATRs (*65, 66*).

The structures of mammalian and bacterial ATRs reveal a homotrimeric organization in which the active sites are located between adjacent subunits (*67*). For the ATR from *Methylobacterium extorquens*, which is the best studied, both AdoCbl and ATP bind with negative cooperativity and only two of the three available active sites are used at any given time (*60, 68*). The non-equivalence of the active sites appears to be an allosteric strategy for controlling the delivery of AdoCbl from ATR (*68*). Binding of ATP triggers the ejection of a single equivalent of AdoCbl, presumably from the low affinity site of ATR to methylmalonyl-CoA mutase, resulting in direct transfer of the cofactor (Fig. 1.4b). This strategy of chaperoned delivery averts loss of the cofactor by dilution in the cellular milieu and its conversion to the

unwanted "base-on" state. The pathogenic C-terminal truncation mutation compromises the ability of ATR to sequester AdoCbl and promotes instead, its release into solution (*69*).

While the DMB "base-off" conformation of AdoCbl in ATR persists in the active site of MCM, the coordination environments are distinct, an important geometric consideration for the inter-protein cofactor transfer process. Thus, in ATR, the cobalamin is four-coordinate and the funnel-shaped B_{12} binding site leaves the DMB tail exposed to solvent. In MCM, the cobalamin is five-coordinate by virtue of a histidine ligand donated by the protein serving as a lower axial ligand. The histidine residue appears to be crucial for the translocation of AdoCbl from the active site of ATR to the mutase, and its substitution by alanine or asparagine impairs the transfer process (*60*). In contrast, the histidine mutations have little impact on the K_D for AdoCbl binding from solution. These results suggest a model for cofactor transfer in which the histidine residue in the mutase transiently coordinates the cobalt in ATR, facilitating the relocation of AdoCbl to the mutase. Interestingly, mutation of conserved residues in a hinged lid motif that enforces the "base-off" conformation in ATR compromises mutase activity *in vivo* (*67*).

1.9 A G-protein Editor of Methylmalonyl-CoA mutase

In the reaction catalyzed by MCM, the only isomerase found in mammals, AdoCbl serves as a radical reservoir, generating cob(II)alamin and the reactive 5′-deoxyadenosyl radical that initiates the radical-based 1,2 rearrangement of the substrate (Fig. 1.4b). The cofactor-derived radicals recombine at the end of each catalytic cycle. Occasional escape of the 5′-deoxyadenosine intermediate during catalytic turnover, leads to inactive enzyme, and is rescued by a G-protein chaperone, which uses the binding energy of GTP to power the expulsion of

inactive cob(II)alamin from the active site (*70*). MCM and the G-protein chaperone are encoded by the *mut* and *cbl*A loci, respectively (Fig. 1.2).

CblA or MMAA (for <u>m</u>ethyl<u>m</u>alonic <u>a</u>ciduria type <u>A</u>) is a P-loop GTPase (*70, 71*). Mutations in the *cbl*A gene are associated with methylmalonic aciduria, reduced AdoCbl levels, and low mutase activity in patient fibroblasts (*72, 73*). A bacterial ortholog of CblA from *M. extorquens*, MeaB, is the best-studied member of this class of G-proteins and has been used as a model for the human CblA protein (*70, 74-77*).

MeaB exhibits nanomolar affinity for MCM that is modulated by the ligands and substrates bound to each protein (*76*). The activities of MeaB and the mutase are each influenced by the other. MeaB has low intrinsic GTPase activity, which is enhanced ~100-fold, in the presence of the mutase. Hence, the mutase is a GTPase-activating protein (GAP) of MeaB. MeaB in turn, enhances the k_{cat} of the mutase reaction by ~2-fold. Additionally, MeaB influences other mutase functions. It (i) allows the mutase to discriminate between inactive cob(II)alamin and active AdoCbl forms of the cofactor during ATR-dependent docking, (ii) protects the mutase against inactivation during turnover, and (iii) promotes the release of cob(II)alamin from inactive mutase.

MeaB exhibits almost equal affinity for GTP and GDP and is expected to be predominantly GTP-loaded in cells due to the higher concentration of this nucleotide form. The GTPase activity of MeaB gates transfer of AdoCbl to the mutase active site (*70*). Thus, MeaB functions as a molecular screen that prevents assembly of MCM with incomplete cofactor precursors. The susceptibility of the mutase to inactivation during turnover would lead to its gradual accumulation in an inactive form. A two-pronged strategy is used by MeaB to avert this situation. First, MeaB diminishes the inactivation rate of the mutase ~3- and 15-fold in the

presence of GDP and GTP, respectively (*75*). CblA has a similar effect on the human mutase (*70*). Second, when inactive MCM is generated by the escape of 5´-deoxyadenosine from the active site, MeaB utilizes the binding energy of GTP to promote ejection of cob(II)alamin from MCM (*70*). CblA appears to utilize a similar mechanism as MeaB (*71*). The remarkable sensing of the 5´-deoxyadenosine moiety by MeaB, avoids inappropriate ejection of cob(II)alamin formed during turnover. The molecular basis of communication between MeaB and MCM awaits elucidation.

Similarly, the mechanistic basis for the intricate bidirectional signaling between MeaB and MCM remain to be elucidated. Interestingly, a pathogenic mutation of a conserved arginine to cysteine at the surface of the B_{12} domain in the mutase nearly abolishes its GAP activity and destabilizes the MCM•MeaB complex (*70*). Strikingly, this mutation also corrupts the ability of MeaB to block cob(II)alamin binding to MCM, and to promote release of cob(II)alamin from the inactive mutase. Most G-proteins use structural motifs known as switch I and II loops that exhibit conformational sensitivity to nucleotide binding and hydrolysis for communicating with client proteins (*77, 78*). Missense mutations in the switch I and II loops are pathogenic and are located at the surface of MeaB and CblA, which might be important for interactions with the mutase (*72, 79*). Interestingly, a conserved region adjacent to the switch I and II regions in both MeaB and CblA also displays nucleotide-dependent conformational plasticity, and mutations in this region are also pathogenic (*80*). We speculate that this region might play a critical role in bidirectional communication between MCM and its G-protein partner.

1.10 Summary

The exciting discoveries over the past decade of genes that are culpable for cobalamin disorders, has opened doors to biochemical investigations of their functions. While homology

17

has served to clue us into function in some cases (e.g., ATR), the lack of relatedness at a sequence level to any known protein (e.g., CblC and CblD) has challenged efforts with others. The recent discovery of a duo of membrane proteins that lead to trapping of the cofactor in the lysosome when mutated, raises questions about their individual function and whether one serves as a bona fide transporter and the other, as an assistant. The multifunctionality of the CblC protein, which keeps busy as a decyanase, a dealkylase and a flavin reductase raises many questions about how this monomeric protein functions as a proverbial "jack-of-all trades", and how it transfers the tightly bound cob(II)alamin product to client proteins. The role of CblD in this transfer process is a complete mystery. Similarly, the identities of the mitochondrial membrane importers for cobalamin are unknown as is the reductase on which the ATR function depends. The mechanism of busy bidirectional signaling between MCM and the G-protein chaperone, which orchestrates gating, guiding and repair functions, awaits elucidation. The combination of structural and functional studies on cobalamin trafficking proteins promises to illuminate this pathway and possibly, general strategies for how rare cofactors are handled within cells.

References

1. Waldron, K. J., Rutherford, J. C., Ford, D., and Robinson, N. J. (2009) Metalloproteins and metal sensing, *Nature 460*, 823-830.
2. Boal, A. K., and Rosenzweig, A. C. (2009) Structural biology of copper trafficking, *Chem Rev 109*, 4760-4779.
3. Hu, Y., and Ribbe, M. W. (2012) Nitrogenase assembly, *Biochim Biophys Acta*, Dec 8. doi: 10.1016/j.bbabio.2012.1012.1001. [Epub ahead of print].
4. Reddi, A. R., Jensen, L. T., and Culotta, V. C. (2009) Manganese homeostasis in *Saccharomyces cerevisiae*, *Chem Rev 109*, 4722-4732.
5. Lutsenko, S. (2010) Human copper homeostasis: a network of interconnected pathways, *Curr Opin Chem Biol 14*, 211-217.
6. Fukada, T., Yamasaki, S., Nishida, K., Murakami, M., and Hirano, T. (2011) Zinc homeostasis and signaling in health and diseases: Zinc signaling, *J Biol Inorg Chem 16*, 1123-1134.
7. Lill, R. (2009) Function and biogenesis of iron-sulphur proteins, *Nature 460*, 831-838.
8. Banerjee, R., Gherasim, C., and Padovani, D. (2009) The Tinker, Tailor, Soldier in intracellular B_{12} Trafficking, *Cur Op Chem Biol 13*, 477-484.
9. Banerjee, R. (2006) B_{12} trafficking in mammals: A for coenzyme escort service, *ACS Chem Biol 1*, 149-159.
10. Shevell, M. I., and Rosenblatt, D. S. (1992) The neurology of cobalamin, *Can. J. Neurol. Sci. 19*, 472-486.
11. Rickes, E. L., Brink, N. G., Koniuszy, F. R., Wood, T. R., and Folkers, K. (1948) Vitamin B_{12}, A Cobalt Complex, *Science 108*, 134.
12. Hodgkin, D. C., Kamper, J., Mackay, M., Pickworth, J. W., Trueblood, K. N., and White, J. G. (1956) Structure of vitamin B_{12}, *Nature (London) 178*, 64-66.
13. Banerjee, R., and Ragsdale, S. W. (2003) The many faces of vitamin B_{12}: Catalysis by cobalamin-dependent enzymes, *Ann. Rev. Biochem. 72*, 209-247.
14. Kim, J., Gherasim, C., and Banerjee, R. (2008) Decyanation of vitamin B_{12} by a trafficking chaperone, *Proc. Natl. Acad. Sci. U.S.A. 105*, 14551-14554.
15. Drennan, C. L., Huang, S., Drummond, J. T., Matthews, R. G., and Ludwig, M. L. (1994) How a protein binds B_{12}: A 3.0 Å X-ray structure of B_{12}-binding domains of methionine synthase, *Science 266*, 1669-1674.
16. Mancia, F., Keep, N. H., Nakagawa, A., Leadlay, P. F., McSweeney, S., Rasmussen, B., Bosecke, P., Diat, O., and Evans, P. R. (1996) How coenzyme B_{12} radicals are generated: the crystal structure of methylmalonyl-coenzyme A mutase at 2 Å resolution, *Structure 4*, 339-350.
17. Brown, K. L., and Hakimi, J. M. (1984) Heteronuclear NMR studies of cobalamins. 3. ^{31}P NMR of aquocobalamin and various organocobalamins, *J. Am. Chem. Soc. 106*, 7894-7899.
18. Brown, K. L., and Zou, X. (1999) Thermolysis of coenzymes B_{12} at physiological temperatures: activation parameters for cobalt-carbon bond homolysis and a quantitative analysis of the perturbation of the homolysis equilibrium by the ribonucleoside triphosphate reductase from Lactobacillus leichmannii, *J Inorg Biochem 77*, 185-195.

19. Waddington, M. D., and Finke, R. G. (1993) Neopentylcobalamin (Neopentyl-B_{12}) Cobalt-Carbon Bond Thermolysis Products, Kinetics, Activation Parameters, and Bond-Dissociation Energy - a Chemical-Model Exhibiting 10^6 of the 10^{12} Enzymatic Activation of Coenzyme-B_{12}s Cobalt-Carbon Bond, *J Am Chem Soc 115*, 4629-4640.

20. Stupperich, E., and Nexo, E. (1991) Effect of the cobalt-N coordination on the cobamide recognition by the human vitamin B_{12} binding proteins intrinsic factor, transcobalamin and haptocorrin, *Eur J Biochem/ FEBS 199*, 299-303.

21. Fedosov, S. N., Berglund, L., Fedosova, N. U., Nexo, E., and Petersen, T. E. (2002) Comparative analysis of cobalamin binding kinetics and ligand protection for intrinsic factor, transcobalamin, and haptocorrin, *J Biol Chem 277*, 9989-9996.

22. Aminoff, M., Carter, J. E., Chadwick, R. B., Johnson, C., Grasbeck, R., Abdelaal, M. A., Broch, H., Jenner, L. B., Verroust, P. J., Moestrup, S. K., de la Chapelle, A., and Krahe, R. (1999) Mutations in CUBN, encoding the intrinsic factor-vitamin B_{12} receptor, cubilin, cause hereditary megaloblastic anaemia 1, *Nat Genet 21*, 309-313.

23. Quadros, E. V. (2010) Advances in the understanding of cobalamin assimilation and metabolism, *Br J Haematol 148*, 195-204.

24. Beedholm-Ebsen, R., van de Wetering, K., Hardlei, T., Nexo, E., Borst, P., and Moestrup, S. K. (2010) Identification of multidrug resistance protein 1 (MRP1/ABCC1) as a molecular gate for cellular export of cobalamin, *Blood 115*, 1632-1639.

25. Hall, C. A. (1977) The carriers of native vitamin B_{12} in normal human serum, *Clin Sci Mol Med 53*, 453-457.

26. Seetharam, B., and Yammani, R. R. (2003) Cobalamin transport proteins and their cell-surface receptors, *Expert Rev Mol Med 5*, 1-18.

27. Wuerges, J., Garau, G., Geremia, S., Fedosov, S. N., Petersen, T. E., and Randaccio, L. (2006) Structural basis for mammalian vitamin B_{12} transport by transcobalamin, *Proc Natl Acad Sci U S A 103*, 4386-4391.

28. Quadros, E. V., Nakayama, Y., and Sequeira, J. M. (2009) The protein and the gene encoding the receptor for the cellular uptake of transcobalamin-bound cobalamin, *Blood 113*, 186-192.

29. Li, N., Seetharam, S., and Seetharam, B. (1995) Genomic structure of human transcobalamin II: comparison to human intrinsic factor and transcobalamin I, *Biochem Biophys Res Commun 208*, 756-764.

30. Kolhouse, J. F., Kondo, H., Allen, N. C., Podell, E., and Allen, R. H. (1978) Cobalamin analogues are present in human plasma and can mask cobalamin deficiency because current radioisotope dilution assays are not specific for true cobalamin, *N Engl J Med 299*, 785-792.

31. Rutsch, F., Gailus, S., Miousse, I. R., Suormala, T., Sagne, C., Toliat, M. R., Nurnberg, G., Wittkampf, T., Buers, I., Sharifi, A., Stucki, M., Becker, C., Baumgartner, M., Robenek, H., Marquardt, T., Hohne, W., Gasnier, B., Rosenblatt, D. S., Fowler, B., and Nurnberg, P. (2009) Identification of a putative lysosomal cobalamin exporter altered in the cblF defect of vitamin B_{12} metabolism, *Nat Genet 41*, 234-239.

32. Coelho, D., Kim, J. C., Miousse, I. R., Fung, S., du Moulin, M., Buers, I., Suormala, T., Burda, P., Frapolli, M., Stucki, M., Nurnberg, P., Thiele, H., Robenek, H., Hohne, W., Longo, N., Pasquali, M., Mengel, E., Watkins, D., Shoubridge, E. A., Majewski, J., Rosenblatt, D. S., Fowler, B., Rutsch, F., and Baumgartner, M. R. (2012) Mutations in ABCD4 cause a new inborn error of vitamin B_{12} metabolism, *Nat Genet 44*, 1152-1155.

33. Rosenblatt, D. S., Hosack, A., Matiaszuk, N. V., Cooper, B. A., and Laframboise, R. (1985) Defect in vitamin B_{12} release from lysosomes: newly described inborn error of vitamin B_{12} metabolism, *Science 228*, 1319-1321.

34. Borths, E. L., Poolman, B., Hvorup, R. N., Locher, K. P., and Rees, D. C. (2005) In vitro functional characterization of BtuCD-F, the Escherichia coli ABC transporter for vitamin B_{12} uptake, *Biochemistry 44*, 16301-16309.

35. Lerner-Ellis, J. P., Tirone, J. C., Pawelek, P. D., Dore, C., Atkinson, J. L., Watkins, D., Morel, C. F., Fujiwara, T. M., Moras, E., Hosack, A. R., Dunbar, G. V., Antonicka, H., Forgetta, V., Dobson, C. M., Leclerc, D., Gravel, R. A., Shoubridge, E. A., Coulton, J. W., Lepage, P., Rommens, J. M., Morgan, K., and Rosenblatt, D. S. (2006) Identification of the gene responsible for methylmalonic aciduria and homocystinuria, cblC type, *Nat Genet 38*, 93-100.

36. Koutmos, M., Gherasim, C., Smith, J. L., and Banerjee, R. (2011) Structural basis of multifunctionality in a vitamin B_{12}-processing enzyme, *J Biol Chem 286*, 29780-29787.

37. Deme, J. C., Miousse, I. R., Plesa, M., Kim, J. C., Hancock, M. A., Mah, W., Rosenblatt, D. S., and Coulton, J. W. (2012) Structural features of recombinant MMADHC isoforms and their interactions with MMACHC, proteins of mammalian vitamin B_{12} metabolism, *Mol Genet Metab 107*, 352-362.

38. Froese, D. S., Krojer, T., Wu, X., Shrestha, R., Kiyani, W., von Delft, F., Gravel, R. A., Oppermann, U., and Yue, W. W. (2012) Structure of MMACHC reveals an arginine-rich pocket and a domain-swapped dimer for its B_{12} processing function, *Biochemistry 51*, 5083-5090.

39. Kim, J., Hannibal, L., Gherasim, C., Jacobsen, D. W., and Banerjee, R. (2009) A human vitamin B_{12} trafficking protein uses glutathione transferase activity for processing alkylcobalamins, *J Biol Chem 284*, 33418-33424.

40. Hannibal, L., Kim, J., Brasch, N. E., Wang, S., Rosenblatt, D., Banerjee, R., and Jacobsen, D. W. (2009) Processing of alkylcobalamins in mammalian cells: a role for the MMACHC (*cbl*C) gene product, *Mol Genet Metabol 97*, 260-266.

41. Coelho, D., Suormala, T., Stucki, M., Lerner-Ellis, J. P., Rosenblatt, D. S., Newbold, R. F., Baumgartner, M. R., and Fowler, B. (2008) Gene identification for the cblD defect of vitamin B_{12} metabolism, *N Engl J Med 358*, 1454-1464.

42. Suormala, T., Baumgartner, M. R., Coelho, D., Zavadakova, P., Kozich, V., Koch, H. G., Berghauser, M., Wraith, J. E., Burlina, A., Sewell, A., Herwig, J., and Fowler, B. (2004) The cblD defect causes either isolated or combined deficiency of methylcobalamin and adenosylcobalamin synthesis, *J Biol Chem 279*, 42742-42749.

43. Stucki, M., Coelho, D., Suormala, T., Burda, P., Fowler, B., and Baumgartner, M. R. (2012) Molecular mechanisms leading to three different phenotypes in the cblD defect of intracellular cobalamin metabolism, *Hum Mol Genet 21*, 1410-1418.

44. Gherasim, C., Hannibal, L., Rajagopalan, D., Jacobsen, D. W., and Banerjee, R. (2013) The C-terminal domain of CblD interacts with CblC and influences intracellular cobalamin partitioning *Biochemie*, Feb 14. doi: 10.1016/j.biochi.2013.1002.1003. [Epub ahead of print].

45. Gulati, S. G., Baker, P., Fowler, B., Li, Y., Kruger, W., Brody, L. C., and Banerjee, R. (1996) Mutations in human methionine synthase in *cbl*G patients, *Hum. Molec. Genet. 5*, 1859-1866.

46. Leclerc, D., Campeau, E., Goyette, P., Adjalla, C. E., Christensen, B., Ross, M., Eydoux, P., Rosenblatt, D. S., Rozen, R., and Gravel, R. A. (1996) Human methionine synthase: cDNA cloning and identification of mutations in patients of the *cbl*G complementation group of folate/cobalamin disorders, *Hum. Molec. Genet. 5*, 1867-1874.

47. Chen, L. H., Liu, M.-L., Hwang, H.-Y., Chen, L.-S., Korenberg, J., and Shane, B. (1997) Human methionine synthase. cDNA cloning, gene localization and expression, *J. Biol. Chem. 272*, 3628-3634.

48. Matthews, R. G., Koutmos, M., and Datta, S. (2008) Cobalamin-dependent and cobamide-dependent methyltransferases, *Curr Opin Struct Biol 18*, 658-666.

49. Watkins, D., and Rosenblatt, D. S. (1989) Functional methionine synthase deficiency (cblE and cblG): clinical and biochemical heterogeneity, *Am J Med Genet 34*, 427-434.

50. Ludwig, M. L., and Matthews, R. G. (1997) Structure-based perspectives on B_{12}-dependent enzymes, *Annu. Rev. Biochem. 66*, 269-313.

51. Olteanu, H., and Banerjee, R. (2001) Human methionine synthase reductase, a soluble P-450 reductase-like dual flavoprotein, is sufficient for NADPH-dependent methionine synthase activation, *J Biol Chem 276*, 35558-35563.

52. Olteanu, H., Munson, T., and Banerjee, R. (2002) Differences in the efficiency of reductive activation of methionine synthase and exogenous electron acceptors between the common polymorphic variants of human methionine synthase reductase, *Biochemistry 41*, 13378-13385.

53. Olteanu, H., Wolthers, K. R., Munro, A. W., Scrutton, N. S., and Banerjee, R. (2004) Kinetic and thermodynamic characterization of the common polymorphic variants of human methionine synthase reductase, *Biochemistry 43*, 1988-1997.

54. Wolthers, K. R., Basran, J., Munro, A. W., and Scrutton, N. S. (2003) Molecular dissection of human methionine synthase reductase: determination of the flavin redox potentials in full-length enzyme and isolated flavin-binding domains, *Biochemistry 42*, 3911-3920.

55. Banerjee, R. V., Harder, S., R., Ragsdale, S. W., and Matthews, R. G. (1990) Mechanism of reductive activation of cobalamin-dependent methionine synthase: an electron paramagnetic resonance spectroelectrochemical study, *Biochemistry 29*, 1129-1137.

56. Yamada, K., Gravel, R. A., Toraya, T., and Matthews, R. G. (2006) Human methionine synthase reductase is a molecular chaperone for human methionine synthase, *Proc Natl Acad Sci U S A 103*, 9476-9481.

57. Gulati, S., Chen, Z., Brody, L. C., Rosenblatt, D. S., and Banerjee, R. (1997) Defects in auxiliary redox proteins lead to functional methionine synthase deficiency, *J Biol Chem 272*, 19171-19175.

58. Dobson, C. M., Wai, T., Leclerc, D., Kadir, H., Narang, M., Lerner-Ellis, J. P., Hudson, T. J., Rosenblatt, D. S., and Gravel, R. A. (2002) Identification of the gene responsible for the *cbl*B complementation group of vitamin B_{12}-dependent methylmalonic aciduria, *Hum Mol Genet 11*, 3361-3369.

59. Leal, N. A., Park, S. D., Kima, P. E., and Bobik, T. A. (2003) Identification of the human and bovine ATP:Cob(I)alamin adenosyltransferase cDNAs based on complementation of a bacterial mutant, *J Biol Chem 278*, 9227-9234.

60. Padovani, D., Labunska, T., Palfey, B. A., Ballou, D. P., and Banerjee, R. (2008) Adenosyltransferase tailors and delivers coenzyme B_{12}, *Nat Chem Biol 4*, 194-196.

61.   Stich, T. A., Yamanishi, M., Banerjee, R., and Brunold, T. C. (2005) Spectroscopic evidence for the formation of a four-coordinate Co^{2+} cobalamin species upon binding to the human ATP:cobalamin adenosyltransferase, *J Am Chem Soc 127*, 7660-7661.

62.   Yamanishi, M., Labunska, T., and Banerjee, R. (2005) Mirror "base-off" conformation of coenzyme B_{12} in human adenosyltransferase and its downstream target, methylmalonyl-CoA mutase, *J Am Chem Soc 127*, 526-527.

63.   Yamanishi, M., Vlasie, M., and Banerjee, R. (2005) Adenosyltransferase: an enzyme and an escort for coenzyme B_{12}?, *Trends Biochem Sci 30*, 304-308.

64.   Lexa, D., and Saveant, J.-M. (1983) The electrochemistry of vitamin B_{12}, *Acc. Chem. Res. 16*, 235-243.

65.   Mera, P. E., and Escalante-Semerena, J. C. (2010) Dihydroflavin-driven adenosylation of 4-coordinate Co(II) corrinoids: are cobalamin reductases enzymes or electron transfer proteins?, *J Biol Chem 285*, 2911-2917.

66.   Leal, N. A., Olteanu, H., Banerjee, R., and Bobik, T. A. (2004) Human ATP:Cob(I)alamin adenosyltransferase and its interaction with methionine synthase reductase, *J Biol Chem 279*, 47536-47542.

67.   Mera, P. E., and Escalante-Semerena, J. C. (2010) Multiple roles of ATP:cob(I)alamin adenosyltransferases in the conversion of B_{12} to coenzyme B_{12}, *Appl Microbiol Biotechnol 88*, 41-48.

68.   Padovani, D., and Banerjee, R. (2009) A Rotary Mechanism for Coenzyme B_{12} Synthesis by Adenosyltransferase, *Biochemistry 48*, 5350-5357.

69.   Lofgren, M., and Banerjee, R. (2011) Loss of allostery and coenzyme B_{12} delivery by a pathogenic mutation in adenosyltransferase, *Biochemistry 50*, 5790-5798.

70.   Padovani, D., and Banerjee, R. (2009) A G-protein editor gates coenzyme B_{12} loading and is corrupted in methylmalonic aciduria, *Proc Natl Acad Sci U S A 106*, 21567-21572.

71.   Takahashi-Iniguez, T., Garcia-Arellano, H., Trujillo-Roldan, M. A., and Flores, M. E. (2011) Protection and reactivation of human methylmalonyl-CoA mutase by MMAA protein, *Biochem Biophys Res Commun 404*, 443-447.

72.   Lerner-Ellis, J. P., Dobson, C. M., Wai, T., Watkins, D., Tirone, J. C., Leclerc, D., Dore, C., Lepage, P., Gravel, R. A., and Rosenblatt, D. S. (2004) Mutations in the *MMAA* gene in patients with the *cbl*A disorder of vitamin B_{12} metabolism, *Hum Mutat 24*, 509-516.

73.   Dobson, C. M., Wai, T., Leclerc, D., Wilson, A., Wu, X., Dore, C., Hudson, T., Rosenblatt, D. S., and Gravel, R. A. (2002) Identification of the gene responsible for the *cbl*A complementation group of vitamin B_{12}-responsive methylmalonic acidemia based on analysis of prokaryotic gene arrangements, *Proc Natl Acad Sci U S A 99*, 15554-15559.

74.   Korotkova, N., and Lidstrom, M. E. (2004) MeaB is a component of the methylmalonyl-CoA mutase complex required for protection of the enzyme from inactivation, *J Biol Chem 279*, 13652-13658.

75.   Padovani, D., and Banerjee, R. (2006) Assembly and protection of the radical enzyme, methylmalonyl-CoA mutase, by its chaperone, *Biochemistry 45*, 9300-9306.

76.   Padovani, D., Labunska, T., and Banerjee, R. (2006) Energetics of interaction between the G-protein chaperone, MeaB and B_{12}-dependent methylmalonyl-CoA mutase, *J. Biol. Chem. 281*, 17838-17844.

77. Hubbard, P. A., Padovani, D., Labunska, T., Mahlstedt, S. A., Banerjee, R., and Drennan, C. L. (2007) Crystal structure and mutagenesis of the metallochaperone MeaB: insight into the causes of methylmalonic aciduria, *J Biol Chem 282*, 31308-31316.

78. Froese, D. S., Kochan, G., Muniz, J. R., Wu, X., Gileadi, C., Ugochukwu, E., Krysztofinska, E., Gravel, R. A., Oppermann, U., and Yue, W. W. (2010) Structures of the human GTPase MMAA and vitamin B_{12}-dependent methylmalonyl-CoA mutase and insight into their complex formation, *J Biol Chem 285*, 38204-38213.

79. Perez, B., Angaroni, C., Sanchez-Alcudia, R., Merinero, B., Perez-Cerda, C., Specola, N., Rodriguez-Pombo, P., Wajner, M., de Kremer, R. D., Cornejo, V., Desviat, L. R., and Ugarte, M. (2010) The molecular landscape of propionic acidemia and methylmalonic aciduria in Latin America, *J Inherit Metab Dis 33*, S307-314.

80. Dempsey-Nunez, L., Illson, M. L., Kent, J., Huang, Q., Brebner, A., Watkins, D., Gilfix, B. M., Wittwer, C. T., and Rosenblatt, D. S. (2012) High resolution melting analysis of the MMAA gene in patients with cblA and in those with undiagnosed methylmalonic aciduria, *Mol Genet Metab 107*, 363-367.

CHAPTER 2

Loss of Allostery and Coenzyme B$_{12}$ Delivery by a Pathogenic Mutation in Adenosyltransferase[3,4]

2.1 Abstract

ATP-dependent cob(I)alamin adenosyltransferase (ATR) is a bifunctional protein: an enzyme that catalyzes the adenosylation of cob(I)alamin and an escort that delivers the product, adenosylcobalamin (AdoCbl or coenzyme B$_{12}$), to methylmalonyl-CoA mutase (MCM), resulting in holoenzyme formation. Failure to assemble holo-MCM leads to methylmalonic aciduria. We have previously demonstrated that only 2 equiv of AdoCbl bind per homotrimer of ATR and that binding of ATP to the vacant active site triggers ejection of 1 equiv of AdoCbl from an adjacent site. In this study, we have mimicked in the *Methylobacterium extorquens* ATR, a C-terminal truncation mutation, D180X, described in a patient with methylmalonic aciduria, and characterized the associated biochemical penalties. We demonstrate

that while k_{cat} and $K_M^{Cob(I)}$ for D180X ATR are only modestly decreased (by 3- and 2-fold, respectively), affinity for the product, AdoCbl, is significantly diminished (400-fold), and the negative cooperativity associated with its binding is lost. We also demonstrate that the D180X mutation corrupts ATP-dependent cofactor ejection, which leads to transfer of AdoCbl from wild-type ATR to MCM. These results suggest that the pathogenicity of the corresponding human truncation mutant results from its inability to sequester AdoCbl for direct transfer to MCM. Instead, cofactor release into solution is predicted to reduce the capacity for holo-MCM formation, leading to disease.

2.2 Introduction

Coenzyme B_{12} or 5′-deoxyadenoslycobalamin (AdoCbl) is a complex organometallic cofactor that is used in all domains of life by enzymes catalyzing diverse reactions including: dehydrations, intramolecular carbon skeleton rearrangements, reductive eliminations, and deaminations (1-3). AdoCbl comprises a central cobalt ion coordinated equatorially by four nitrogen atoms donated by the corrin macrocycle. A novel nucleotide base, dimethylbenzimidazole (DMB), occupies the lower axial coordination position while the upper axial position is occupied by the 5′-deoxyadenosyl group, via the organometallic cobalt–carbon bond.

AdoCbl is a "high value" product that is either biosynthesized *de novo* by some bacteria or generated via adenosylation of cob(I)alamin in organisms such as mammals, which lack a *de novo* pathway for its synthesis (4). There are at least three families of ATP-dependent cob(I)alamin adenosyltransferases (ATR): EutT, PduO, and CobA, which catalyze the addition of the 5′-deoxyadenosyl group from ATP to cob(I)alamin; however, their roles in metabolism are

distinct. Members of the three ATR subfamilies do not share sequence or structural homology and represent examples of convergent evolution. In some organisms, such as *Salmonella enterica*, members of all three ATR subfamilies are used to meet metabolic requirements under distinct physiological conditions (4). The EutT- and PduO-type ATRs of *S. enterica* furnish AdoCbl for the B_{12}-dependent enzymes, diol dehydratase, and ethanolamine ammonia lyase, for catabolism of alkane diols and growth on ethanolamine, respectively (2, 5). In contrast, CobA is involved in the *de novo* synthesis of AdoCbl (6). Humans use a PduO-type ATR for supplying AdoCbl to the only enzyme that uses this cofactor, i.e., MCM, for catabolism of cholesterol, branched chain amino acids, and odd-chain fatty acids (7, 8).

To overcome the twin challenges posed by the lability of the cofactor in the three biologically relevant cobalt oxidation states and its low tissue concentration in humans, it has been proposed that, following intracellular delivery, B_{12} remains protein-bound as it is processed and delivered to its target enzymes (9,10). In support of this model, it has been demonstrated that, following AdoCbl synthesis by ATR, the cofactor is directly transferred to the active site of MCM via a transient protein–protein interaction (11-13). Mutations in ATR lead to deficiencies in the enzymatic activity of MCM, resulting in methylmalonic aciduria (7, 14, 15).

Structure–function studies on PduO-type ATRs from *Lactobacillus reuteri* (16-19) and *Methylbacterium extorquens* (13, 20, 21) have provided mechanistic insights into these enzymes. Cob(II)alamin binds to ATR in a "base-off" conformation in which the lower axial DMB base is displaced from the cobalt ion (22, 23). A yet unknown mitochondrial oxidoreductase catalyzes the one electron reduction of mammalian ATR-bound cob(II)alamin, yielding cob(I)alamin (24) (eq 2.1). Cob(I)alamin is a potent nucleophile and attacks the C-5′ribosyl carbon of ATP forming PPP_i and AdoCbl, which is "base-off" and five-coordinate (16, 25, 26). In contrast,

27

AdoCbl bound to MCM is in a six-coordinate "base-off/His-on" conformation in which a histidine residue donated by MCM occupies the lower axial position (1). This difference in coordination number results in large differences in the absorption spectra and is experimentally useful for locating the cofactor (13). Thus, "base-off" AdoCbl bound to ATR exhibits an absorbance maximum at 458 nm while "base-off/His-on" AdoCbl bound to MCM or free in solution has a maximum at 525 nm (13).

$$\text{Cob(II)alamin} \rightarrow \text{Cob(I)alamin} + \text{ATP} \rightarrow \text{AdoCbl} + \text{PPP}_i \qquad \text{(eq 2.1)}$$

PduO-type ATR is a homotrimer that appears to use only two of its three active sites at a time and exhibits negative cooperativity for substrate and product binding (13, 20, 27). In the crystal structure of human PduO-type ATR, 2 equivalents of ATP are bound per homotrimer (28). ATP binding to the vacant site in the *M. extorquens* ATR triggers ejection of only 1 of 2 equiv of AdoCbl, providing a mechanism for driving transfer to MCM in what has been described as a "rotary mechanism" (Figure 2.1) (27). However, the crystal structures of the *L. reuteri* ATR show occupancy of all three active sites with either ATP or cob(II)alamin (18). This difference may arise from altered behavior in the crystalline versus solution state or differences between PduO-type ATRs from different organisms. The apparent conservation of function between human and *M. extorquens* PduO-type ATR suggests that the *M. extorquens* ATR is a viable model for the human enzyme.
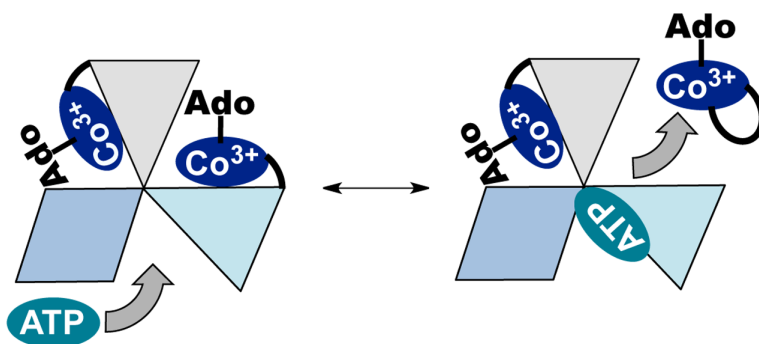
Figure 2.1. The rotary mechanism of ATP-depenent AdoCbl release/transfer. ATP binding triggers AdoCbl release. The ATR•product complex has two of three active sites occupied by AdoCbl. The three subunits of ATR are depicted in shades of blue an grey. ATP binds to the ATR•2AdoCbl complex and triggers the release of one equivalent of AdoCbl.

The ATR monomer comprises a five-helix bundle arranged in a head-to-tail fashion relative to the neighboring subunit. The active sites are located at the subunit interfaces (Figure 2.2) (18, 28). Residues at the N-terminus become ordered in response to ATP binding, and residues from the adjacent monomer contribute to the ATP binding site. Cobalamin binds in a C-terminal crevice, and backbone amides from the adjacent subunit participate in the majority of hydrogen-bonding interactions with the amide substituents on the corrin ring (18). Two conformational changes accompany binding of B_{12}: the ordering of the C-terminus and positioning of a mobile loop proximal to the lower axial face of B_{12}. This loop is hydrogen bonded to B_{12}, and its movement facilitates generation of four-coordinate cob(II)alamin (17). In contrast, the significance of the C-terminal ordering for ATR function is less well understood. Truncation of the final 16 residues in human ATR due to the nonsense Q234X mutation results in early onset methylmalonic aciduria (15). Structural studies on *Lr*PduO-Δ183–188, an *L. reuteri* ATR missing the terminal six amino acids, revealed decreased conformational rigidity of the mobile loop, although cob(II)alamin was nonetheless bound in a four-coordinate "base-off" state (17). The *Lr*PduO-Δ183–188 mutant exhibited a modest decrease in the catalytic efficiency

relative to wild-type ATR, providing limited insight into the role of the C-terminal tail and the biochemical basis of pathogenicity of the Q234X patient mutation (17).

In this study, we have mimicked the Q234X mutation in the *M. extorquens* ATR by introducing the D180X mutation, which corresponds to the site of the nonsense mutation in the human sequence (Figure 2.3). We demonstrate that while this C-terminal truncation has modest effects on the steady-state kinetic parameters, the affinity for the product, AdoCbl, and allosteric communication between active sites leading to negative cooperativity are adversely affected. These changes lead to corruption of the direct transfer mechanism of AdoCbl from ATR to MCM and provide insights into the importance of the C-terminal loop in gating cofactor transfer and for communication between adjoining active sites.
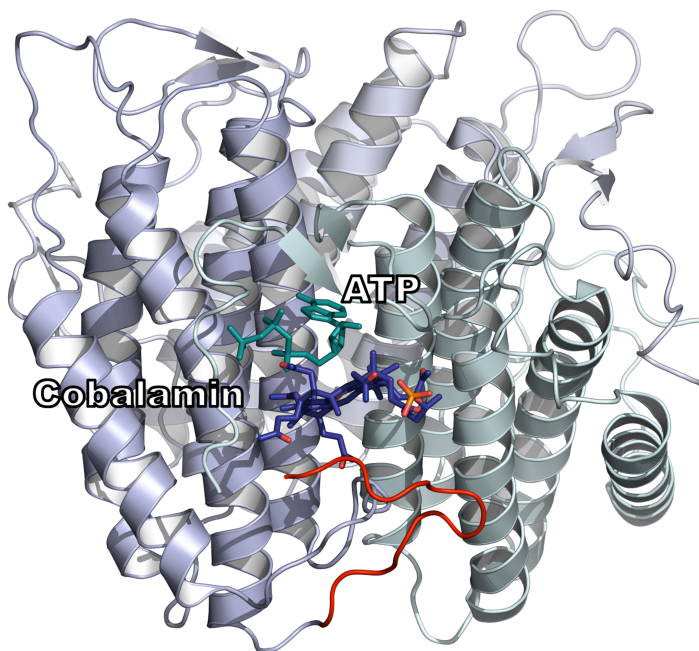
Figure 2.2. **Structure of PduO-type ATR from *L. reuteri* with Cob(II)alamin and ATP bound (PDB entry 3CI1).** The ATR holoenzyme is shown in ribbon representation with the individual subunits of the ATR trimer are colored as in Fig. 1. ATP and cobalamin are shown in stick representation in cyan and dark blue, respectively. The C-terminal loop (red) in one subunit corresponds to the boundaries of the truncation in *M. extorquens* D180X ATR (D180–R190).

2.3 Experimental Procedures

2.3.1 Materials – MANT-ATP (2′(3′)-*O*-(*N*-methylanthraniloyl)-ATP) was purchased from Jen Biosciences (Germany). ATP, AdoCbl, phenylmethylsulfonyl fluoride, lysozyme, and all other chemical reagents were purchased from Sigma. The Stratagene Quikchange II XL Site-Directed Mutagenesis Kit was purchased from Agilent.

2.3.2 Construction of the D180X ATR Mutant – The mutation was created using the Quikchange kit and the following primers: sense: 5′-CAACCGCGACGGCGCCTAGGACGTGCTCTGGGTG-3′ and an antisense primary containing the complementary sequence. The 6xHis-wild-type ATR expression plasmid described previously (20) was used as template. The mutation was confirmed by nucleotide sequence determination at the University of Michigan DNA Sequencing Core.

2.3.3 Expression and Purification of ATR – *Escherichia coli* (BL21 (DE3)) was transformed with plasmids encoding recombinant D180X ATR or 6xHis-wild-type ATR and grown at 37 °C in 1 L of Luria–Bertani media containing kanamycyin (50 μg/mL). Cultures were grown to an optical density at 600 nm of 0.5–0.6 and induced with either 0.1 mM (for D180X ATR) or 1 mM (for wild-type ATR) isopropyl-β-D-thiogalactopyranoside. Cultures were then grown at 20 °C for 14–16 h (D180X ATR) or at 37 °C for 6–10 h (wild-type ATR) prior to harvesting.

ATR (wild-type and D180X) was purified as follows. Bacterial pellets were suspended in 50 mM sodium phosphate buffer, pH 8.0, containing 0.3 M KCl, 20 mM imidazole, and 1 mM phenylmethylsulfonyl fluoride (buffer A). Cells were lysed first by treatment with lysozyme (25 mg/L culture; 40 000 U/mg) for 1 h with stirring at 4 °C and then disrupted by sonication as described previously (20). The pellet was separated by centrifugation at 19000*g* at 4 °C. The supernatant was filtered through a 0.4 μm syringe filter and diluted to 4–5 mg protein/mL before

31

loading onto a 50 mL nickel–nitrilotriacetic acid–Sepharose column pre-equilibrated with 10–20

column volumes of buffer A. The column was washed with 10 column volumes of buffer A and

eluted with a linear gradient of 20–300 mM imidazole in buffer A. Fractions containing the

target protein were pooled, concentrated, dialyzed extensively against 50 mM HEPES, pH 8, 0.3

M KCl, 5% glycerol (buffer B) at 4 °C, and then dialyzed extensively against buffer B

containing 10 mM MgCl$_2$ at 4 °C. This purification protocol typically yielded 15–20 mg of

≥95% pure protein per liter of culture.

```
M. extorquens   ----------------------------------------------------MVKLNRIYT  9
S. enterica     -----------------------------------------------------MAIYT  5
L. reuteri      -----------------------------------------------------MKIYT  5
H. sapien       MAVCGLGSRLGLGSRLGLRGCFGAARLLYPRFQSRGPQGVEDGDRPQPSSKTPRIPKIYT 60
B. taurus       ----------------------------QSRGPQGVEDGDRPQPSSKTPKVPKIYT 28

M. extorquens   RTGDQGTTGLANGERRSKADLRVEAYGTVDETNACIGLAR-LTAEPA--LDAMLARIQND 66
S. enterica     RTGDAGTTSLFTGQRVSKTHPRVEAYGTLDELNAALSLCACAAADEN--HRTLLEAIQQQ 63
L. reuteri      KNGDKGQTRIIGKQILYKNDPRVAAYGEVDELNSWVGYTKSLINSHTQVLSNELEEIQQL 65
H. sapien       KTGDKGFSSTFTGERRPKDDQVFEAVGTTDELSSAIGFALELVTEKGHTFAEELQKIQCT 120
B. taurus       KTGDKGFSSTFTGERRSKDDQVFEAVGTTDELSSAIGFAMELIAEKGHPFVEELQKIQCS 88

M. extorquens   LFDLGADLATPP-SDKPLGYEPLRIVPAQVQRLETEIDALNANIPPLKSFVLPGGSAAAA 125
S. enterica     LFWFSAELASD--SEQPS-PKQRYISSEEISALEAAIDRAMARVEPLHSFILPGRCEAAS 120
L. reuteri      LFDCGHDLATPA-DDERHSFKFKQEQP--TVWLEEKIDNYTQVVPAVKKFILPGGTQLAS 122
H. sapien       LQDVGSALATPCSSAREAHLKYTTFKAGPILELEQWIDKYTSQLPPLTAFILPSGGKISS 180
B. taurus       LQDVGSALATPRSSAREAHLKHATFEAGPILELEQWIDKYSRQLPPLTAFILPSGGKSSS 148

M. extorquens   ALHLARTVCRRAERLVVALSGVESEAISGEALQYLNRLSDFLFVASRAAN---------R 176
S. enterica     RLHFARTLARRAERRLVELA--TEVNVRQVLMRYINRLSDCLYALARAEDSDAHQANIIR 178
L. reuteri      ALHVARTITRRAERQIVQLMR--EEQINQDVLIFINRLSDYFFAAARYAN--------YL 172
H. sapien       ALHFCRAVCRRAERRVVPLVQMGETDAN--VAKFLNRLSDYLFTLARYAA--------MK 230
B. taurus       ALHFCRAVCRRAERRVVPLVQTGETDAN--VVKFLNRLSDYLFTLARYTA--------MK 198

                    *
M. extorquens   DGADDVLWVPGQNR------ 190
S. enterica     EVSKRYLAASQPTR------ 192
L. reuteri      EQQPDMLYRNSKDVFR---- 188
H. sapien       EGNQEKIYMKNDPSAESEGL 250
B. taurus       EGNPEKIYKKNDLSDRT--- 215
```

Figure 2.3. **Sequence comparison of select PduO-type ATRs.** Multiple sequence alignment of PduO-type ATRs in which amino acids that are identical (black) or conserved (grey) are highlighted. The sequence of the human ATR includes an N-terminal 32 amino acid mitochondrial leader sequence. An asterisk indicates the position of residue D180.

2.3.4 ATR Activity Assays − ATR activity was monitored in a steady-state assay as described

previously and data were fit to the Michaelis–Menten equation to obtain the kinetic parameters

(20). The K_M for ATP was determined at saturating HOCbl (55 µM) and varying ATP (from 0.5 to 300 µM). The K_M for HOCbl was determined at saturating ATP (1 mM) and varying HOCbl (from 0.5 to 60 µM) concentrations.

2.3.5 Thermal Denaturation Assays – Thermal denaturation of ATR was performed to assess the relative stabilities of the wild-type and mutant proteins. For this, 0.5 mg/mL of purified ATR in buffer B containing 10 mM MgCl$_2$was placed in a cuvette, and the temperature was increased from 4 to 68 °C in a Cary 100 Bio UV/vis spectrophotometer with a heating block connected to a Fisher Scientific Isotemp 3016S water bath. Unfolding was measured by increased light scattering at 600 nm in 5 °C increments until no further change in the optical density was observed. Data were analyzed as described previously (29).

2.3.6 Isothermal Titration Calorimetry (ITC) – ITC experiments were performed as described previously (13, 30) with the exception that the temperature was maintained at 4 °C due to the instability of D180X ATR at ambient temperature for prolonged periods. ITC experiments, conducted in triplicate, were analyzed with MicroCal ORIGIN software to determine the bimolecular association constant (K_A), binding enthalpy ($\Delta H°$), and binding entropy ($\Delta S°$). Briefly, 40–45 µM D180X ATR in 50 mM HEPES, 0.3 M KCl, 10 mM MgCl$_2$, 5% glycerol at pH 8 was titrated with 45 6 µL aliquots of 1–2 mM ATP or AdoCbl. Following integration of the calorimetric signals in MicroCal ORIGIN software, ITC data for the titration of D180X ATR with ATP were fitted to a two-sites model that describes two populations of active sites that bind ATP with distinct thermodynamic parameters. When D180X ATR was titrated with AdoCbl, a single-site model was used to fit the data. The Gibbs free energy of binding either ligand was calculated using eqs 2 and 3.

$$\Delta G° = -RT \ln(K_A) \qquad \text{(eq 2.2)}$$

$$\Delta G^\circ = \Delta H^\circ - T\Delta S^\circ \qquad \text{(eq 2.3)}$$

2.3.7 Fluorescence and UV/vis Titrations – For the UV/vis titration of AdoCbl with D180X ATR, experiments were performed in quadruplicate, and the large hypsochromic shift from 525 to 458 nm associated with the "base-on" to "base-off" transition for AdoCbl was used to monitor binding. Titrations were performed at 4 °C, and all stock solutions were kept chilled throughout the experiment. Briefly, 1.5–10 μM AdoCbl in 50 mM HEPES, pH 8 containing 0.3 M KCl, 10 mM MgCl$_2$ and 5% glycerol was titrated with 1–100 μM D180X ATR in the same buffer. Spectra were recorded 8–10 min after each addition of enzyme to allow binding to reach equilibrium. Data were fit to a hyperbolic binding isotherm to determine the dissociation constant, K_D, for binding of AdoCbl to D180X ATR. For wild-type ATR, titrations were performed using 4 μM enzyme +8 μM AdoCbl and aliquots of a 1 mM ATP stock solution. The corresponding titration with D180X ATR was performed using 130 μM enzyme, 2 μM AdoCbl, and aliquots of a 20 mM ATP stock solution. Titrations of MANT-ATP with D180X were monitored via the quenching of MANT fluorescence upon binding. Briefly, 10–15 μM of MANT-ATP in 50 mM HEPES, 0.3 M KCl, 10 mM MgCl$_2$, 5% glycerol at pH 8 was titrated with 100 μM D180X ATR in the same buffer to a final concentration of 35 μM protein at 4 °C. Fluorescence quenching was monitored at 444 nm (360 nm excitation), and its dependence on D180X ATR concentration was fitted to a hyperbolic binding isotherm. The MANT-ATP titrations were performed in triplicate.

2.4 Results

2.4.1 Stability of Wild-Type and D180X ATR

During purification, the stability of the D180X mutant was noted to be lower than for wild-type ATR, as evidenced by precipitation, especially during concentration. Comparison of the

thermal denaturation profiles confirmed that the D180X mutant is indeed less stable relative to wild-type ATR with a $\Delta T_m = 11.1 \pm 0.4$ °C (Figure 2.4).
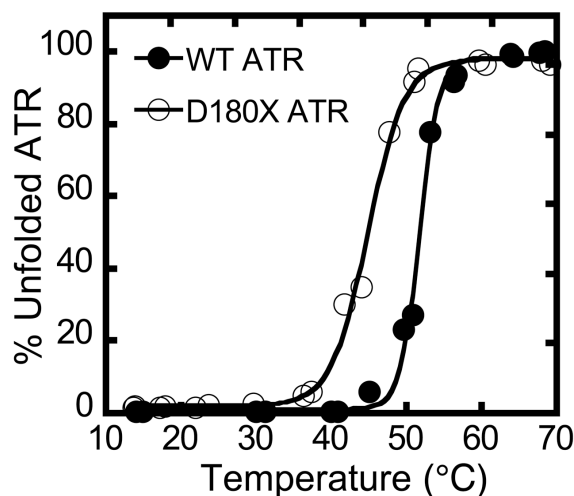
Figure 2.4. **Thermal melting curves for wild-type ATR (filled circles) and D180X ATR (hollow circles)**. Plots were normalized to the maximum turbidity observed at 600 nm. Protein unfolding was monitored as described under Experimental Procedures.

2.4.2 Kinetic Characterization of Wild-Type and D180X ATR

The initial velocity of the adenosylation reaction was monitored at 390 nm (corresponding to conversion of cob(I)alamin to AdoCbl) by varying the concentration of cob(I)alamin at saturating concentrations of ATP, or vice versa (Table 1). The apparent K_M^{ATP} (8.4 ± 1.4 μM) for wild-type ATR is similar to previously reported values for the N-terminally His$_8$-tagged human (K_M, 7.2 μM) and *L. reuteri* (K_M, 2 μM) ATRs. Similarly, the $K_M^{Cob(I)}$ for wild-type ATR is similar to values reported for other PduO-type ATRs (K_M, 0.2–5 μM (8, 31-33)) but 5-fold lower than the value reported for His-tagged human ATR (31). The k_{cat} for wild-type *M. extorquens* ATR is 4-fold larger than any value previously reported for a PduO-type ATR.

The D180X mutation has modest effects on the steady-state kinetic parameters: $K_M^{cob(I)}$ and k_{cat} are 2- and 3.5-fold smaller, respectively, resulting in a 7-fold lower catalytic efficiency with

respect to the cob(I)alamin substrate (Table 2.1). The K_M for ATP is unaffected by the D180X mutation.

| Enzyme | k_{cat} (s^{-1}) | ATP-dependence | | Cob(I)alamin-dependence | |
		K_M (μM)	k_{cat}/K_M (M^{-1}s^{-1})	K_M (μM)	k_{cat}/K_M (M^{-1}s^{-1})
WT	$(8.9 \pm 0.1) \times 10^{-1}$	8.4 ± 1.4	$(1.1 \pm 0.3) \times 10^{5}$	0.4 ± 0.1	$(2.5 \pm 0.2) \times 10^{6}$
D180X	$(2.5 \pm 0.1) \times 10^{-1}$	9.5 ± 1.2	$(2.7 \pm 0.1) \times 10^{4}$	0.8 ± 0.1	$(3.5 \pm 0.1) \times 10^{5}$

[a]The values represent the mean ± SD from at least three independent experiments in the adenosylation reaction.

Table 2.1. Kinetic parameters of wild-type and D180X ATR[a].

2.4.3 Thermodynamic Characterization of ATP and AdoCbl Binding

Binding of ATP to D180X ATR was characterized by ITC and by fluorescence spectroscopy using MANT-ATP (Figure 2.5A). A monophasic binding isotherm was obtained from the fluorescence titration and yielded a K_D value of 5.4 ± 1.1 μM for binding of MANT-ATP to D180X ATR. This value is comparable to the K_D value of 5.9 ± 1.4 μM reported for binding of the second equivalent of ATP to wild-type ATR (27). In contrast, ITC data for ATP binding to D180X ATR exhibits biphasic behavior (Figure 2.5B). The discrepancy between the fluorescence and ITC data may be derived from the low amplitude of fluorescence quenching upon binding of MANT-ATP to site 1 and is consistent with prior data on MANT-ATP binding to ATR by stopped-flow fluorescence spectroscopy (27).

Analysis of the ITC data yielded $\Delta G_1°$ and $\Delta G_2°$ values of −8.1 kcal/mol and −6.9 kcal/mol for binding of ATP to sites 1 and 2 in D180X ATR (Table 2.2), which are virtually identical to those reported for wild-type ATR (−8.3 kcal/mol and −6.6 kcal/mol, respectively). However, the

relative contributions of the entropic and enthalpic terms to the $\Delta G°$ values differ between the

D180X mutant and wild-type ATR. Thus, binding of ATP to sites 1 and 2 is enthalpically

dominated ($\Delta H_1° = -8.1$ kcal/mol and $\Delta H_2° = -6.0$ kcal/mol) in wild-type ATR, while it is

entropically driven in the D180X mutant ($T\Delta S_1° = 7.9$ kcal/mol and $T\Delta S_2° = 3.4$ kcal/mol).
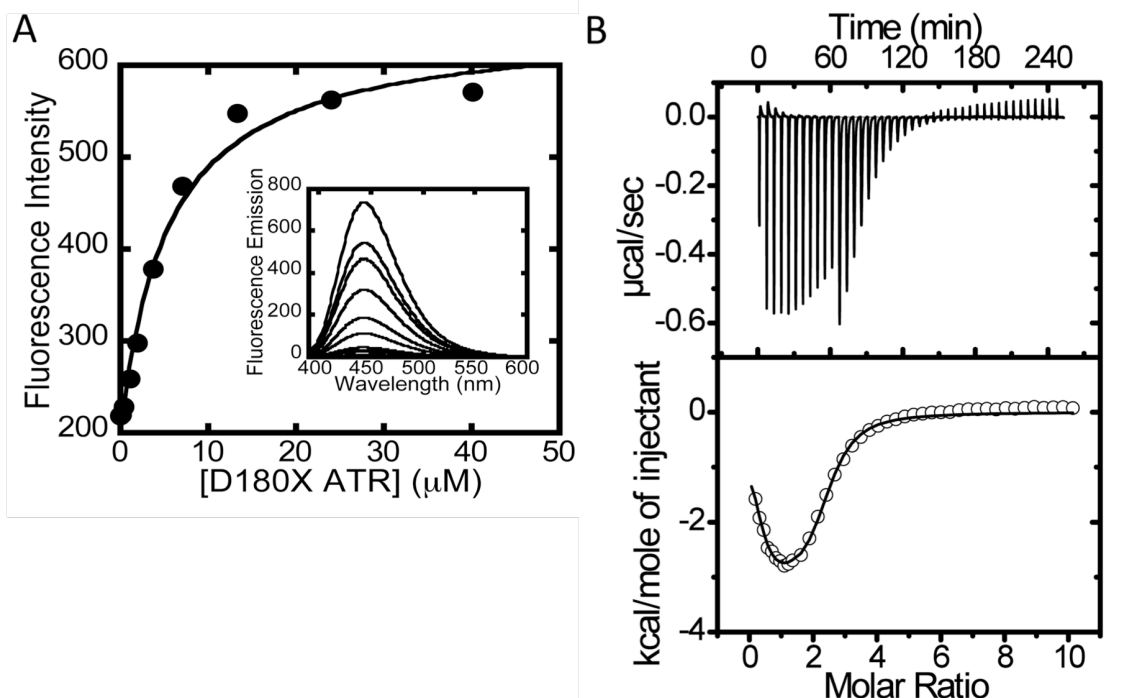
Figure 2.5. **Binding of ATP to D180X ATR.** (A) The inset shows a representative fluorescence titration of MANT-ATP (15 μM) with D180X ATR (0–40 μM) at 10 °C. (B) Representative calorimetric titration data for binding of ATP to ATR (50 μM) in buffer B at 4 °C. The top panel depicts the raw data for ATP binding in power versus time. The lower panel shows integration of data in the top panel, which is proportional to the heat release that accompanies binding as a function of time. The data in the lower panel were best fit to a two-sites binding model and yielded the thermodynamic parameters that govern ATP binding to D180X ATR at 4 °C (shown in Table 2).

Binding of AdoCbl is significantly impacted in the D180X mutant, which exhibits

a K_D^{AdoCbl} of 71 ± 24 μM (Figure 2.6A) in comparison to the 0.1 and 2.0 μM values for sites 1

and 2 reported for the wild-type enzyme (27). The relatively low affinity of the D180X mutant

for AdoCbl necessitated high protein concentrations during spectrophotometric titrations and was

limited by the instability of the mutant protein. Hence, only ~83% saturation with AdoCbl could be observed in the spectrophotometric binding assay (Figure 2.6A). In principle, the inability to observe binding of 2 equiv of AdoCbl in the "base-off" state per trimer could arise from two possibilities: (i) only 1 equiv of AdoCbl binds to the D180X mutant in the "base-off" conformation while the second equivalent binds in the "base-on" conformation and (ii) the dissociation constant for AdoCbl binding at site 2 is ≫70 μM measured by spectral titration. To distinguish between these possibilities, AdoCbl binding was also monitored by ITC (Figure 6B).
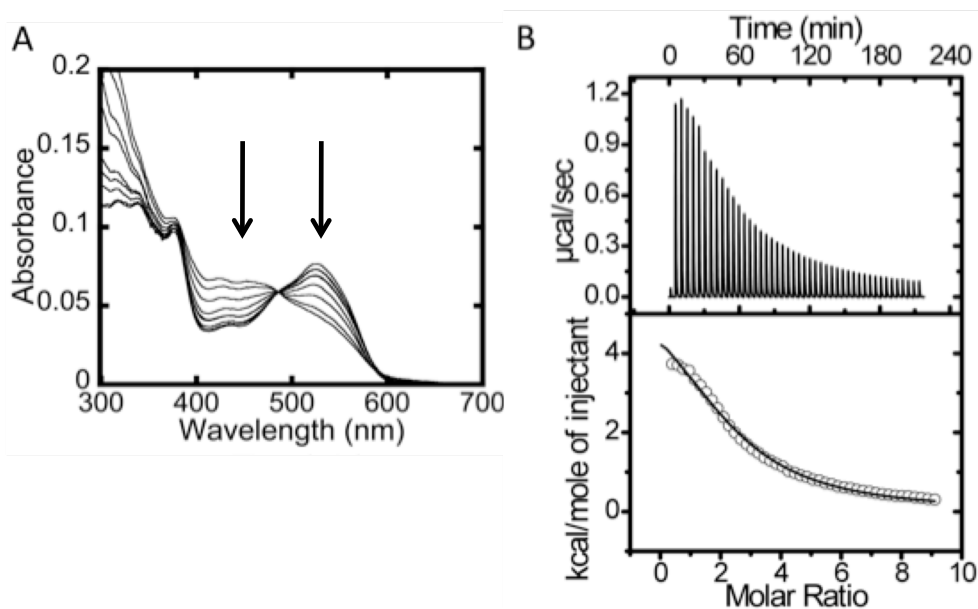
Figure 2.6. Binding of AdoCbl to D180X ATR. (A) The UV/vis spectra were obtained by titrating a fixed concentration of AdoCbl (7.5 μM) with increasing concentrations of D180X ATR (0–150 μM). Approximately 83% saturation of the two AdoCbl binding sites per trimer was achieved based on $\Delta\varepsilon 525 = 6.69$ M–1 cm–1. (B) Representative ITC data for binding of AdoCbl to D180X ATR (50 μM) in buffer B at 4 °C. The top panel depicts the raw data for AdoCbl-binding in power versus time. The lower panel shows integration of data in the top panel. The data in the lower panel were best fit to a single-site binding model and gave the thermodynamic parameters associated with binding of AdoCbl to D180X ATR at 4 °C.

The calorimetric titrations showed monophasic behavior for AdoCbl binding, and the data were best fit to a single-binding site model with $N = 2$ per ATR homotrimer (Table 2.2). The ITC data confirm that AdoCbl binds to D180X ATR with an ~700- and 35-fold weaker binding affinity at

sites 1 and 2 compared to wild-type enzyme. Hence, the C-terminal deletion leads to loss of negative cooperativity associated with AdoCbl binding to wild-type ATR.

	ATP[a]		AdoCbl[b]
	Site 1	Site 2	Sites 1 and 2
K_D (μM)	0.48 ± 0.02	4.01 ± 0.61	44.1 ± 3.2
ΔH^o (kcal/mol)	-0.27 ± 0.02	-3.40 ± 0.40	5.61 ± 0.26
$T\Delta S^o$ (kcal/mol)	7.86 ± 0.91	3.41 ± 0.04	11.10 ± 0.63
ΔG^o (kcal/mol)	-8.12 ± 0.90	-6.87 ± 0.61	-5.49 ± 0.89
N^c (sites)	0.38 ± 0.08	1.43 ± 0.07	2.07 ± 0.07

[a]ITC data for ATP binding were fitted to a 2-site model. [b]The isotherms for binding of AdoCbl to D180X ATR were best fit to a one-site model. [c]N represents the number of unique sites described by the binding model.

Table 2.2. Thermodynamic parameters for binding ATP and AdoCbl to D180X ATR[c].

2.4.4 Corruption of the ATP-Triggered Mechanism for AdoCbl Unloading

A characteristic of AdoCbl transfer from ATR to MCM is the ATP-stimulated ejection of 1 equiv of AdoCbl from ATR (Figure 2.1) (20). To determine whether ATP triggers product release irrespective of whether one or two AdoCbl molecules are bound, wild-type ATR was loaded under conditions where a vast excess of active sites over AdoCbl (i.e., 100:1) resulted statistically, in the predominance of the 1:1 ATR:AdoCbl complex. Addition of 0–30 mM ATP to this complex (corresponding to a 0–200-fold excess of ATP over ATR) failed to trigger release of AdoCbl into solution, demonstrating that binding of ATP only releases AdoCbl from the low affinity site when 2 equiv of AdoCbl are bound (Figure 2.7).
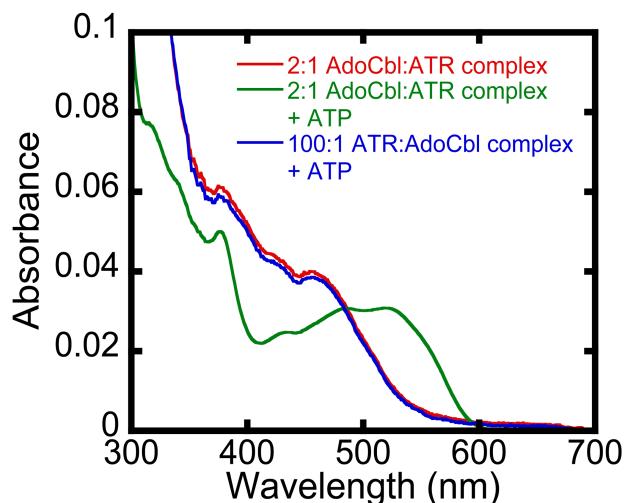
Figure 2.7. **ATP-triggered release of AdoCbl only from the low affinity site in wild-type ATR homotrimer.** The difference in K_Ds for the two AdoCbl sites on ATR implies that when [ATR] >> [AdoCbl] (i.e., 100:1), site 2 is predominantly vacant and site 1 is occupied. The spectrum of "base-off" AdoCbl in the 2:1 (AdoCbl·wild-type ATR) complex where the concentration of AdoCbl is identical to the concentration of AdoCbl-binding sites is shown by the red spectrum. The green spectrum represents the release of 50% of bound Adocbl resulting from the addition of 30 mM ATP to the solution of 2:1 AdoCbl:ATR (red spectrum). The blue spectrum is of "base-off" AdoCbl when AdoCbl·ATR is 1:100 in the presence of 30 mM ATP. ATP is unable to stimulate release of AdoCbl under these conditions (i.e., [ATR] >> [AdoCbl]) when only the high affinity binding site in ATR is occupied by AdoCbl and the low affinity site is vacant. Titrations were performed at 4 °C and recorded after 20 min to allow binding equilibration.

Next, the fidelity of the ATP-dependent AdoCbl release mechanism was assessed in the D180X mutant. The spectrum obtained upon mixing AdoCbl with a 50-fold excess of D180X ATR indicates that at least 85% of the cofactor is bound in the "base-off" conformation (Figure 2.8). The low affinity and equivalence of AdoCbl binding to sites 1 and 2 in D180X ATR results in a statistical distribution of populations with 0, 1, or 2 equiv of AdoCbl bound per ATR trimer. Addition of 5 mM ATP to this sample resulted in full displacement of all bound AdoCbl into solution as evidenced by the appearance of the "base-on" spectrum. The presence of free AdoCbl in solution was confirmed by separation using a Centricon filter.
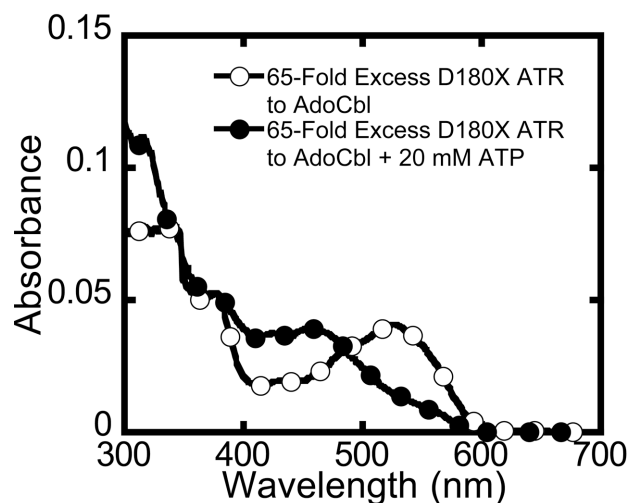
Figure 2.8. **Corruption of the ATP-dependent mechanism for release of a single equivalent of AdoCbl in the D180X mutant.** Mixing AdoCbl with a 65-fold excess of D180X ATR generated the spectrum (filled circles) with 90% bound AdoCbl at 4 °C in buffer B. Because of the equivalence of sites 1 and 2 for AdoCbl binding in D180X ATR, the spectrum represents a statistical distribution of ATR with 0, 1, or 2 equiv of AdoCbl bound at the active site. Addition of 20 mM ATP resulted in the complete displacement of AdoCbl from D180X ATR (open circles). Thus, whereas ATP is only capable of displacing AdoCbl from the low affinity site in wild-type ATR when 2 equiv of AdoCbl are bound, the D180X mutant binds AdoCbl with equal and low affinity at both binding sites and ejects both equivalents of AdoCbl in response to ATP binding.

2.5 Discussion

In this study, we have mimicked the pathogenic Q243X truncation found in human ATR (17) to assess the role of the C-terminal tail in AdoCbl synthesis and transfer to MCM. AdoCbl levels are reduced ~70% in cultured fibroblasts harboring the Q234X deletion, and supplementation with exogenous B_{12} provides only mild stimulation of MCM activity (15). The corresponding *M. extorquens* D180X mutant exhibits lower protein stability (Figure 2.4), and the steady-state kinetic parameters for adenosylation of cob(I)alamin are only modestly impacted (Table 2.1). The steady-state kinetic parameters of the *Lr*PduOΔ*S*183–188 mutant, designed to mimic the Q243X mutation in the human sequence, are similarly mildly affected compared to wild-type ATR. These results suggest that the C-terminus does not play a critical role in synthesis of AdoCbl, at least under *in vitro* conditions (17). However, as indicated by both the

primary sequence alignment and the crystal structure of the *Lr*PduO ATR holoenzyme, residue P176 of *Lr*PduO, and not residue S183, corresponds to Q234 in the human sequence. Hence, the *Lr*PduO-ΔS183–188 sequence represents a shorter C-terminal truncation than that resulting from the human Q234X mutation. Importantly, while the wild-type *Lr*PduO gene can rescue the growth of a ΔCobA strain of *S. enterica* on minimal media, *Lr*PduO-ΔS183–188 is unable to do so. This is consistent with our results on the *M. extorquens* D180X mutant, which reveal that the C-terminal truncation impairs AdoCbl transfer from ATR to MCM rather than AdoCbl synthesis *per se*.

In the structure of the *L. reuteri* ATR, cobalamin is bound in a hydrophobic cavity that is capped by an ordered C-terminal tail (18). Modeling the corresponding Q234X mutation into the*Lr*PduO ATR structure suggests loss of the C-terminal cap of the B_{12} binding site (Figure 2.9). Thus, a predicted outcome of the Q234X mutation is weaker binding of AdoCbl, which is borne out by the significant reduction in the affinity of the D180X mutant for AdoCbl (Table 2).

The C-terminal truncation is also predicted to lead to loss of key hydrogen-bonding interactions with AdoCbl and the mobile loop (Figure 2.10A). In the structure of *Lr*PduO holoenzyme, residues R188, V186, and K184 participate in either direct or water-mediated hydrogen bonds, via backbone amides with the amide substituents of the corrin ring (Figure 2.10) (18). The low C-terminal sequence conservation among the PduO-type ATRs from different organisms is likely due to the use of backbone amides rather than side chains for hydrogen bonding. Additionally, ordering of the C-terminus triggers the formation of hydrogen-bonding contacts between B_{12} and residues I113 and L114 in the mobile loop. Thus, while
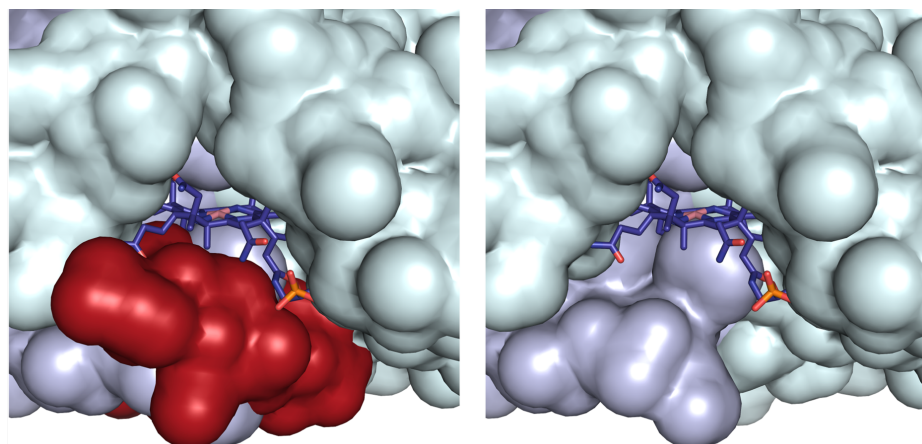
Figure 2.9. Surface representation of the cobalamin binding site in ATR. (A) Cob(II)alamin is shown in stick representation, while adjacent subunits colored as in Figure 2.2 are shown in surface representation. The C-terminal loop residues deleted in the D180X mutant are shown in red in (A) and are deleted in (B). The figure was created using the PDB file 3CI4.

A   B
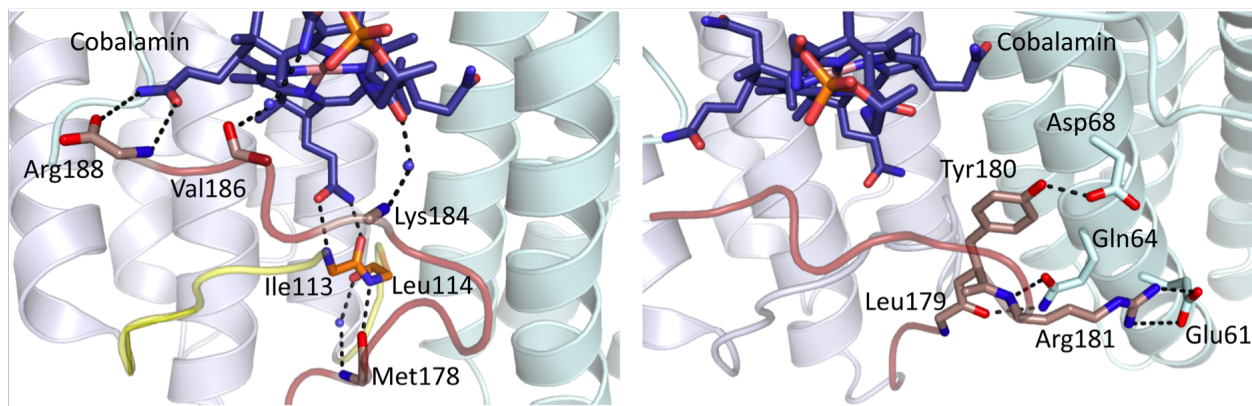
Figure 2.10. Map of interactions between cob(II)alamin and LrPduO ATR. (A) Shown are the intermolecular hydrogen-bonding interactions formed between the peptide backbone of the C-terminus with cobalamin and the peptide backbone of the mobile loop. All side chains have been excluded for clarity. The C-terminal loop missing in the D180X mutant is shown in red, and the backbone of residues M178, K184, V186, and R188 are shown as sticks. The mobile loop is shown in yellow, and the amide backbone of residues I113 and L114 are indicated. Hydrogen bond interactions are depicted as black dashes. (B) Shown are the proposed allosteric contacts between residues of the C-terminus in one subunit and helix 2 residues on the adjacent subunit. The C-terminus and residues L179, Y180, and R181, shown as sticks, are colored red. For clarity, only the amide backbone of L179 is shown. Residues E61, Q64, and D68 of the adjacent subunit are shown as sticks. Cobalamin is colored dark blue and shown in stick representation.

ordering of the C-terminus may contribute to orienting the mobile loop over the lower face of cobalamin, it is not required for generating "base-off" AdoCbl.

It is unclear how the C-terminal truncation leads to loss of allosteric communication between adjacent active sites. The binding of ATP to the vacant site in the wild-type ATR·2AdoCbl product complex triggers ejection of only a single equivalent of AdoCbl, presumably from the low affinity site (Figure 2.7). In D180X ATR, the two binding sites are equivalent, and both display low affinity for AdoCbl. Binding of ATP leads to release of both equivalents of AdoCbl from the trimer (Figures 2.6 and 2.8). Comparison of the apo- and holo-LrPduO crystal structures suggests a possible mechanism for signal transmission between neighboring subunits (16, 18, 19). B_{12}binding induces interactions between the C-terminus of one subunit and helix 2 residues in the adjacent subunit (Figure 2.10B). These interactions include a salt bridge between R181 in the C-terminus and E61 and a hydrogen bond network between the side chains of residues D68 and Q64 and peptide backbone of R181 and L179 and the phenolic oxygen of Y180 in the neighboring C-terminus (18). A two amino acid deletion of helix 2 residues in the human sequence I117-Q118del results in methylmalonic aciduria. Although this deletion mutation has been found in a compound heterozygous state, i.e., the other ATR allele carries a different mutation, it would be of interest to further investigate the importance of this deletion mutation and other helix 2 residues in allosteric communication (14).

In summary, our studies on the *M. extorquens* D180X mutation designed to mimic the patient Q243X mutation provide insights into the functions of ATR not only as an enzyme but also as an escort responsible for conveying AdoCbl to the client enzyme, MCM. The observations of decreased MCM activity and lower AdoCbl levels in the Q234X patient cell lines this study. We propose that the lower AdoCbl levels in patient fibroblasts likely reflect a combination of

instability of the Q234X mutant and weaker affinity for cobalamin. Supplementation of fibroblasts that are homozygous for the Q234X mutation with OHCbl leads to a modest increase in MCM activity and may result from an increased free AdoCbl pool, which facilitates reconstitution of MCM.

References

1.   Banerjee, R., and Ragsdale, S. W. (2003) The many faces of vitamin B_{12}: catalysis by cobalamin-dependent enzymes, *Annu Rev Biochem 72*, 209-247.
2.   Bandarian, V. a. R., G.H (1999) *Ethanolamine ammonia-lyase. In: Banerjee, R. (ed) Chemistry and Biochemistry of B_{12}*, Wiley, New York.
3.   Banerjee, R. a. C., S (1999) *Methylmalonly-CoA mutase. In: Banerjee, R. (ed) Chemistry and Biochemistry of B12*, Wiley, New York.
4.   Mera, P. E., and Escalante-Semerena, J. C. (2010) Multiple roles of ATP:cob(I)alamin adenosyltransferases in the conversion of B12 to coenzyme B_{12}, *Appl Microbiol Biotechnol 88*, 41-48.
5.   Tsang, A. W., and Escalante-Semerena, J. C. (1996) cobB function is required for catabolism of propionate in Salmonella typhimurium LT2: evidence for existence of a substitute function for CobB within the 1,2-propanediol utilization (pdu) operon, *J Bacteriol 178*, 7016-7019.
6.   Suh, S., and Escalante-Semerena, J. C. (1995) Purification and initial characterization of the ATP:corrinoid adenosyltransferase encoded by the cobA gene of Salmonella typhimurium, *J Bacteriol 177*, 921-925.
7.   Dobson, C. M., Wai, T., Leclerc, D., Kadir, H., Narang, M., Lerner-Ellis, J. P., Hudson, T. J., Rosenblatt, D. S., and Gravel, R. A. (2002) Identification of the gene responsible for the *cbl*B complementation group of vitamin B_{12}-dependent methylmalonic aciduria, *Hum Mol Genet 11*, 3361-3369.
8.   Leal, N. A., Park, S. D., Kima, P. E., and Bobik, T. A. (2003) Identification of the human and bovine ATP:Cob(I)alamin adenosyltransferase cDNAs based on complementation of a bacterial mutant, *J Biol Chem 278*, 9227-9234.
9.   Banerjee, R. (2006) B_{12} trafficking in mammals: A for coenzyme escort service, *ACS Chem Biol 1*, 149-159.
10.   Banerjee, R., Gherasim, C., and Padovani, D. (2009) The Tinker, Tailor, Soldier in intracellular B12 Trafficking, *Current Op Chem Biol 13*, 477-484.
11.   Kim, J., Hannibal, L., Gherasim, C., Jacobsen, D. W., and Banerjee, R. (2009) A human vitamin B_{12} trafficking protein uses glutathione transferase activity for processing alkylcobalamins, *J Biol Chem 284*, 33418-33424.
12.   Kim, J., Gherasim, C., and Banerjee, R. (2008) Decyanation of vitamin B12 by a trafficking chaperone, *Proc Natl Acad Sci U S A 105*, 14551-14554.
13.   Padovani, D., Labunska, T., Palfey, B. A., Ballou, D. P., and Banerjee, R. (2008) Adenosyltransferase tailors and delivers coenzyme B_{12}, *Nat Chem Biol 4*, 194-196.
14.   Jorge-Finnigan, A., Aguado, C., Sanchez-Alcudia, R., Abia, D., Richard, E., Merinero, B., Gamez, A., Banerjee, R., Desviat, L. R., Ugarte, M., and Perez, B. (2010) Functional and structural analysis of five mutations identified in methylmalonic aciduria *cbl*B type, *Hum Mutat 31*, 1033-1042.
15.   Lerner-Ellis, J. P., Gradinger, A. B., Watkins, D., Tirone, J. C., Villeneuve, A., Dobson, C. M., Montpetit, A., Lepage, P., Gravel, R. A., and Rosenblatt, D. S. (2006) Mutation and biochemical analysis of patients belonging to the cblB complementation class of vitamin B_{12}-dependent methylmalonic aciduria, *Mol Genet Metab 87*, 219-225.

16.   Mera, P. E., St Maurice, M., Rayment, I., and Escalante-Semerena, J. C. (2007) Structural and functional analyses of the human-type corrinoid adenosyltransferase (PduO) from Lactobacillus reuteri, *Biochemistry 46*, 13829-13836.

17.   Mera, P., St Maurice, M., Rayment, I., and Escalante-Semerena, J. (2009) Residue Phe112 of the Human-type Corrinoid Adenosyltransferase (PduO) Enzyme of Lactobacillus reuteri is Critical to the Formation of the Four-coordinate Co(II) Corrinoid Substrate and to the Activity of the Enzyme, *Biochemistry 48*, 3138-3145.

18.   St Maurice, M., Mera, P., Park, K., Brunold, T. C., Escalante-Semerena, J. C., and Rayment, I. (2008) Structural characterization of a human-type corrinoid adenosyltransferase confirms that coenzyme B_{12} is synthesized through a four-coordinate intermediate, *Biochemistry 47*, 5755-5766.

19.   St Maurice, M., Mera, P. E., Taranto, M. P., Sesma, F., Escalante-Semerena, J. C., and Rayment, I. (2007) Structural characterization of the active site of the PduO-type ATP:Co(I)rrinoid adenosyltransferase from Lactobacillus reuteri, *J Biol Chem 282*, 2596-2605.

20.   Padovani, D., and Banerjee, R. (2009) A Rotary Mechanism for Coenzyme B_{12} Synthesis by Adenosyltransferase, *Biochemistry 48*, 5350-5357.

21.   Padovani, D., and Banerjee, R. (2009) A G-protein editor gates coenzyme B_{12} loading and is corrupted in methylmalonic aciduria, *Proc Natl Acad Sci U S A 106*, 21567-21572.

22.   Stich, T. A., Buan, N. R., Escalante-Semerena, J. C., and Brunold, T. C. (2005) Spectroscopic and computational studies of the ATP:corrinoid adenosyltransferase (CobA) from Salmonella enterica: insights into the mechanism of adenosylcobalamin biosynthesis, *J Am Chem Soc 127*, 8710-8719.

23.   Stich, T. A., Yamanishi, M., Banerjee, R., and Brunold, T. C. (2005) Spectroscopic evidence for the formation of a four-coordinate Co^{2+} cobalamin species upon binding to the human ATP:cobalamin adenosyltransferase, *J Am Chem Soc 127*, 7660-7661.

24.   Mera, P. E., and Escalante-Semerena, J. C. (2010) Dihydroflavin-driven adenosylation of 4-coordinate Co(II) corrinoids: are cobalamin reductases enzymes or electron transfer proteins?, *J Biol Chem 285*, 2911-2917.

25.   Park, K., Mera, P. E., Escalante-Semerena, J. C., and Brunold, T. C. (2008) Kinetic and spectroscopic studies of the ATP:corrinoid adenosyltransferase PduO from Lactobacillus reuteri: substrate specificity and insights into the mechanism of Co(II)corrinoid reduction, *Biochemistry 47*, 9007-9015.

26.   Yamanishi, M., Labunska, T., and Banerjee, R. (2005) Mirror "base-off" conformation of coenzyme B_{12} in human adenosyltransferase and its downstream target, methylmalonyl-CoA mutase, *J Am Chem Soc 127*, 526-527.

27.   Padovani, D., and Banerjee, R. (2009) A rotary mechanism for coenzyme B(12) synthesis by adenosyltransferase, *Biochemistry 48*, 5350-5357.

28.   Schubert, H. L., and Hill, C. P. (2006) Structure of ATP-bound human ATP:cobalamin adenosyltransferase, *Biochemistry 45*, 15188-15196.

29.   Zoldak, G., Zubrik, A., Musatov, A., Stupak, M., and Sedlak, E. (2004) Irreversible thermal denaturation of glucose oxidase from *Aspergillus niger* is the transition to the denatured state with residual structure, *J Biol Chem 279*, 47601-47609.

30.   Padovani, D., Labunska, T., and Banerjee, R. (2006) Energetics of interaction between the G-protein chaperone, MeaB, and B_{12}-dependent methylmalonyl-CoA mutase, *J Biol Chem 281*, 17838-17844.

31. Leal, N. A., Olteanu, H., Banerjee, R., and Bobik, T. A. (2004) Human ATP: Cob(I)alamin adenosyltransferase and its interaction with methionine synthase reductase, *J Biol Chem 279*, 47536-47542.

32. Saridakis, V., Yakunin, A., Xu, X., Anandakumar, P., Pennycooke, M., Gu, J., Cheung, F., Lew, J. M., Sanishvili, R., Joachimiak, A., Arrowsmith, C. H., Christendat, D., and Edwards, A. M. (2004) The structural basis for methylmalonic aciduria. The crystal structure of archaeal ATP:cobalamin adenosyltransferase, *J Biol Chem 279*, 23646-23653.

33. Johnson, C. L., Buszko, M. L., and Bobik, T. A. (2004) Purification and initial characterization of the Salmonella enterica PduO ATP:Cob(I)alamin adenosyltransferase, *J Bacteriol 186*, 7881-7887.

CHAPTER 3

A Switch III Motif Relays Signaling between a B$_{12}$ Enzyme and its G-protein Chaperone[5,6]

3.1 Abstract

Fidelity during cofactor assembly is essential for the proper functioning of metalloenzymes and is ensured by specific chaperones. MeaB, a G-protein chaperone for the coenzyme B$_{12}$-dependent radical enzyme, methylmalonyl-CoA mutase (MCM), utilizes the energy of GTP binding and/or hydrolysis to regulate cofactor loading into MCM, protect MCM from inactivation, and rescue MCM inactivated during turnover. Typically, G-proteins signal to client proteins using the conformationally mobile switch I and II loops. Crystallographic snapshots of MeaB reported herein reveal a novel switch III element, which exhibits substantial conformational plasticity. Using alanine-scanning mutagenesis, we demonstrate that the switch III motif is critical for bidirectional signal transmission of the GTPase activating protein activity of MCM and the chaperone functions of MeaB in the MeaB:MCM complex. Mutations in the switch III loop

identified in patients corrupt this inter-protein communication and lead to methylmalonic aciduria, an inborn error of metabolism.

3.2 Introduction

Metallochaperones control the specificity of metal insertion into active sites that harbor mononuclear sites, metalloclusters or organometallic cofactors *(1-3)*. The bacterial protein MeaB *(4)* and its human ortholog CblA *(5)* are chaperones that regulate docking of coenzyme B_{12} (5´-deoxyadenosylcobalamin or AdoCbl) into the radical enzyme methylmalonyl-CoA mutase (MCM) *(6,7)*. MCM uses AdoCbl to catalyze the chemically challenging 1,2-rearrangement of (*R*)-methylmalonyl-CoA to succinyl-CoA *(8)*. Mutations in MCM or in MMAA result in methylmalonic aciduria, an inborn error of metabolism *(5, 9)*.

MeaB belongs to the G3E family of G-proteins that include other metallochaperones needed for insertion of nickel into varied client proteins[10]. It forms a tight complex with MCM with affinity that is modulated by the ligand bound to each protein and that varies from 34-524 nM *(11)*. MeaB binds guanosine 5´-triphosphate (GTP) and guanosine 5´-diphosphate (GDP) with almost equal affinity, and its low intrinsic GTPase activity is enhanced ~100-fold in the presence of MCM, which exhibits GTPase activating protein (GAP) activity *(11)*. MeaB in turn, orchestrates a complex series of actions powered by the energy of GTP binding or hydrolysis *(6)*. These functions include: (i) gating the transfer of AdoCbl from adenosyltransferase (ATR) to MCM while excluding the inactive precursor, cob(II)alamin, (ii) protecting MCM from oxidative inactivation during turnover, and (iii) reactivating via cofactor exchange, MCM that is inactivated during the catalytic cycle *(6, 12)*. Chaperones with roles limited to reactivation have been described for methycobalamin-dependent methyltransferases and the AdoCbl-dependent

subfamily of eliminases *(13-18)*. These chaperones either promote an adenosine 5´-triphosphate (ATP)-dependent exchange of inactive cobalamin for AdoCbl *(16-19)* or reduction of cob(II)alamin to cob(I)alamin during in situ repair of the cofactor on methyltransferases *(13, 20)*. Insights into the mechanism by which complex bidirectional communication occurs between the active sites of MeaB and MCM have been lacking.

Classically, small G-proteins involved in signal transduction communicate via conformational changes in conserved switch I and II regions in response to nucleotide binding, exchange and/or hydrolysis *(21)*. MeaB is a homodimer and each subunit contains a central α/β G-domain core (Fig. 3.1a, light gray), a helical C-terminal extension (dark gray) contributing to the dimer interface and an N terminal extension *(22)* (medium gray). MeaB was previously crystallized in a nucleotide-free form (PDB ID: 2QM8; MeaB:2Pi) and in the presence of GDP (PDB ID: 2QM7; MeaB:2GDP)[22]. The location of the conformationally flexible switch I (residues 92-108) and II (residues 154-162) regions in MeaB used by G proteins for signal transmission via the canonical "spring-loaded" mechanism *(23)*, had raised questions about how structural transitions accompanying nucleotide binding and GTP hydrolysis are communicated from MeaB to MCM *(22)*. The presence of phosphate in the crystallization conditions used to obtain the nucleotide-free structure had resulted in ordering of both P loops (residues 62-70) in the dimer. A comparison of MeaB structures has led us to identify switch III, a third mobile loop whose proximity to the GTPase active site and to the conserved switch II region, suggested the hypothesis that this structural element is utilized for nucleotide-responsive communication between the MeaB and the MCM active sites. Herein, we report the structures of apo- and 5´-guanylyl-β,γ-imidophosphate (GMPPNP)-bound MeaB and demonstrate using alanine scanning mutagenesis, the pleiotropic consequences of alterations to the switch III sequence. Our study

identifies switch III as a critical structural element for bidirectional signaling between MeaB and MCM that is compromised by disease-causing mutations in the switch III loop identified in methylmalonic aciduria patients.

3.3 Results

3.3.1 Structure of Apo-MeaB and of MeaB•2GMPPNP

We report two new crystal structures of apo-MeaB in the absence of phosphate or sulfate and in the presence of the non-hydrolyzable GTP analogue, GMPPNP (Table 3.1). The structure of apo-MeaB, unlike the earlier structures *(22)*, comprises two dimers instead of a single dimer in the asymmetric unit (Figure 3.2). Although the overall basic dimeric unit is very similar to the ones reported previously (Fig. 3.1a), there are discrete differences that are localized to the active site and the switch regions (Figs. 3.1a, 3.2, 3.3). In one apo-MeaB dimer, the active sites are empty and the P-loops have conformations distinct from the reported MeaB structures. Thus, in the absence of nucleotides or phosphates, the P-loop rearranges and part of it forms an extra helical turn at the base of helix α4, increasing the number of turns from four to five (Fig. 3.2). This conformation is not conducive to substrate binding since the groove required for phosphate binding is not present. In the second dimer, there is a single GDP bound in one active site while the second active site is phosphate- and nucleotide-free with the P-loop in a conformation permissive for nucleotide binding (Fig. 3.2). We typically isolate "apo-MeaB" with 0.04 equivalents of bound GDP, which presumably represents nucleotide that remains associated with the protein during purification from cell extracts.

The MeaB•2GMPPNP structure exhibits an overall arrangement comparable to that of the other MeaB structures (Fig. 3.1a, Fig. 3.3). The overall conformation of the two monomers in each dimer is very similar. Although Mg^{2+} is required for the low intrinsic GTPase activity of

MeaB (Fig. 3.4), it is not observed in any of the structures presumably because its binding site is not fully formed in the absence of MCM.

The MeaB•2GMPPNP structure exhibits an overall arrangement comparable to that of the other MeaB structures (Fig. 3.1a, Fig. 3.3). The overall conformation of the two monomers in each dimer is very similar. Although Mg^{2+} is required for the low intrinsic GTPase activity of MeaB (Fig. 3.4), it is not observed in any of the structures presumably because its binding site is not fully formed in the absence of MCM. The differences between the two monomers are primarily observed in the nucleotide-binding site and in the position of a loop (residues 177-188) referred to hereafter as Switch III (Fig 3.1a, right panel).

There is clear electron density for GMPPNP in one of the monomers and residues K68, S69 and R108 contact the β- and γ-phosphates (Fig. 3.1b, chain A). In the second monomer (chain B), GMPPNP is bound in a different conformation in which the γ-phosphate, which exhibits only partial occupancy, is re-positioned and oriented away from the active site (Fig. 3.1b). It is more solvent exposed and interacts only with S69 (Fig. 3.1b). In fact, the hydroxyl group of S69 in chain B is rotated by almost 180° and reoriented to interact directly with the oxygen atoms of the α- and γ-phosphate groups and with the bridging N atom. Similarly, the ε-amino group of K68 is rotated by ~180° with respect to its position in chain A and forms an ionic interaction with E154, which in turn forms a salt bridge with R108. Comparison of the structures of MeaB with other G-proteins such as HypB *(24)*, suggest that residues E154 and D105 serve as Mg^{2+} ligands. Thus, E154 is likely to disengage from R108 to bind to Mg^{2+} in the activated MeaB:MCM complex.
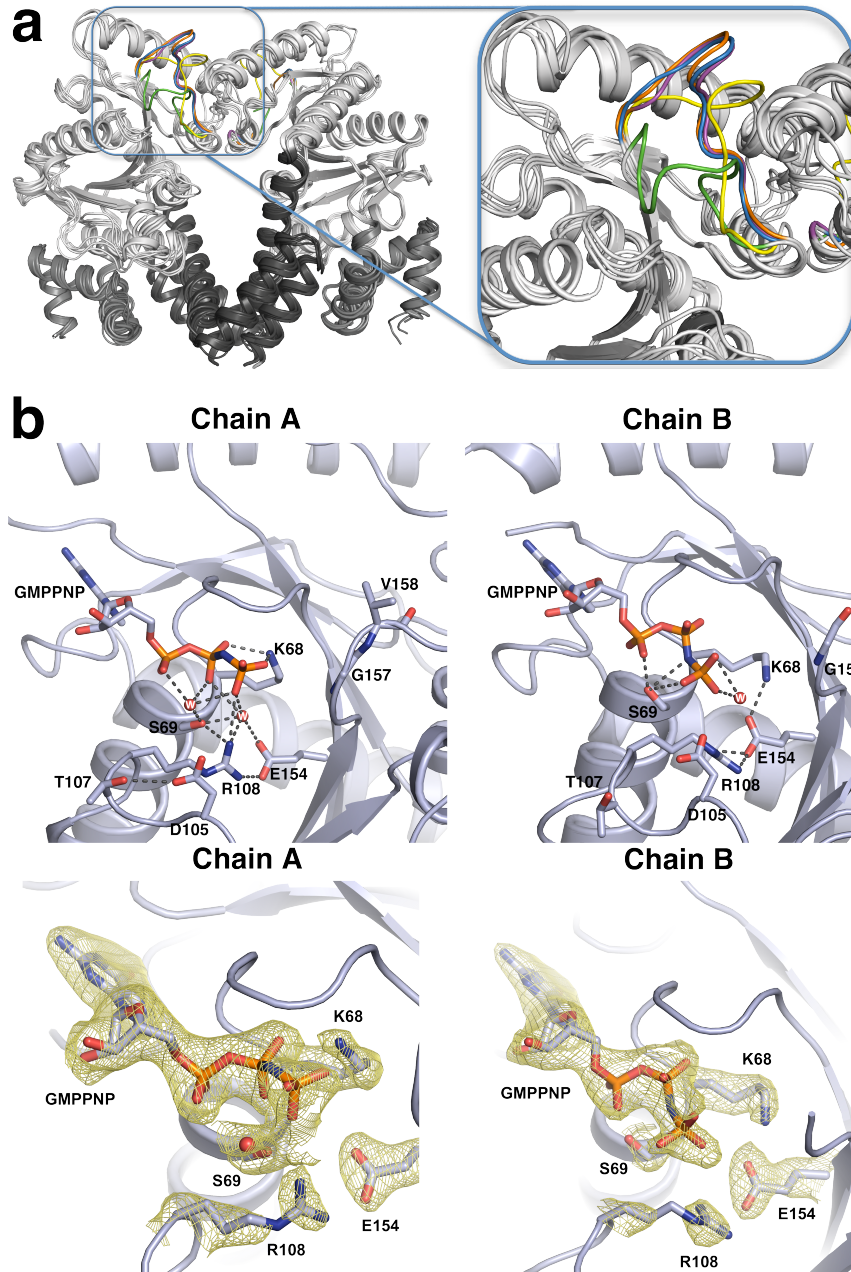
Figure 3.1. Crystal structure of MeaB reveals a mobile switch III loop. (**a**) Comparison of MeaB crystal structures (gray) and the mobile Switch III regions (various colors). Apo-MeaB (green), MeaB•2GMPPNP (blue), MeaB•2GDP (yellow), MeaB•1GDP (mangenta), MeaB•2Pi (orange). (**b**) Close-up of the two active sites (designated as chains A and B) in the MeaB•2GMPPNP structure showing interactions between active site residues and the nucleotide (top) and composite omit electron density of the two GMPPNP ligands in the active site contoured at 1σ (bottom). The GMPPNP ligands as well as active site residues K68, S69, R108 and E154 are shown in sticks.

	Apo-MeaB[1]	MeaB:2GMPPNP[2]
Data Collection		
Space group	*C*2	*C*2
Cell dimensions		
a, *b*, *c* (Å)	185.5, 58.4, 155.3	185.6, 58.2, 76.4
a, b, g (°)	90, 110.1, 90	90, 106.3, 90
Resolution (Å)	50-2.20 (2.33-2.20)	50-2.10 (2.15-2.10)
R_{sym} or R_{merge}	8.6 (50.6)	6.5 (33.6)
I / s*I*	11.8 (3.2)	14.3 (4.3)
Completeness (%)	96.9 (93.4)	99.1 (98.1)
Redundancy	6.6 (6.6)	4.1 (4.1)
Refinement		
Resolution (Å)	48.6-2.2	44.5-2.1
No. reflections	77430	43385
R_{work} / R_{free}	0.197 / 0.252	0.199 / 0.242
No. atoms		
Protein	9399	4751
Ligands	28	64
Water	403	302
B-factors		
Protein	40.7	42.6
Ligands	35.0	53.8
Water	39.4	45.8
R.m.s. deviations		
Bond lengths (Å)	0.011	0.011
Bond angles (°)	1.393	1.388

Table 3.1. Data collection and refinement statistics (molecular replacement) for apo-MeaB and MeaB:2GMPPNP. [1]Apo-MeaB (PDB ID 4JYC) has two unique dimers in the asymmetric unit; one has no ligands in the active site and the other dimer has one GDP bound to one of the two active sites. [2]This structure (PDB ID 4JYB) refers to the dimer of MeaB containing two equivalents of GMPPNP.
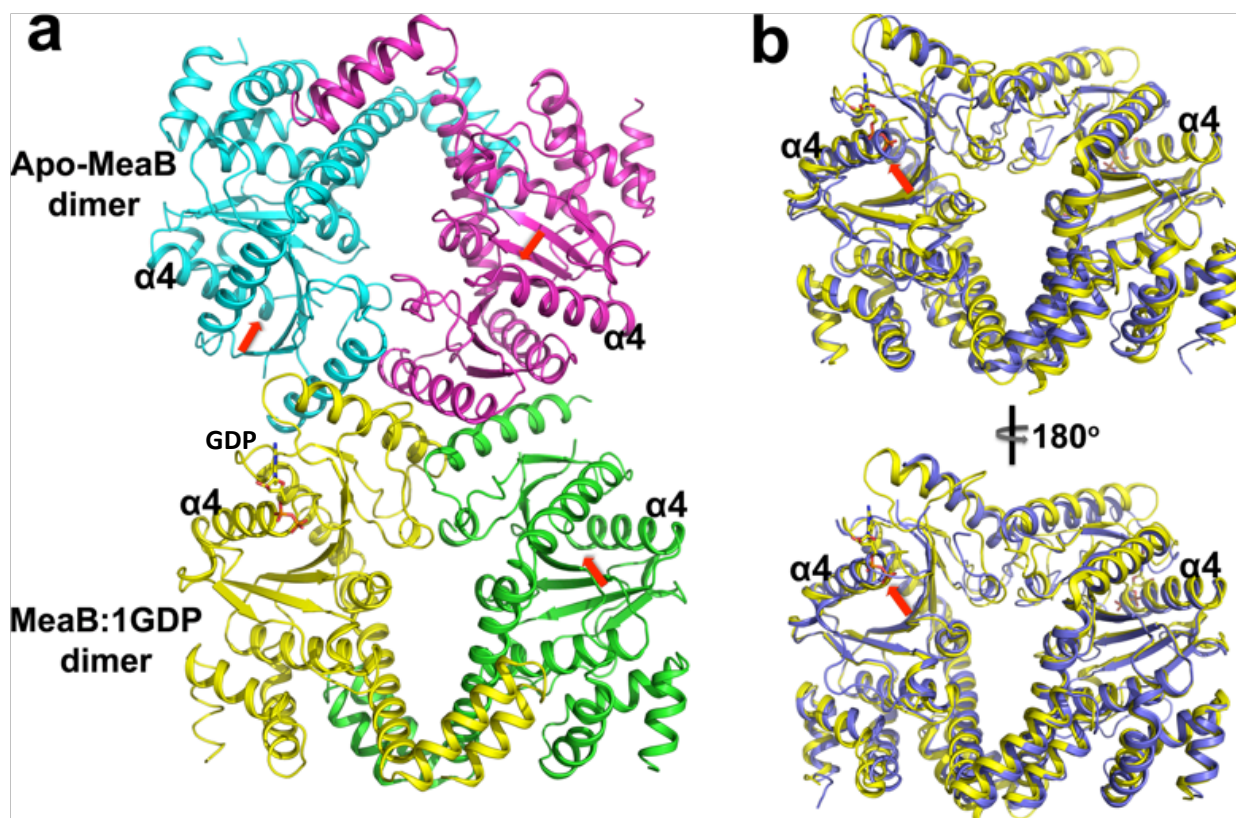
Figure 3.2. Structure of Apo-MeaB. (**a**). MeaB in its apo form crystallized as a dimer of dimers. One of the dimers (apo-MeaB; cyan and magenta) has no ligands (i.e. nucleotides or phosphates) in the active site, whereas the other has one GDP molecule in one of the active sites (MeaB:1GDP, yellow and green). (**b**) Superposition of the apo-MeaB dimer (blue) with the MeaB:2GDP dimer (yellow). Both faces of the dimer, related by 180° rotation are shown. The area of the P-loop that reorders into a helical turn in the absence of substrate is highlighted with a red arrow.

The available MeaB structures have fairly similar dimeric arrangements and overall conformations as evidenced by their small comparative rmsd values (Table 3.2). The main differences are evident in the P-loop, switch-I and -II regions, and most significantly, in the switch III region. The switch III loop is found in one of three conformations or is disordered. We postulate that switch III exists in an ensemble of conformations and that the equilibrium between these conformations is influenced by the nucleotide bound in the active site in the MCM:MeaB

56

complex. The substantial conformational flexibility of the switch III region prompted us to test its potential role in signaling.
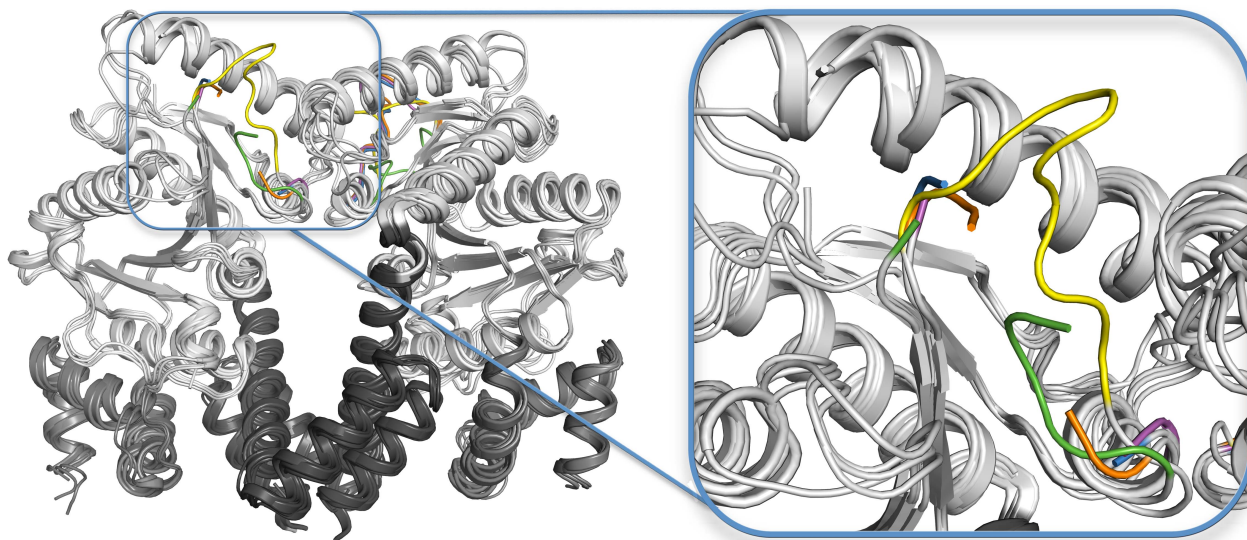
Figure 3.3. Comparison of MeaB crystal structures. Structures are shown in gray with the mobile Switch III regions shown in color as in Fig 1a but rotated by 180° so as to reveal the opposite face of the MeaB dimers. Apo-MeaB (green), MeaB:2GMPPNP (blue), MeaB:2GDP (yellow), MeaB:1GDP (magenta), MeaB:2Pi (orange). The Switch III region is disordered in all of these MeaB monomers with the exception of the MeaB:2GDP structure.
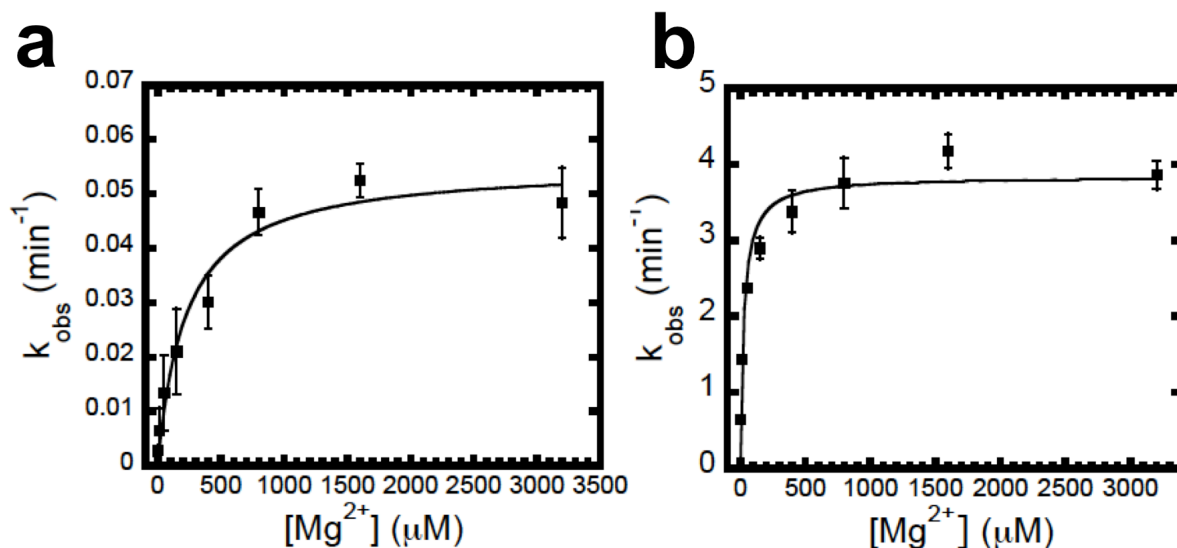
Figure 3.4. Mg^{2+} ion concentration dependence of GTP hydrolysis by MeaB. GTP hydrolysis in the (**a**) absence and (**b**) presence of MCM. The data represent the average ±S.D. of at least 3 independent experiments.

Rmsds (Å) **	MeaB no ligands	MeaB:1GDP	MeaB:2Pi	MeaB:2GDP	MeaB:2GMPPNP
MeaB no ligands		0.57	0.79	1.10	0.7
MeaB:1GDP	0.57		0.59	0.91	0.57
MeaB:2Pi	0.79	0.59		0.76	0.50
MeaB:2GDP	1.10	0.91	0.76		0.51
MeaB:2GMPPNP	0.70	0.57	0.50	0.51	

Table 3.2. Comparative Rmsd values for MeaB dimers*. *MeaB:2Pi; PDB ID 2QM8. MeaB:2GDP; PDB ID 2QM7. MeaB:2GMPPNP; PDB ID 4JYB. Apo-MeaB (PDB ID 4JYC) has two unique dimers in the asymmetric unit; one has no ligands in the active site and is designated MeaB no ligands, and the other dimer has only one GDP bound to one of the two active sites and is designated MeaB:1GDP. **based on Cα atoms

3.3.2 Alanine Substitution Mutagenesis of Switch III Loop

The following switch III residues conserved in MeaB-like proteins (Fig. 3.5) were targeted for substitution with alanine: D182, E183, Q185, and K188. The resulting mutant proteins retained the ability to form high affinity complexes with apo-MCM yielding K_D values ranging from 61 ± 9 to 117 ± 17 nM in the absence and from 30 ± 13 to 65 ± 14 nM in the presence of GMPPNP and exhibited similar thermodynamic parameters as wild-type MeaB (Table 3.3). The affinity of the two MeaB active sites for nucleotide is unequal (Table 3.4). The K_{DS} for GMPPNP in the mutants were comparable to that of wild-type MeaB indicating that the mutations in switch III do not significantly impact binding of GMPPNP, particularly at site 1. The K_{DS} for GDP binding to the mutant MeaBs were also comparable to the wild-type protein within a 2- to 3-fold range (Table 3.4) as were the nucleotide affinities in the MeaB•apo-MCM complex, which were within a 5-8-fold range (Table 3.5). Interestingly, the stoichiometry of nucleotide binding to MeaB changes from two in the absence to one in the presence of MCM indicating half of sites

activity of MeaB in the complex. Collectively, these results establish that the switch III mutations

do not significantly perturb binding of nucleotides to MeaB or formation of the complex between

MeaB and apo-MCM.
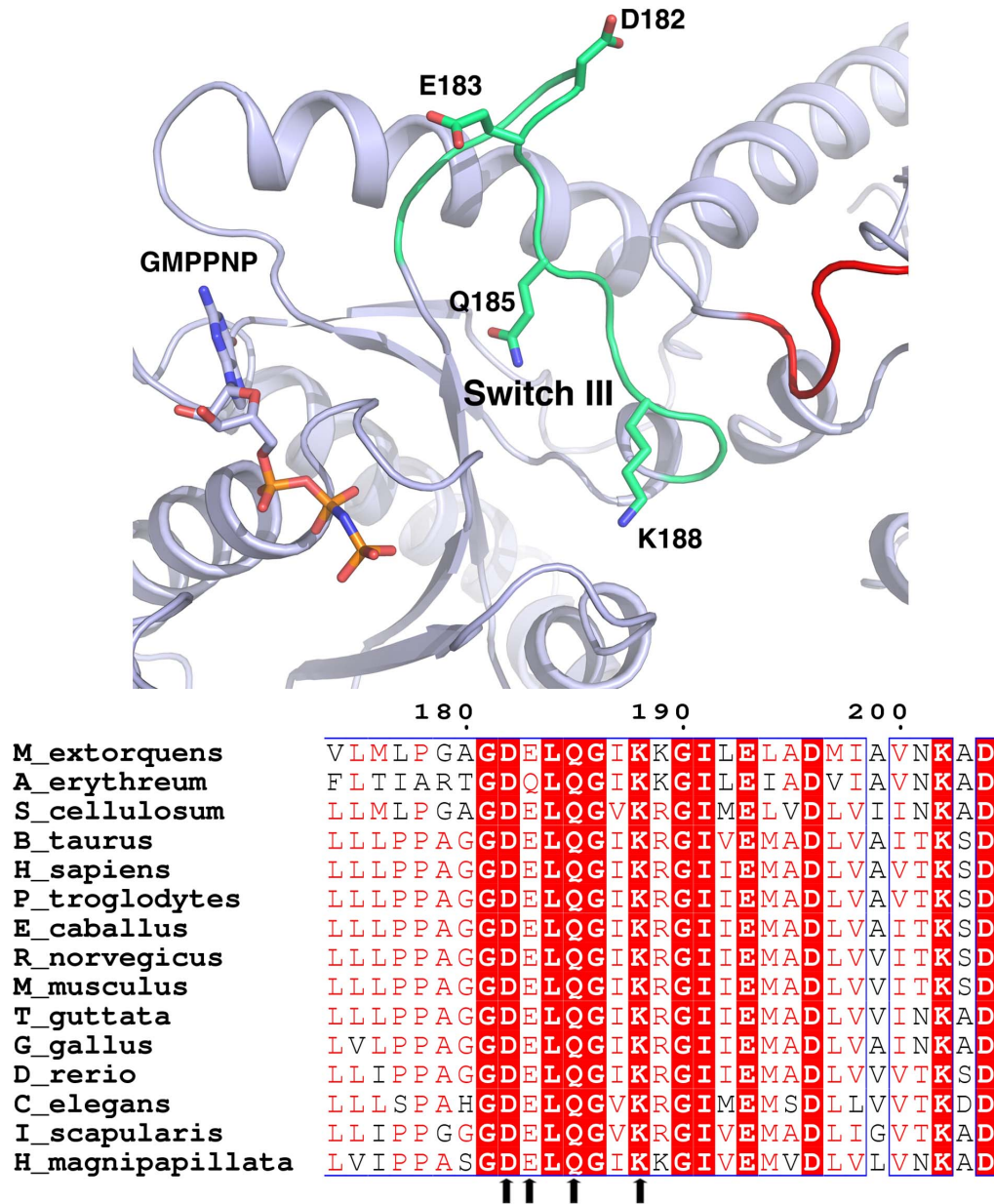
Figure 3.5. Conservation of Switch III loop residues. Conformation of a switch III loop in the MeaB:2GMPPNP structure (top) and sequence alignment of the switch III sequences of MeaB and its orthologs (bottom). Invariant residues investigated in this study are highlighted with red arrows and mapped in the structure with sticks.

	GMPPNP	K_D (nM)	ΔH^o (kcal/mol)	$T\Delta S^o$ (kcal/mol)	ΔG^o (kcal/mol)
Wild-type	-	88 ± 16	-31.3 ± 1.0	-21.8 ± 1.4	-9.5 ± 1.4
	+[1]	155 ± 24	-24.1 ± 0.5	-15.0 ± 0.8	-9.2 ± 0.3
D182A	-	113 ± 19	-26.3 ± 0.9	-17.0 ± 0.4	-9.3 ± 1.0
	+	53 ± 11	-23.3 ± 0.6	-14.4 ± 0.9	-8.9 ± 0.8
E183A	-	61 ± 9	-33.8 ± 1.6	-24.0 ± 0.4	-9.8 ± 0.8
	+	65 ± 14	-26.6 ± 0.4	-16.9 ± 0.8	-9.7 ± 0.3
Q185A	-	117 ± 17	-27.9 ± 0.3	-19.1 ± 0.7	-8.8 ± 0.6
	+	30 ± 14	-32.4 ± 0.2	-21.9 ± 1.1	-10.5 ± 0.5
K188A	-	67 ± 9	-29.9 ± 0.7	-19.9 ± 1.5	-10.0 ± 1.1
	+	30 ± 13	-24.4 ± 0.8	-13.9 ± 1.4	-10.5 ± 0.9
G186S	-	568 ± 49	-32.4 ± 0.9	-24.5 ± 0.7	-7.9 ± 0.2
	+	58 ± 20	-22.8 ± 1.3	-11.1 ± 0.6	-11.7 ± 0.7
K188E	-	73 ± 33	-23.7 ± 1.2	-13.1 ± 1.1	-10.6 ± 1.4
	+	38 ± 13	-30.2 ± 2.5	-19.0 ± 2.1	-11.2 ± 0.4

Table 3.3 Thermodynamic parameters for the binding of apo-MCM to switch III mutants of MeaB. These experiments were performed as described under Materials and Methods and the values represent the mean of at least three experiments ± S.D. [1]These values are from Ref 8.

	nucleotide	K_D (µM) site 1	site 2
Wild-type	GDP	0.8 ± 0.5	9.5 ± 1.9
	GMPPNP	0.6 ± 0.2	9.3 ± 1.6
D182A	GDP	0.6 ± 0.3	6.9 ± 0.4
	GMPPNP	0.3 ± 0.1	4.2 ± 1.1
E183A	GDP	1.3 ± 0.2	9.9 ± 0.6
	GMPPNP	0.2 ± 0.1	1.3 ± 0.4
Q185A	GDP	2.6 ± 0.5	21.2 ± 4.3
	GMPPNP	0.3 ± 0.1	3.5 ± 0.9
K188A	GDP	1.4 ± 0.4	27.5 ± 2.6
	GMPPNP	0.6 ± 0.1	11.8 ± 0.6
G186S	GDP	0.6 ± 0.3	13.8 ± 0.8
	GMPPNP	0.7 ± 0.4	7.1 ± 0.3
K188E	GDP	0.9 ± 0.4	10.7 ± 2.1
	GMPPNP	0.8 ± 0.4	11.2 ± 2.3

Table 3.4 Comparison of nucleotide affinities between wild-type MeaB and switch III mutants. These experiments were performed as described under Methods and represent the mean of at least three experiments ± S.D.

	K_D (µM)	
	GMPPNP	**GDP**
Wild-type	0.11 ± 0.01	0.20 ± 0.01
D182A	0.09 ± 0.06	0.32 ± 0.03
E183A	0.16 ± 0.06	0.87 ± 0.19
Q185A	0.54 ± 0.24	1.74 ± 0.61
K188A	0.33 ± 0.09	0.92 ± 0.33
G186S	0.60 ± 0.14	0.20 ± 0.03
K188E	0.13 ± 0.02	0.47 ± 0.06

Table 3.5. **Nucleotide binding affinities in the MCM:MeaB complex.** These experiments were performed as described under Methods and represent the mean of at least three experiments ± S.D.

3.3.3 GAP function of MCM is Impaired in Switch III Mutants.

The intrinsic GTPase activity of the switch III mutants is low (k_{obs} = 0.039 to 0.043 min^{-1}) and comparable to that of wild-type MeaB (Table 3.6). When MCM binds MeaB, the GTPase activity of Meab is increased by 100-fold. The GAP function of MCM is suppressed 10- to 25-fold by mutants, and the Q185A and K188A mutations show the largest impairment. The presence of AdoCbl had no effect on the GAP activity of MCM (data not shown). Mg^{2+} is not required for nucleotide binding and in its absence MeaB binds GDP (K_D = 1.4 ± 0.1 µM and 7.9 ± 2.1 µM for sites 1 and 2) and GMPPNP (0.9 ± 0.2 µM and 6.7 ± 1.7 µM for sites 1 and 2) well, albeit with slightly lower affinity. The K_{act} for Mg^{2+} in the GTPase assay decreases from 225 ± 22 µM in the absence to 27 ± 8 µM in the presence of MCM (Fig. 3.4b). The 10-fold decrease in the K_{act} for Mg^{2+} in the presence of MCM is consistent with the organization of a higher affinity

binding-site in the complex versus in MeaB alone. We speculate that the occurrence of an incomplete active site in MeaB alone is a strategy for suppressing its intrinsic GTPase activity, which is activated in the MCM:MeaB complex. Collectively, these results indicate that the switch III loop is important for transmitting the GAP function of MCM to MeaB, which is expressed in part by promoting high-affinity binding of Mg^{2+}.

	k_{cat} (min^{-1})	
Enzyme	- MCM	+ MCM
Wild-type	0.039 ± 0.003	4.20 ± 0.21
D182A	0.042 ± 0.004	0.50 ± 0.05
E183A	0.040 ± 0.005	0.30 ± 0.04
Q185A	0.043 ± 0.004	0.17 ± 0.03
K188A	0.039 ± 0.001	0.14 ± 0.02
G186S	0.050 ± 0.006	0.21 ± 0.03
K188E	0.047 ± 0.004	0.28 ± 0.02

Table 3.6 Kinetic Parameters for GTP hydrolysis by switch III mutants of MeaB. These experiments were performed as described under Methods and represent the mean of at least three experiments $\pm$ S.D.

3.3.4 AdoCbl Loading into MCM is Impaired in Switch III Mutants.

ATR catalyzes the transfer of the 5´-deoxyadenosyl group of ATP to cob(I)alamin to form the active cofactor, AdoCbl. However, in addition to functioning as an enzyme in the cobalamin assimilation pathway, ATR also functions as an escort, transferring AdoCbl directly to the MCM:MeaB complex in a process that is gated by GTP hydrolysis by MeaB *(6,25-27)* and driven by binding of ATP to ATR *(26)* (Fig. 3.6a). ATP binding triggers either the transfer of one of the two bound equivalents of AdoCbl from ATR to the wild-type MCM:MeaB complex in the presence of GTP or the release of AdoCbl into solution in the presence of the non-hydrolyzable analog, GMPPNP *(26)* (Fig. 3.6b, *inset*).
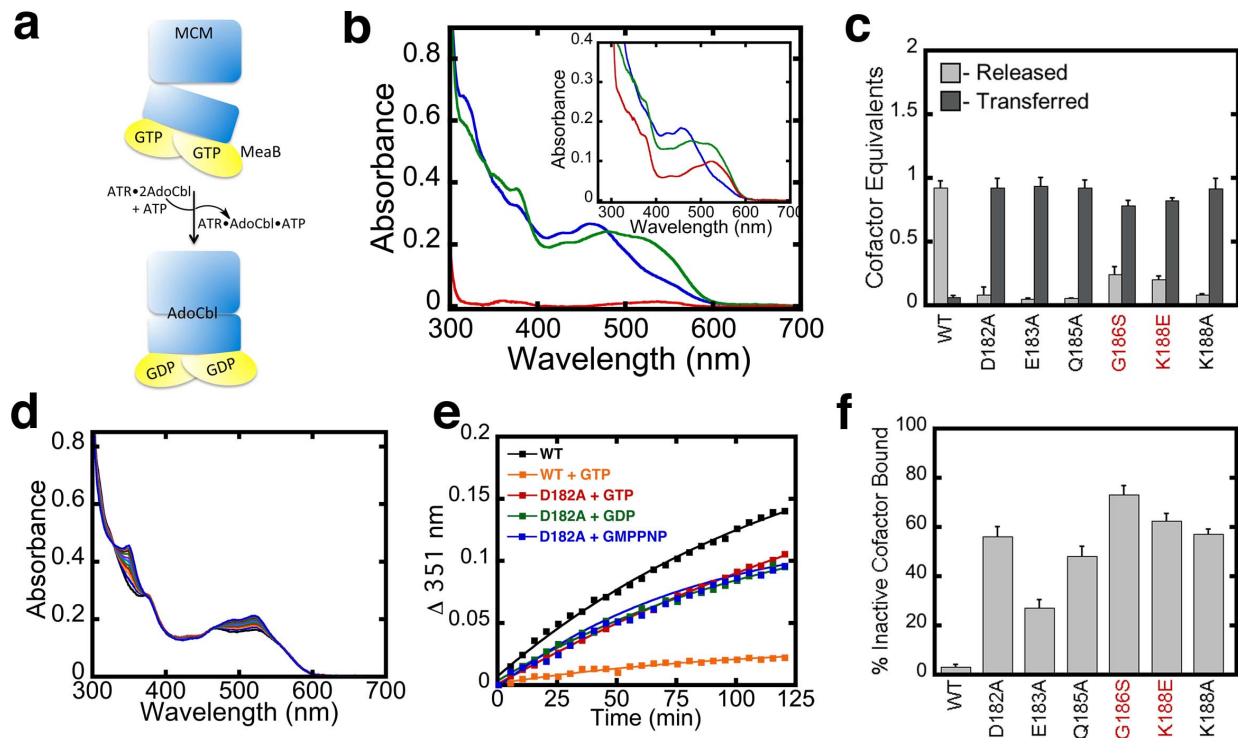
Figure 3.6. The pleiotropic effects of switch III mutations. (**a**) Model for AdoCbl transfer from ATR to MCM:MeaB gated by GTP hydrolysis and triggered by ATP binding to ATR. (**b**) Representative spectra showing changes associated with the transfer of one of two equivalents of AdoCbl from ATR (blue) to MCM in the MCM:mutant MeaB•2GMPPNP complex (green) upon addition of ATP. Very little cofactor is released into solution (red). The *inset* shows the corresponding spectra in the presence of wild-type MeaB and GMPPNP in which one equivalent of AdoCbl is lost from ATR (blue) to solution (green) following addition of ATP. The red spectrum represents free AdoCbl recovered after filtration. (**c**) Comparison of AdoCbl equivalents transferred to MCM versus released into solution from ATR in the presence of switch III mutants of MeaB containing bound GMPPNP. (**d**) Spectroscopic changes accompanying oxidative inactivation of MCM during turnover under aerobic conditions. The increase in absorbance at 351 nm corresponds to oxidation of the cob(II)alamin formed during catalytic turnover of MCM, to H_2OCbl. (**e**) Comparison of the inactivation time course for MCM in the presence of wild-type versus the D182A MeaB with GTP, GMPPNP or GDP. Inactivation was monitored at 351 nm. (**f**) Comparison of inactive cobalamin that remains bound to MCM in the presence of wild-type and mutant MeaBs with bound GMPPNP. The mutations in MeaB that are equivalent to pathogenic switch III mutations in CblA are shown in red in c and f and the data represent the mean ± SD of ≥3 (c) and ≥2 (f) independent experiments as described under Methods.

Mutations in the switch III region of MeaB corrupt GTPase-gated inter-protein cofactor transfer (Fig. 3.6b-c). Hence, in the presence of ATP, ~1 equivalent of AdoCbl is transferred

from the ATR to the MCM active site in the presence of GMPPNP rather than being released into solution as seen with wild-type MeaB (Fig. 3.6c). These results demonstrate that mutations in switch III uncouple the dependence of AdoCbl transfer from ATR to MCM on GTP hydrolysis in MeaB. Hence, mutations in switch III corrupt the GTPase-dependent gating mechanism used by wild-type MeaB *(6)*.

3.4.5 Switch III Mutants Affect MCM Turnover and Repair.

Multiple cycles of catalytic turnover in MCM requires (i) the deployment of a highly reactive, enzyme-bound radical adenosine group that facilitates substrate isoerization and (ii) geminal recombination between cob(II)alamin and the radical adenosine group *(8)*. Inadvertent dissociation of adenosine from the MCM active site during turnover strands a reactive cob(II)alamin in the MCM active site. Under aerobic conditions, enzyme-boudn cob(II)alamin undergoes oxidation to H_2OCbl and results in the terminal inactivation of MCM *(12)*. It was previously shown that loss of the 5′-deoxyadenosine moiety from the active site, which precludes reformation of AdoCbl at the end of the catalytic cycle, is "sensed" by MeaB and triggers cofactor ejection in a process that utilizes the binding energy of GTP *(6)*. Inactivation of MCM during enzyme-monitored turnover can be followed spectrophotometrically by formation of aquocobalamin (H_2OCbl, 351 nm) (Fig. 3.6d-e). Under steady-state turnover conditions, H_2OCbl forms at a rate of 9.5×10^{-3} min^{-1} in the MCM:MeaB complex in the absence of nucleotides. The presence of GTP decreases cob(II)alamin oxidation ~30-fold ($k_{obs} = 3.0 \times 10^{-4}$ min^{-1}). Although the switch III mutant E183A protects MCM from oxidation to a similar degree as wild-type MeaB (data not shown), the K188A ($k_{obs} = 0.9 \times 10^{-4}$ min^{-1}) and Q185A ($k_{obs} = 1.7 \times 10^{-4}$ min^{-1}) mutants offer less protection. By comparison to wild-type MeaB, the protective capacity of the D182A mutant is substantially less. The k_{obs} for oxidative inactivation of MCM in the presence of

64

D182A MeaB and GTP, GMPPNP or GDP are 8.9, 8.4, and 8.2 x 10^{-3} min^{-1}, respectively, and corresponds to an ~30-fold increase compared to wild-type MeaB (Fig. 3.6e).

If the adenosine group is lost from the MCM active site, MeaB facilitates the ejection of cob(II)alamin from the MCM active site (6). To assess the role of the switch III loop in rescue of MCM, cob(II)alamin was mixed with an excess of apo-MCM in complex with the MeaB mutants followed by addition of GMPPNP. The amount of free (i.e. released) cob(II)alamin obtained in the filtrate following centrifugation was then estimated. In the presence of D182A, Q185A, or K188A variants, ~50-60% of cob(II)alamin remained bound to MCM whereas only ~30% of the cofactor was associated with MCM in the presence of the E183A MeaB mutant (Fig. 3.6f). In contrast, ~3% of cob(II)alamin was bound to MCM in the presence of wild-type MeaB. Hence the efficacy of cofactor expulsion is reduced 16-20-fold in three of the switch III mutants and 10-fold in the E183 mutant.

3.3.6 Mutations in Switch III Lead to Methylmalonic Aciduria.

Mutations in the switch III motif of MeaB, designed to mimic disease associated switch III mutations in CblA, impair bidirectional signaling in the MCM:MeaB complex. Switch III mutations, G274S and K276E, in human CblA have been reported recently in patients with methylmalonic aciduria (7). The intrinsic GTPase activity and affinity for nucleotides or for MCM are largely unaffected in the corresponding MeaB mutants (G186S and K188E) as also seen with the corresponding alanine mutations in the switch III region (Tables 3.3-3.6). The pleiotropic biochemical penalties associated with the patient mutations mimicked in MeaB are virtually identical to the set of alanine mutants described above. Thus, the two patient mutations: (i) diminish the GAP activity of MCM (Table 3.6), (ii) uncouple AdoCbl transfer from ATR from the GTPase activity of MeaB in the MCM:MeaB complex (Fig. 3.6c), and (iii) inhibit release of

inactive cofactor from MCM (Fig. 3.6f). In the presence of GMPPNP and either K188E or G186S MeaB, MCM undergoes oxidative inactivation at rates of 4.1×10^{-4} min^{-1} and 2.5×10^{-4} min^{-1}, respectively. These values compare closely to the wild-type and K188A variants of MeaB, indicating a comparable level of protection against inactivation of MCM during catalytic turnover. These results establish the biological import of the switch III loop in the function of MeaB and by inference, MMAA.

3.5 Discussion

In this study, we have demonstrated that mutations of the conserved polar residues in the switch III region in MeaB impact several aspects of bidirectional signaling ranging from uncoupling AdoCbl transfer from GTP hydrolysis, to protection against inactivation of MCM, to rescue of inactivated MCM, to GAP signaling from MCM to MeaB (Figs. 3b-f and Table 1). Importantly, switch III mutations do not substantially impair nucleotide binding or hydrolysis by MeaB alone or the affinity of MeaB for MCM (Tables 3.3-3.6).

Switch III loops, previously considered to be unique to heterotrimeric G-proteins, are deployed for bidirectional conveyance of signals from cell surface receptors to intracellular effector proteins. The switch III loops in the Gα_s and Gα_T subunits are important for β-adrenergic receptor-dependent adenylate cyclase activation (28) and rhodopsin-dependent cyclic GMP phosphodiesterase activation via transducin (29), respectively. The crystal structure of G$_s\alpha$ revealed acidic residues in switch III that interact with basic ones in switch II and suggested that coupled dynamical changes in these two loop regions might be important for G-protein activation. Indeed, mutation of a conserved glutamate residue in switch III impairs receptor-mediated G$_s\alpha$ activation and the same residue is mutated in a patient with

pseudohypoparathyroidism *(30)*. Mutation of the corresponding E232 residue in transducin decreases its downstream function, i.e., effector activation *(29)*. Comparison of the crystal structures of $G\alpha_T$ with various nucleotide ligands reveals a network of primarily ionic interactions between switch II and III that differ in the GDP versus GTP bound states *(31)*. Exchange of GDP by GTP induces conformational changes in switch II, which are propagated to switch III.
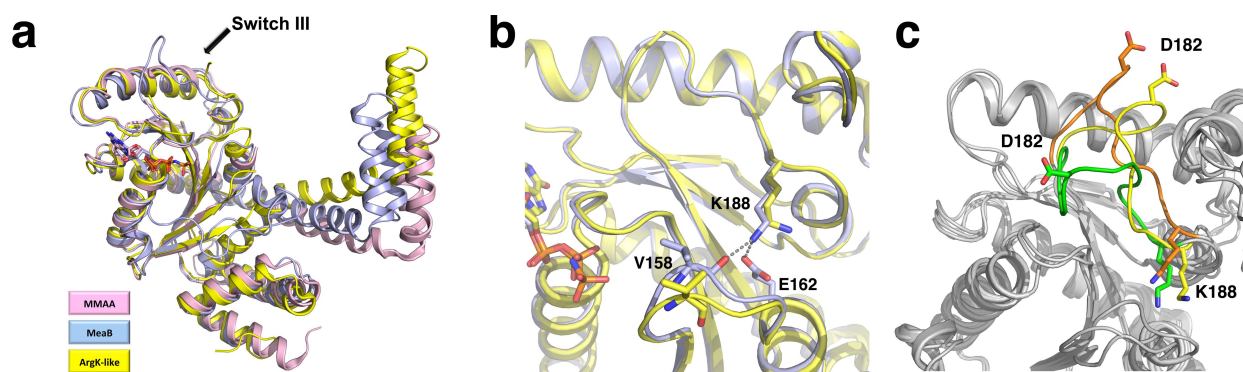
Figure 3.7. Switch III loop conformations. (a) Superposition of monomers of MeaB•GMPPNP, ArgK-like protein (PDB ID; 2P67) and MMAA (PDB ID; 2WWW). (b) Interactions between the switch III residue, K188 and switch II residues, V158 and E162 in the structures of MeaB•2GDP (yellow) and MeaB•2GMPPNP (blue). (**c**) Position of D182 and K188 in apo-MeaB (green), MeaB•2GDP (yellow), and MeaB•2Pi (orange).

We posit that the switch III loop in MeaB and its orthologs are functionally equivalent to the corresponding element in $G\alpha$ proteins. The switch III regions in the MeaB orthologs, ArgK and MMAA *(32)* are disordered in the respective crystal structures (Fig. 3.7a). Although not as well characterized, human CblA, like MeaB, also protects MCM against oxidative inactivation during turnover and reactivates it in a GTPase-dependent manner *(33)*. While further work is needed to understand the relationship between nucleotide identity/occupancy and switch III conformation particularly in the MCM:MeaB complex, the disorder observed in the switch III region of the MeaB crystal structures indicates conformational plasticity of switch III in MeaB and related

proteins. In the MeaB•2GMPPNP monomers, K188 in the switch III loop interacts with the backbone carbonyl of V158 and a carboxylate oxygen of E162 in switch II (Fig. 3.7b), communications that are either broken or rearranged in the other MeaB structures (Fig. 3.8). Moreover, D182 in the conformationally mobile switch III loop in the MeaB structures is excursive and found in multiple and divergent orientations (Fig. 3.7c). We postulate that nucleotide hydrolysis triggers a conformational change in the switch I/II regions that is propagated via switch II to switch III, where it modulates upstream (AdoCbl docking) and downstream (protection and rescue of MCM) functions. The lack of sequence homology between the switch III loops in MeaB and the Gα proteins suggests convergent evolution of a signaling strategy. Collectively, the results we have reported herein suggest that switch III motifs may be more prevalent among the various classes of G-proteins than previously understood, and where found, are critical for the signaling functions of G-proteins.
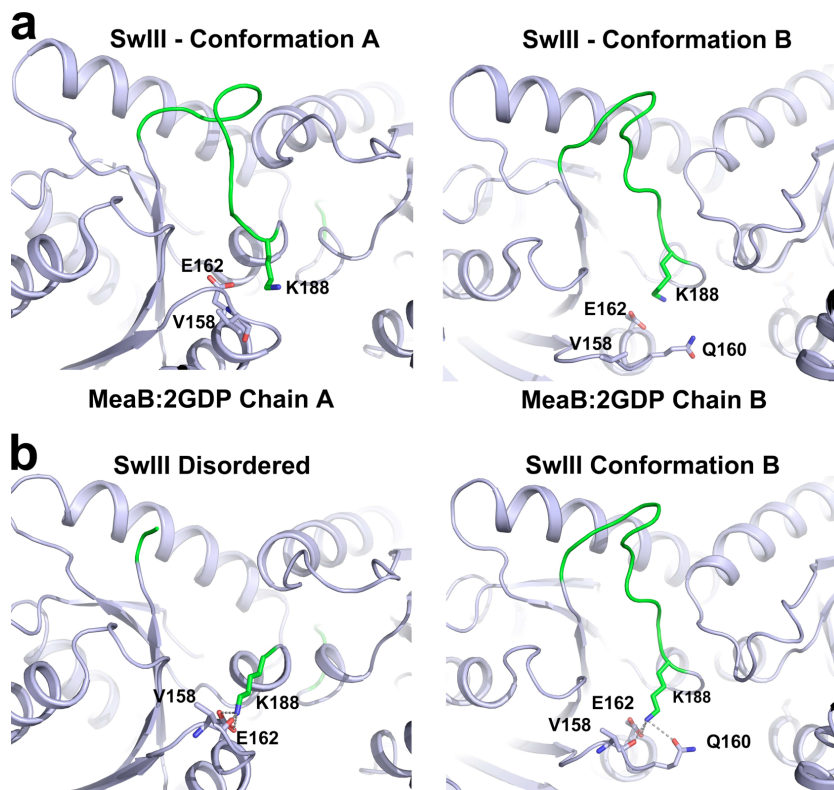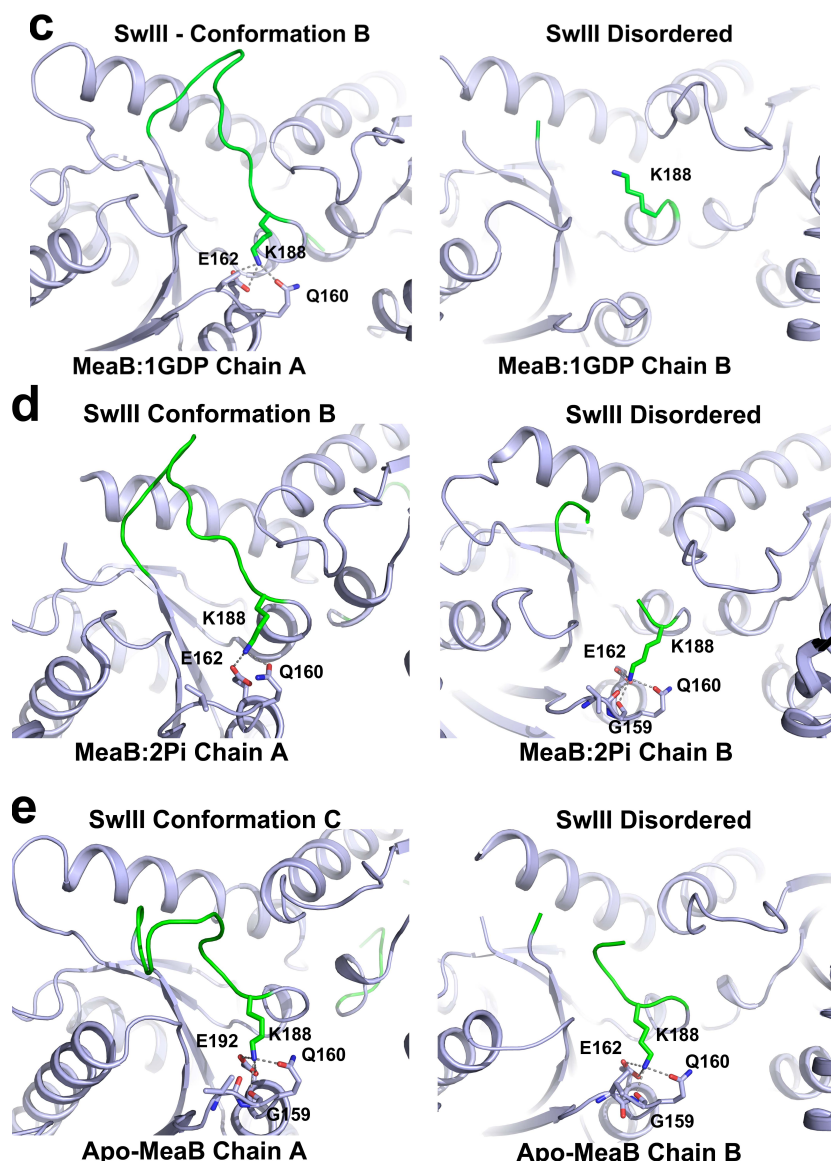
Figure 3.8. Switch III loop conformations, K188 positioning and interactions in (a) MeaB:2GDP, (b) MeaB:GMPPNP, (c) MeaB:1GDP, (d) MeaB:2Pi, and (e) apo-MeaB dimers. In every panel both faces, related by 180° rotation, of the MeaB dimers are shown. The B average values for each chain (B_{all}) and SwIII regions (B_{SwIII}) are as follows: (a) Conformation A: B_{all}=29.5 B_{SwIII}=23.6; Conformation B: B_{all}=22.9 B_{SwIII}=25.7 (b) Conformation B: B_{all}=42.3 B_{SwIII}=50.2 (c) Conformation B: B_{all}=40.9 B_{SwIII}=35.2 (d) Conformation B: B_{all}=20.3 B_{SwIII}=27.1 (e) Conformation C: B_{all}=45.4 B_{SwIII}=68.9 ($B_{average}$ for D182 and E183 side chains > 100).

3.5 Methods

3.5.1 Plasmids and construction of site-specific mutants–The plasmids containing the

Methylobacterium extorquens AM1 MCM and ATR were described previously *(6)*. A synthetic

69

gene (GenScript Corp.) encoding *M. extorquens* AM1 MeaB with a 5´-Nco1 site and 3´-Xho1 site was generated for optimal codon usage in *E. coli*. The synthetic MeaB gene was restriction digested with Nco1 and Xho1 (New England Biolabs) and sub-cloned into a pET-21d(+) (Novagen). Site-directed mutants were generated using a Quikchange II XL site-directed mutagenesis kit (Agilent) using the following mutagenic primers and the corresponding antisense primers:

D182A: 5´-GCCGGGTGCAGGTGCTGAACTGCAAGGCATCAAAAAAGG-3´

E183A: 5´-GCCGGGTGCAGGTGATGCACTGCAAGGCATCAAAAAAGG-3´

Q185A: 5´-GGGTGCAGGTGATGAACTGGCAGGCATCAAAAAAGG-3´

K188A: 5´-GGTGATGAACTGCAAGGCATCGCAAAAGGTATCCTGGAACTG-3´

K188E: 5´-GATGAACTGCAAGGCATCGAAAAAGGTATCCTGGAACTGG-3´

G186S: 5´-GCAGGTGATGAACTGCAAAGCATCAAAAAAGGTATCCTG-3´

Mutations generated according to the Quickchange protocol were confirmed by nucleotide sequence determination at the DNA Sequencing Core Facility (University of Michigan, Ann Arbor).

3.5.2 Enzyme expression and purification–Recombinant MeaB, MCM, ATR, and malonyl-CoA synthetase were expressed and purified from One Shot® BL21 (DE3) chemically competent *E. coli* (Invitrogen) as described previously *(6,34,35)*. Following purification, the enzymes were stored at -80 °C in 50 mM Hepes buffer, pH 8.0, 0.3 M KCl, 10 mM $MgCl_2$, 5 % glycerol (Buffer A).

3.5.3 Enzymatic synthesis and purification of methylmalonyl-CoA–Recombinant malonyl-CoA synthetase was employed for synthesis of methylmalonyl-CoA as described previously

(34). The identity and purity of the product was determined by HPLC using a known standard *(34)*.

3.5.4 Thermodynamic characterization of complex formation and nucleotide binding– Isothermal titration calorimetry experiments were performed at 10 °C in Buffer A using a VPITC calorimeter (Microcal, Inc.) equipped with a 1.43 ml cell and a 300 µl injection syringe. Prior to each titration, samples were degassed using a ThermoVac degasser (Microcal, Inc.) at 5 °C for 10 min. Each titration was performed at least in duplicate and the data were analyzed using the MicroCal ORIGIN program. Titrations of MeaB with nucleotides were performed with 10-25 µM MeaB protein with 8 µl additions of 150–375 µM GDP or GMPPNP (Sigma). The binding affinity of MeaB to MCM was determined by titrating 4-8 µM apo-MCM ± GMPPNP (250 µM) with 10 µl additions of 50-100 µM MeaB ± GMPPNP (250 µM) (Sigma). The binding of nucleotides to the MCM:MeaB complex (with wild-type or mutant MeaBs) was performed using 7.5–15 µM MeaB and a 2-fold molar excess of MCM to ensure saturation of the MCM:MeaB complex. The complexes were titrated with 8–10 µl aliquots of GDP or GMPPNP ranging in concentration from 100-250 µM. Single- or two-site binding models selected based on Chi-squared distribution values for each model, were used to estimate the association constant, K_A, entropy, $T\varDelta S^o$, and enthalpy, $\varDelta H^o$ values. The Gibbs free energy, $\varDelta G^o$, was calculated using the following equation: $\varDelta G^o = \varDelta H^o - T\varDelta S^o$.

3.5.5 The effect of switch III mutants on oxidative inactivation of MCM–The inactivation of MCM under steady-state turnover conditions in the presence of MeaB ± GMPPNP or GDP was followed by UV/visible spectroscopy by monitoring conversion of MCM-bound AdoCbl to H_2OCbl at 20 °C *(12)*. To generate the MCM:MeaB complex in 50 mM potassium phosphate, pH 7.5, containing 10 mM $MgCl_2$, 3-4 mM GMPPNP was added to 35-40 µM MeaB and

incubated at 20 °C prior to reconstitution with 25-30 μM MCM reconstituted with an equimolar concentration of AdoCbl. An excess of MeaB•2GMPPNP was added to MCM to fully populate the MCM:MeaB complex. The reaction was initiated by addition of methylmalonyl-CoA to a final concentration of 7-10 mM. The rate of inactivation was monitored at 351 nm and plotted as a function of time. The data were fit to a single-exponential equation, $A = A_o - A_p e^{(-kt)}$, where A is the absorbance at 351 nm, A_o represents the initial absorbance of cobalamin, A_p is the final amplitude for the conversion of AdoCbl to H_2OCbl, and k is the rate constant for H_2OCbl formation during turnover. The goodness of fit was evaluated according to the R^2 value using a cutoff R^2 value of 0.95 for each data set. The data shown are representative of at least two independent experiments.

3.5.6 Cofactor transfer assays–The transfer of AdoCbl from holo-ATR to MCM in the MCM:MeaB•GMPPNP complex was performed in the presence of stoichiometric holo-ATR and an excess of GMPPNP, following addition of excess ATP. The transfer or release of AdoCbl was monitored by UV/visible spectroscopy at 20 °C in Buffer A as described previously *(6)*. Two equivalents of AdoCbl were added to ATR to generate holo-ATR. The apo-MCM:MeaB•GMPPNP complex was reconstituted by mixing MCM with two equivalents of MeaB and 1 mM GMPPNP in Buffer A. The two enzyme solutions were then mixed to obtain a final concentration of 15 μM holo-ATR (30 μM in bound AdoCbl) and 15 μM of the MCM:MeaB•GMPPNP complex. In control samples, the reaction mixture was centrifuged at this stage using a Centricon YM10 concentrator (4 °C, 30 min., 16,000 x *g*) (Millipore). The presence of the "base-off" absorption spectrum of ATR-bound AdoCbl (λ_{max} = 458 nm) verified that ATR did not release AdoCbl into solution upon sample dilution (i.e. when the MCM:MeaB•GMPPNP solution was added to it). AdoCbl transfer/release was then initiated by

addition of 10 mM ATP and the amount of AdoCbl released was calculated using $\Delta\varepsilon_{525} = 6.69$ mM^{-1} cm^{-1}. The amount of AdoCbl transferred to the MCM active site was independently determined by centrifugation of the mixture through a Centricon YM10 concentrator (4 °C, 30 min., 16,000 x g) (Millipore) and determining the concentration of AdoCbl in the filtrate using an $\varepsilon_{525} = 8.0$ mM^{-1} cm^{-1}. The average ± S.D. of ≥ 3 independent experiments was used for reporting these results.

3.5.7 Cob(II)alamin release assays–Loss of cob(II)alamin from MCM in the presence of MeaB was evaluated under anaerobic conditions in the dark, following taddition of excess GMPPNP. The released cob(II)alamin was quantified by absorption spectroscopy of H$_2$OCbl (formed upon air oxidation) following separation of bound and free cofactor. Briefly, MCM (25-40 μM) was mixed with a 1.5-fold excess of D182A, E183A, Q185A, G186S, K188E, or K188A MeaB and incubated for 10 min with 20-35 μM cob(II)alamin at 20 °C in anaerobic Buffer A. Then, GMPPNP was added to a final concentration of 1-2 mM and the mixture was incubated for 10 min at 20 °C. The sample was then removed from anaerobic conditions, incubated at 20 °C, and cob(II)alamin was converted to H$_2$OCbl by air oxidation for 2 h before filtration through a Centricon YM10 concentrator (Millipore). H$_2$OCbl does not dissociate from the MCM:MeaB•GMPPNP complex *(6)*. The UV/visible spectra of total and released cofactor were recorded in the unfiltered sample and the filtrate, respectively. The concentration of bound and free cob(II)alamin was determined using $\varepsilon_{350} = 26.2$ mM^{-1}cm^{-1}. The percentage of inactive cofactor bound was determined as the average ± S.D. of ≥ 2 independent experiments.

3.5.8 GTPase activity of MeaB mutants–The k_{cat} values for GTP hydrolysis by wild-type and mutant MeaB in the presence or absence of a 2-fold molar excess of MCM were determined under V_{max} conditions using a discontinuous HPLC assay at a fixed and a saturating

concentration of GTP (10 mM) and 10 mM Mg^{2+} at 20 °C in Buffer A. To study the dependence of the GTPase activity on Mg^{2+}, 1 mM GTP and a variable concentration of Mg^{2+} (0-3 mM) was employed in Buffer A at 20 ˚C. Briefly, reactions were quenched at 10, 20, or 30 min using 10% (vol/vol) 2 N trichloroacetic acid and centrifuged (4 °C, 10 min, 16,000 x g) to remove precipitated protein. The samples were then applied to a μ Bondapak HPLC column (Waters) (NH2 10 μm, 125 Å 3.9 x 300 mm) and the eluent was monitored at 254 nm. GTP and GDP were separated using the following HPLC program at a flow rate of 1 ml/min: 100% of Buffer 1 (0.05 M potassium phosphate, pH 4.5) from 0-5 minutes, a linear gradient to 70 % Buffer 2 (0.80 M potassium phosphate, pH 4.5) from 5-20 min, isocratic elution with 70% Buffer 2 from 20-25 min, a linear gradient of 0 to 100% Buffer 1 from 25-26 min and isocratic elution with 100% Buffer 1 from 26-35 min. Under these conditions, GTP and GDP eluted at ~15.5 min and ~11.8 min, respectively. Values of k_{cat} ± S.D. represent the average at least 3 independent experiments.

3.5.9 Crystallization and crystal harvesting–Crystals of apo-MeaB and MeaB•2GMPPNP were obtained at 4 °C and 20 °C, respectively, by the vapor diffusion method from 4 μl 1:1 mixtures of protein to reservoir solutions. All protein samples were concentrated to 11 mg/ml in 50 mM Hepes buffer, pH 8.0, 2.5 mM $MgCl_2$, 5 mM GMPPNP and 5 % glycerol for MeaB with GMPPNP co-crystallization and in 50 mM Hepes buffer, pH 8.0, 2.5 mM $MgCl_2$, and 5 % glycerol for apo-MeaB**.** The reservoir solutions contained 28 % PEG400 in 50 mM HEPES, pH 7.5, for apo-MeaB, and 28 % PEG550MME in 50 mM MES, pH 6.5 for MeaB with GMPPNP. Crystals of MeaB with GMPPNP were cryoprotected for a few minutes prior to flash freezing in liquid N_2, by transfer to a solution of 22 % glycerol, 5 mM GMPPNP and 21 % PEG550MME in 50 mM MES pH 6.75. Crystals of apo-MeaB were harvested directly from the crystallization drop and were subsequently flash frozen in liquid N_2. Crystals of MeaB with GMPPNP were of

space group *C*2 (a= 185.6, b= 58.2, c= 76.4, β= 106.3) with 2 monomers in the asymmetric unit. Crystals of apo-MeaB were of space group *C*2 (a= 185.5, b= 58.4, c= 155.3, β= 110.1) with 4 monomers in asymmetric unit.

3.5.10 Data collection and structure determination–Diffraction data for apo-MeaB and MeaB•2GMPPNP were collected at 100 K on beamline GM/CA-CAT 23-ID-D at the Advanced Photon Source, Argonne National Laboratory (Argonne, IL). Data for apo-MeaB and MeaB•2GMPPNP were recorded on a Mar300 detector and processed with XDS *(36)* to 2.2 Å, and 2.1 Å resolution respectively. Phases were obtained by molecular replacement with the program PHASER *(37)* using a single monomer of the MeaB•GDP structure *(22)* (PDB ID 2QM7) as a search model. Loops containing residues 62-67, 95-100, 181-186, and 225-231 were removed from the search model to eliminate bias. Initial simulated annealing refinement (torsional and cartesian) was performed for the model obtained from molecular replacement with phenix.refine *(38)* in order to remove potential model bias. Subsequently, restrained individual atomic refinement, and restrained isotropic individual B-factor refinement with maximum likelihood targets using the Babinet model for bulk solvent scaling was performed using REFMAC5 *(39)* of the CCP4 suite *(40)*. COOT *(41)* was used to manually correct the incorrectly modeled residues. Through successive iterative rounds of refinement and manual model building, the remaining residues were traced in the electron density to afford the structural models. In later rounds of refinement, electron density near the nucleotide binding sites for one chain in Apo-MeaB and in both chains in MeaB•GMPPNP, were assigned and modeled with GDP and GMPPNP respectively. Crystallographic information as well as refinement statistics are provided in Supplementary Table 1. The geometric quality of the models was assessed with MolProbity *(42)*. For Apo-MeaB, Molprobity reported a clash and a Molprobity score of 4.5

(99th percentile) and 1.73 (95th percentile) respectively, while 97.2% of the residues were in the favored Ramachandran plot regions with 3 outliers (0.24%). For MeaB•2GMPPNP Molprobity reported a clash and a molprobity score of 4.59 (99th percentile) and 1.54 (97th percentile) respectively, while 98.1% of the residues were in the favored Ramachandran plot regions with no outliers. PyMOL *(43)* was used to create molecular images.

3.5.11 Summary of Statistical Analysis–Kinetic data were analyzed using either Kaleidograph or Microsoft Excel. MicroCal Origin was used to determine Chi-squared distribution of one- and two-site models ITC calorimetric titrations.

3.5.12 Accession Codes–The crystal structure coordinates for MeaB•2GMPPNP and Apo-MeaB were deposited to the RCSB Protein Data Bank under PDB codes 4JYB and 4JYC, respectively.

3.6 References

1. Boal, A. K. & Rosenzweig, A. C. Structural biology of copper trafficking. *Chem Rev* **109**, 4760-4779, (2009).
2. Gherasim, C., Lofgren, M. & Banerjee, R. Navigating the B_{12} road: assimilation, delivery and disorders of cobalamin. *J Biol Chem*, (2013).
3. Reddi, A. R., Jensen, L. T. & Culotta, V. C. Manganese homeostasis in *Saccharomyces cerevisiae*. *Chem Rev* **109**, 4722-4732, (2009).
4. Korotkova, N. & Lidstrom, M. E. MeaB is a component of the methylmalonyl-CoA mutase complex required for protection of the enzyme from inactivation. *J Biol Chem* **279**, 13652-13658, (2004).
5. Dobson, C. M. *et al.* Identification of the gene responsible for the *cbl*A complementation group of vitamin B_{12}-responsive methylmalonic acidemia based on analysis of prokaryotic gene arrangements. *Proc Natl Acad Sci U S A* **99**, 15554-15559, (2002).
6. Padovani, D. & Banerjee, R. A G-protein editor gates coenzyme B_{12} loading and is corrupted in methylmalonic aciduria. *Proc Natl Acad Sci U S A* **106**, 21567-21572, (2009).
7. Dempsey-Nunez, L. *et al.* High resolution melting analysis of the MMAA gene in patients with cblA and in those with undiagnosed methylmalonic aciduria. *Mol Genet Metab* **107**, 363-367, (2012).
8. Banerjee, R. Radical carbon skeleton rearrangements: catalysis by coenzyme B_{12}-dependent mutases. *Chem Rev* **103**, 2083-2094, (2003).
9. Ledley, F. D., Lumetta, M., Nguyen, P. N., Kolhouse, J. F. & Allen, R. H. Molecular Cloning of L-Methylmalonyl CoA Mutase: Gene Transfer and Analysis of mut Mell Lines. *Proc. Natl. Acad. Sci. U.S.A* **85**, 3518-3521, (1988).
10. Leipe, D. D., Wolf, Y. I., Koonin, E. V. & Aravind, L. Classification and evolution of P-loop GTPases and related ATPases. *J Mol Biol* **317**, 41-72, (2002).
11. Padovani, D., Labunska, T. & Banerjee, R. Energetics of interaction between the G-protein chaperone, MeaB and B_{12}-dependent methylmalonyl-CoA mutase. *J. Biol. Chem.* **281**, 17838-17844, (2006).
12. Padovani, D. & Banerjee, R. Assembly and protection of the radical enzyme, methylmalonyl-CoA mutase, by its chaperone. *Biochemistry* **45**, 9300-9306, (2006).
13. Hennig, S. E., Jeoung, J. H., Goetzl, S. & Dobbek, H. Redox-dependent complex formation by an ATP-dependent activator of the corrinoid/iron-sulfur protein. *Proc Natl Acad Sci U S A* **109**, 5235-5240, (2012).
14. Fujii, K., Galivan, J. H. & Huennekens, F. M. Activation of methionine synthase: Further characterization of the flavoprotein system. *Arch. Biochem. Biophys.* **178**, 662-670, (1977).
15. Olteanu, H. & Banerjee, R. Human methionine synthase reductase, a soluble P-450 reductase-like dual flavoprotein, is sufficient for NADPH-dependent methionine synthase activation. *J Biol Chem* **276**, 35558-35563, (2001).
16. Mori, K., Tobimatsu, T., Hara, T. & Toraya, T. Characterization, sequencing, and expression of the genes encoding a reactivating factor for glycerol-inactivated adenosylcobalamin- dependent diol dehydratase. *J Biol Chem* **272**, 32034-32041., (1997).

17. Mori, K., Bando, R., Hieda, N. & Toraya, T. Identification of a reactivating factor for adenosylcobalamin-dependent ethanolamine ammonia lyase. *J Bacteriol* **186**, 6845-6854, (2004).

18. Mori, K. & Toraya, T. Mechanism of reactivation of coenzyme B12-dependent diol dehydratase by a molecular chaperone-like reactivating factor. *Biochemistry* **38**, 13170-13178, (1999).

19. Shibata, N. *et al.* Release of a damaged cofactor from a coenzyme B12-dependent enzyme: X-ray structures of diol dehydratase-reactivating factor. *Structure* **13**, 1745-1754, (2005).

20. Olteanu, H. & Banerjee, R. Redundancy in the pathway for redox regulation of mammalian methionine synthase: reductive activation by the dual flavoprotein, novel reductase 1. *J Biol Chem* **278**, 38310-38314, (2003).

21. Sprang, S. R., Chen, Z. & Du, X. Structural basis of effector regulation and signal termination in heterotrimeric Galpha proteins. *Adv Prot Chem* **74**, 1-65, (2007).

22. Hubbard, P. A. *et al.* Crystal structure and mutagenesis of the metallochaperone MeaB: insight into the causes of methylmalonic aciduria. *J Biol Chem* **282**, 31308-31316, (2007).

23. Wittinghofer, A. & Vetter, I. R. Structure-function relationships of the G domain, a canonical switch motif. *Annu Rev Biochem* **80**, 943-971, (2011).

24. Gasper, R., Scrima, A. & Wittinghofer, A. Structural insights into HypB, a GTP-binding protein that regulates metal binding. *J Biol Chem* **281**, 27492-27502, (2006).

25. Padovani, D., Labunska, T., Palfey, B. A., Ballou, D. P. & Banerjee, R. Adenosyltransferase tailors and delivers coenzyme B_{12}. *Nat Chem Biol* **4**, 194-196, (2008).

26. Padovani, D. & Banerjee, R. A Rotary Mechanism for Coenzyme B_{12} Synthesis by Adenosyltransferase. *Biochemistry* **48**, 5350-5357, (2009).

27. Yamanishi, M., Vlasie, M. & Banerjee, R. Adenosyltransferase: an enzyme and an escort for coenzyme B_{12}? *Trends Biochem Sci* **30**, 304-308, (2005).

28. Grishina, G. & Berlot, C. H. Mutations at the domain interface of GSalpha impair receptor-mediated activation by altering receptor and guanine nucleotide binding. *J Biol Chem.* **273**, 15053-15060, (1998).

29. Li, Q. & Cerione, R. A. Communication between switch II and switch III of the transducin alpha subunit is essential for target activation. *J Biol Chem* **272**, 21673-21676, (1997).

30. Ahmed, S. F. *et al.* GNAS1 mutational analysis in pseudohypoparathyroidism. *Clin Endocrinol* **49**, 525-531, (1998).

31. Lambright, D. G., Noel, J. P., Hamm, H. E. & Sigler, P. B. Structural determinants for activation of the alpha-subunit of a heterotrimeric G protein. *Nature* **369**, 621-628, (1994).

32. Froese, D. S. *et al.* Structures of the human GTPase MMAA and vitamin B_{12}-dependent methylmalonyl-CoA mutase and insight into their complex formation. *J Biol Chem* **285**, 38204-38213, (2010).

33. Takahashi-Iniguez, T., Garcia-Arellano, H., Trujillo-Roldan, M. A. & Flores, M. E. Protection and reactivation of human methylmalonyl-CoA mutase by MMAA protein. *Biochem Biophys Res Commun* **404**, 443-447, (2011).

34. Padovani, D. & Banerjee, R. Alternative pathways for radical dissipation in an active site mutant of B_{12}-dependent methylmalonyl-CoA mutase. *Biochemistry* **45**, 2951-2959, (2006).

35. Lofgren, M. & Banerjee, R. Loss of allostery and coenzyme B_{12} delivery by a pathogenic mutation in adenosyltransferase. *Biochemistry* **50**, 5790-5798, (2011).

36. Otwinowski, Z. & Minor, W. in *Macromolecular Crystallography, Pt A* Vol. 276 *Methods in Enzymology* 307-326 (1997).

37. McCoy, A. J. *et al.* Phaser crystallographic software. *Journal of Applied Crystallography* **40**, 658-674, (2007).

38. Adams, P. D. *et al.* PHENIX: building new software for automated crystallographic structure determination. *Acta Crystallogr D Biol Crystallogr* **58**, 1948-1954, (2002).

39. Murshudov, G. N., Vagin, A. A. & Dodson, E. J. Refinement of macromolecular structures by the maximum-likelihood method. *Acta Crystallogr D Biol Crystallogr* **53**, 240-255, (1997).

40. The CCP4 suite: programs for protein crystallography. *Acta crystallographica. Section D, Biological crystallography* **50**, 760-763, (1994).

41. Emsley, P. & Cowtan, K. Coot: model-building tools for molecular graphics. *Acta Crystallogr D Biol Crystallogr* **60**, 2126-2132, (2004).

42. Davis, I. W. *et al.* MolProbity: all-atom contacts and structure validation for proteins and nucleic acids. *Nucleic Acids Res* **35**, W375-383, (2007).

43. Schrodinger, LLC. *The PyMOL Molecular Graphics System, Version 1.3r1* (2010).

CHAPTER 4

Autoinhibition and Signaling by the Switch II Motif in the G-protein Chaperone of a

Radical B$_{12}$ Enzyme[7,8]

4.1 Abstract

MeaB is an accessory GTPase protein involved in the assembly, protection, and reactivation of 5′-deoxyadenosylcobalamin-dependent methyl-malonyl-CoA mutase (MCM). Mutations in the human ortholog of MeaB, CblA, result in methylmalonic aciduria, an inborn error of metabolism. G-proteins typically utilize conserved switch I and II motifs for signaling to effector proteins via conformational changes elicited by nucleotide-binding and hydrolysis. Our recent discovery that MeaB employs a novel switch III region for bidirectional signaling with MCM raised questions about the roles of the switch I and II motifs in MeaB. In this study, we have addressed the functions of conserved switch II residues by mutating these residues to alanine. Our results demonstrate that the GTPase activity of MeaB is auto-inhibited by switch II and that this loop is important for coupling nucleotide-sensitive conformational changes in switch III for

eliciting the multiple chaperone functions of MeaB. Furthermore, we report the structure of MeaB crystallized in the presence of a putative transition state analog, GDP•AlF$_4^-$. The absence of AlF$_4^-$ in the resulting crystal structure and its comparison to related G-proteins supports the hypothesis that the catalytic site of MeaB is incomplete in the absence of the GTPase-activating protein, MCM, and therefore unable to stabilize the transition state analog. Favoring an inactive conformation in the absence of the client MCM protein represents a strategy for suppressing the intrinsic GTPase activity of MeaB in which the switch II loop plays an important role.

4.2 Introduction

MeaB from Methylobacterium extorquens and its human ortholog CblA, play critical roles in the docking of coenzyme-B$_{12}$ (or 5′-deoxyadenosyl cobalamin or AdoCbl) into the active site of the client enzyme, methylmalonyl-CoA mutase (MCM) (1-4). MCM belongs to the class of AdoCbl-dependent mutases that catalyze 1,2-rearrangement reactions (5). Dietary cobalamin is assimilated into AdoCbl and delivered to MCM in a complex trafficking pathway (6-8). In humans, MCM functions in the mitochondrial catabolism of branched-chain amino acids, odd-chain fatty acids and cholesterol, by converting methylmalonyl-CoA to succinyl-CoA. Mutations in the auxiliary proteins or in MCM itself, give rise to methylmalonic acidemia, an inborn error of metabolism that is inherited as an autosomal recessive disease (9-12). Nearly thirty pathogenic mutations have been described in CblA (also known as MMAA) and lead to lower AdoCbl levels and consequent impairment of MCM (11).

Our understanding about the function of CblA is derived primarily from biochemical studies on MeaB, which belongs to the G3E family of SIMIBI (Signal recognition paticle, MinD, and BioD) phosphate-binding loop (P-loop) G-proteins (13). Several members of this family of

81

NTPases serve as metallochaperones. These include CooC, HypB, and UreG, accessory proteins involved in the maturation of nickel-containing enzymes. CooC is a Ni^{2+}-binding ATPase that undergoes metal and nucleotide-dependent dimerization and catalyzes the insertion of nickel into carbon monooxide dehydrogenase (14). UreG is a GTPase that is needed for the insertion of nickel into urease (15). HypB is activated by GTP-dependent dimerization and is needed for nickel insertion into the [Ni-Fe]-hydrogenase (16). Some metallochaperones bind the transition metal and transfer it directly to the target protein while others facilitate metal insertion but do not directly bind the cofactor. MeaB is an example of the latter class as it gates the transfer of AdoCbl from adenosyltransferase (ATR), to MCM (3) but does not itself bind the metal-containing cofactor. GTP hydrolysis by MeaB is required for transfer of AdoCbl from ATR to MCM *(3)*. Furthermore, MCM and MeaB form a complex whose affinity depends on the ligand bound to each protein, but is predicted to be a stable complex *in vivo (4)*.

Most G-proteins, including the G3E GTPases, are predicted to signal via conserved sequence motifs known as switch I and switch II (17-21). Together, switch I and II function as loaded springs that interact with the Mg^{2+} ion in the GTPase site and signal to target proteins by undergoing conformational changes in response to nucleotide binding, hydrolysis and exchange. In G3E G-proteins, the ExxG peptide defines the minimal consensus sequence for the switch II region (13). The switch I sequence is not strongly conserved with the exception of the nearly ubiquitously present threonine and glutamate residue in Ras-like GTPases (22). The γ-phosphate of GTP makes direct hydrogen bonding contacts with the main-chain amides of the conserved threonine and glycine residues in the switch I and II sequences, respectively. The carboxylate of the switch II glutamate residue forms a water-mediated contact with the Mg^{2+} ion that is also coordinated by the β- and γ-phosphate oxygen atoms. In Ras proteins, an active site water

molecule is activated via interaction with a conserved glutamine residue in the switch II consensus motif, DxxGQ, and serves as the attacking nucleophile in the GTPase reaction. In G3E proteins such as HypB, NifH, and SRP, the activating residue is predicted to be a conserved aspartate residue at position 1 in switch I (23-25). The corresponding aspartate in MeaB, D92, is not positioned for catalysis. It is displaced 11-14 Å from the active site in the reported structures (26). CblA and MeaB comprise seven central and parallel-stranded β-sheets in the G-domain and flanking N- and C-terminal α-helical extensions (26,27). The C-terminal extension forms a dimerization arm. In addition to the switch I (residues 92-108) and II (residues 154-162) loops two other signature G-protein motifs are present in MeaB: the P-loop and the base-specificity loop that extend between residues 62-70 and 200-204, respectively. The P-loop has a GxxGxGKST consensus sequence that interacts with the phosphate moiety of nucleotides.

The switch II motif in MeaB-like GTPases has the following consensus sequence: ETVGVGQSE. In a subset of SIMIBI G-proteins, GTP-dependent conformational changes in the switch regions expose dimerization surfaces that are essential for their biological function (28). In Ras-like GTPases, GTP hydrolysis elicits a conformational change in the switch I region that exposes an effector domain involved in recognition of downstream target proteins (21). In the G3E G-proteins, the functions of switch I and II motifs in the context of their metallochaperone functions have not been addressed.

In MeaB, an additional conformationally dynamic region, switch III, plays a critical role in bidirectional signal transduction with MCM (29). Although unrelated at a primary sequence level, the switch III region in the Gα-subunits of heterotrimeric G proteins is used for signal transmission (30-33).

MeaB exhibits similar affinities for GTP and GDP and, due to the relative tissue concentrations of each nucleotide, is expected to be predominantly GTP-loaded in the cell (2). The MeaB•GTP complex prevents assembly of the MCM active site by inactive precursors of AdoCbl (3). Comparison of the apo- and GDP-bound structures of MeaB with other G3E family members suggests that switch I and II are not in their catalytically active conformations (Fig. 4.1). The association of MeaB with MCM results in an ~100-fold rate enhancement of the GTPase reaction and also increases the affinity for GTP (2). Thus, MCM functions as a GTPase-activating protein (GAP) for MeaB. Two models for GAP activation of MeaB by MCM include: (i) contribution *in trans* of one or more catalytic residues by MCM to the active site of MeaB and (ii) induction of a conformational change in the MeaB•MCM complex that brings the active site residues of MeaB into catalytic register (34,35).
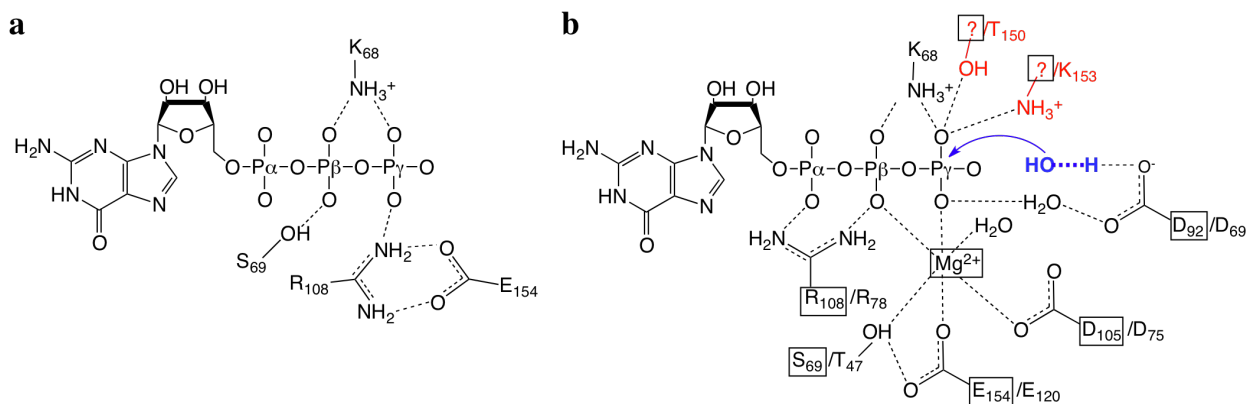
Figure 4.1. **Schematic representation of the interactions between GTP and MeaB or HypB.** The active sites of a) MeaB•GMPPNP (PDB 4JYC) and b) HypB•GTPγS (PDB 2HF8) are shown. The residues in MeaB that, based on sequence and structural homology to other G3E proteins, are predicted to be equivalent to those in the HypB active site are shown on the left and are boxed. Residues on the rate of the back slash identify active site residues in HypB.

In addition to gating the transfer of AdoCbl from ATR to MCM, MeaB also functions to protect MCM from inactivation during catalytic turnover and to rescue MCM that is inactivated (2,3). Thus, in the presence of either GDP or GTP, MeaB slows the rate of MCM inactivation

during catalysis by 30-fold and the exchange of GDP for GTP drives the ejection of inactive cofactor from the active site of MCM. While limited, biochemical studies support a role for CblA that is analogous to the better-characterized MeaB in forming a complex with MCM, protecting MCM from inactivation, and rescuing inactive MCM (36). Furthermore, human MCM also exhibits GAP activity with respect to CblA (27).

In this study, we have interrogated the role of the switch II motif in mediating the chaperone functions of MeaB and in transmitting the GAP function of MCM. To this end, we have employed alanine-substitution mutagenesis at conserved positions in switch II to learn about their role in MeaB function. We demonstrate that switch II mutations compromise regulation of AdoCbl transfer from ATR to the MCM•MeaB complex, reduce protection of MCM from inactivation during turnover, and impair ejection of inactive cofactor from the active site of MCM. Remarkably, a subset of switch II mutations activates the intrinsic GTPase activity of MeaB while disrupting its activation by MCM. We also report the structure of MeaB crystallized in the presence of GDP and AlF_4^-. Our results suggest a strategy for switch II-dependent auto-inhibition of the intrinsic GTPase activity of MeaB, which exists predominantly in an inactive conformation. Complexation with MCM is predicted to switch the MeaB conformation thereby activating its GTPase function.

4.3 Methods and Materials

4.3.1 Materials-AdoCbl, 5′-guanylyl-β,γ-imidophosphate (GMPPNP), ATP, GTP, methylmalonic acid, coenzyme-A, and other reagent grade chemicals were purchased from Sigma. Trifluoroacetic acid was purchased from Aldrich. Methylmalonyl-CoA was synthesized using malonyl-CoA synthetase, purified as described previously (37). The HPLC column used to

quantify guanosine nucleotides was a μBondapak^{TM} NH2 10 μm, 125 Å 3.9 x 300 mm column purchased from Waters.

4.3.2 Construction of site-specific mutants–Plasmids encoding the *M. extorquens* ATR and MCM were generous gifts from Mary E. Lidstrom (University of Washington, Seattle). A synthetic gene encoding *M. extorquens* AM1 MeaB with 5′-Nco1 and 3′-Xho1 restriction sites was generated by GenScript Corporation (New Jersey, USA) to optimize codon usage in *E. coli* and reduce the GC content. The synthetic MeaB gene was cloned into the pET-21d(+) expression vector (Novagen, Gibbstown, NJ) using the Nco1 and Xho1 sites. Site-specific mutants of MeaB were generated using a Quickchange kit (Agilent, Santa Clara, CA) according to the manufacturers protocol. The following forward primers were used to generate the mutants and the reverse primers had the complimentary sequences.

E154A: 5′-CGATGTCATTCTGGTGGCAACC GTTGGCGTCGGTCAGAGCG-3′

T155A: 5′-CGATGTCATTCTGGTGGCAAGCC GTTGTTGGCGTCGGTCAGAGCG-3′

Q160A:5′-GGAAACCGTTGGCGTCGGTGCGA GCGAAACCGCCGTTGC-3′

S161A: 5′- GGAAACCGTTGGCGTCGGTCAG GCCGAAACCGCCGTTGGCAG-3′

E162A: 5′-CCGTTGGCGTCGGTCAGAGCGCA ACCGCCGTTGGCAGATCTG-3′

Following sequence confirmation, the Q160A plasmid and E162A primer pair were used to generate the Q160A/E162A double mutant.

4.3.3 Enzyme Expression and Purification–Recombinant *M. extorquens* MeaB, MCM, and ATR were expressed and purified from *E. coli* BL-21 (DE3) as described previously (4,38). The purified enzymes were flash frozen in liquid nitrogen and stored at -80 °C in 50 mM HEPES buffer, pH 8.0, containing 0.3 M KCl, 10 mM MgCl$_2$, 10% glycerol (Buffer A).

4.3.4 Crystallization of MeaB-Protein samples were concentrated to 11 mg ml^{-1} in 50 mM HEPES buffer at pH 8.0, 2.5 mM MgCl$_2$, 5 mM GDP, 1 mM [AlF$_4$]$^-$. MeaB:GDP•AlF$_4^-$ crystals were grown by the sitting drop vapor diffusion method at 20 ℃ by mixing 2 µL of protein solution with 2 µL of reservoir solution. The reservoir solution contained 20 % (w/v) PEG3350, and 0.2 M sodium sulfate. Crystals were cryoprotected for a few minutes before being flash frozen in liquid N$_2$, by transfer to a solution of 20% glycerol, 15% (w/v) PEG3350, 0.15 M sodium sulfate, 5 mM GDP, and 1 mM [AlF$_4$]$^-$ in 25 mM HEPES, pH 7.5. Crystals of MeaB:GDP•AlF$_4^-$ were of space group $P2_1$ (a= 63.7, b= 78.6, c= 69.6, β= 108.6) with 2 monomers in the a.u.

4.3.5 Data collection and structure determination–Diffraction data for MeaB:GDP•AlF$_4^-$ were collected at 100 K on beamline GM/CA-CAT 23-ID-B at the Advanced Photon Source, Argonne National Laboratory (Argonne, IL). Data were recorded on a Mar300 detector and processed with XDS (39) to 1.8 Å resolution (Table 1). EPMR (40) was used to determine initial phases for the MeaB:GDP•AlF$_4^-$ through molecular replacement using a single monomer of the MeaB:GDP structure (PDB ID 2QM7 (26)) as a search model. Loops containing residues 62-67, 95-100, 181-186, and 225-231 were removed from the search model to eliminate bias. Initial density allowed for ligand to be modeled and added. REFMAC (41) of the CCP4 suite (42) was subsequently employed for restrained refinement of the model using isotropic individual B-factors to a final R_{work} of 0.190 and R_{free} of 0.236. Model building and modification was performed with Coot (43), and the geometric quality of the models and their agreement with the structure factors were assessed with MolProbity (44). Crystallographic information as well as refinement statistics are provided in Table 1. Figures were generated with PyMOL (45).

4.3.6 Thermodynamics of GMPPNP-binding–Isothermal titration calorimetry (ITC) experiments were performed at 10 °C in Buffer A using a 300 μl injection syringe and a 1.43 ml injection cell. Samples were prepared by filtration through a 0.2 μm filter and then degassed under vacuum at 4 °C using a ThermoVac sample degasser. Each titration was performed at least in duplicate. GMPPNP (10 μl injections of 150-400 μM) was added to 10-25 μM MeaB. The data were analyzed using a two-site binding model using the MicroCal ORIGIN program. Values for the dissociation constant at sites 1 and 2 were then compared to the values obtained from the solution of the Gibbs free energy equation $\Delta G^o = -RTln(K_A)$.

4.3.7 Enzyme Inactivation Assays–Inactivation of MCM during steady-state was examined by enzyme-monitored turnover using UV/visible spectroscopy to follow the conversion of MCM-bound cob(II)alamin to aquocob(III)alamin (H_2OCbl) at 20 °C in 0.1 M potassium phosphate at pH 7.5 containing 10 mM $MgCl_2$. The reactions and sample preparations were performed in the dark to avert spurious H_2OCbl formation by photolysis of AdoCbl. Samples were prepared by the addition of reaction components in the order described below. MCM (25-30 μM) was reconstituted with an equimolar concentration AdoCbl. 35-40 μM of MeaB was added to the MCM holoenzyme to generate and fully populate the 1:1 MCM:MeaB complex. GMPPNP was then added to the reaction mixtures to a final concentration of 1-2 mM. The reaction was initiated by the addition of methylmalonly-CoA to a final concentration of 4.5-5 mM. The rates of inactivation were determined by plotting the change in absorbance at 351 nm, corresponding to H_2OCbl formation, as a function of time. The kinetic traces were best fit by a single exponential equation: $\Delta A_t = A_o - \Delta A_p e^{(-kt)}$, where ΔA_t is the absorbance at 351 nm as a function of time, A_o is the initial absorbance of cob(II)alamin, ΔA_p is the reaction phase amplitude for OHCbl formation, and k is the observed rate constant for MCM inactivation.

4.3.8 Assay for transfer of AdoCbl from ATR to MCM–The ATP-dependent transfer of AdoCbl from ATR to the MCM:MeaB•GMPPNP complex was performed in the dark at 20 °C and monitored by UV/visible spectroscopy. Two equivalents of AdoCbl were added to one equivalent of ATR in Buffer A to generate holo-ATR. The apo-MCM:MeaB•GMPPNP complex was reconstituted in Buffer A by mixing 40-50 μM apo-MCM with an equimolar concentration of AdoCbl and 50-60 μM of MeaB to give 40-50 μM of the complex. GMPPNP was added to a final concentration of 1 mM. Holo-ATR (2:1 AdoCbl:ATR) and the MCM:MeaB•GMPPNP complex (40-50 μM) were mixed and incubated for 10 min at 20 °C before that addition of ATP to a final concentration of 5 mM. Release/transfer of AdoCbl from ATR was calculated using a $\Delta\epsilon_{525} = 6.69$ mM^{-1}cm^{-1}. Bound versus free cofactor was separated using an Amicon centrifuge filter (10 kDa cutoff, 20 min, 4 °C, 16,000 x g). The concentration of free AdoCbl in the filtrate was calculated using $\epsilon_{525} = 8.0$ mM^{-1}cm^{-1}.

4.3.9 Release of Cob(II)alamin–MCM (30-40 μM) was mixed with 45-60 μM of wild-type, E154A, T155A, Q160A, S161A, E162A, or Q160A/E162A MeaB in Buffer A such that [MCM]:[MeaB] was 1:1.5 at 20 °C and under strictly anaerobic. Cob(II)alamin was generated by reduction of H$_2$OCbl with tris (2-carboxyethyl) phosphine hydrochloride (TCEP) and was added to a final concentration equal to that of the MCM:MeaB (wild-type or mutant) complex. The reaction mixture was incubated for 10 min at 20 °C. GMPPNP in anaerobic Buffer A was added to a final concentration of 2 mM. The mixture was then incubated for 20 min at 20 °C. Subsequently, the sample was made aerobic by air oxidation for 2 h and then filtered through to a Centricon YM10 filter (10 kDa cutoff) to separate free from bound H$_2$OCbl. Cob(II)alamin (but not H$_2$OCbl) can be released from MCM and is subsequently oxidized to H$_2$OCbl, which was quantified using $\epsilon_{350} = 9.3$ mM^{-1}cm^{-1}.

4.3.10 GTPase activity of MeaB–The GTPase activity of MeaB was determined using an HPLC assay as described previously (46).

4.3.11 Size-Exclusion Chromatography–Samples were prepared in Buffer A containing 0.5 mM GDP and 80-90 μM of wild-type or mutant MeaB ± equimolar MCM and 0.5 mM AdoCbl in a total volume of 150 μl, was prepared in the dark and loaded onto A Superdex-200 HR 10/30 column equilibrated with Buffer A. The protein complexes were eluted in the dark to minimize photolysis of AdoCbl.

4.4 Results

4.4.1 Structural characterization of MeaB:GDP•AlF$_4^-$

MeaB was crystallized in the presence of GDP•AlF$_4^-$, a potential transition state mimic. All the crystals were treated with a cryoprotectant solution containing an excess of GDP and AlF$_4^-$. MeaB crystallizes in the presence of GDP and AlF$_4^-$ in the $P2_1$ space group, and a unit cell similar to that reported for MeaB crystallized in the presence of GDP (Table 4.1). However, AlF$_4^-$ was not observed in any of the more than ten structures that were solved. Furthermore, despite inclusion of Mg^{2+} in the crystallization conditions it was also not observed in the crystal structure of MeaB. Although the structures of MeaB crystallized in the presence of GDP and AlF$_4^-$ (MeaB•GDP•AlF$_4^-$) appears to be identical to that of MeaB•GDP (Fig. 4.2a), closer inspection revealed two significant differences as described below.

Superposition of the MeaB•GDP(+AlF$_4^-$) and MeaB•GDP structures (Fig. 4.2a) yielded rmsd values of 2.31 Å for the Cα atoms of all residues, suggesting the two structures were similar in their overall tertiary and dimeric structure. Superimposition of the MeaB dimers and alignment with respect to the nucleotides, revealed no differences in the nucleotide binding sites between the MeaB•GDP and MeaB•GDP(+AlF$_4^-$) structures. However, R108 in the MeaB•GDP

90

structure (Fig. 4.2b, yellow) is solvent exposed and facing away from the active site cavity. In

contrast, R108 is swung toward the β-phosphate group of GDP and engages in a salt bridge

contact with the carboxylate of E154 in the structure of MeaB•GDP(+AlF$_4^-$) (Fig. 4.2b, blue). To

assess whether the observed structural differences were due to the slightly different

crystallization conditions, the structure of MeaB in the presence of GDP was re-determined

under conditions used to obtain the MeaB•GDP(+AlF$_4^-$) structure. The new and published (PDB

ID 2QM7) structures of MeaB•GDP were found to be identical (data not shown).

	MeaB•GDP(+AlF$_4^-$)
Data Collection	
Space Group	$P2_1$
Unit cell parameters	a= 63.7
	b= 78.6
	c= 69.6
	β= 108.6
Resolution range (Å)	50-1.80
Measured reflections [a]	273351 (40670)
Unique reflections [a]	60064 (9605)
Redundancy [a]	4.5 (4.2)
Completeness (%) [a]	99.5 (97.7)
I/σ$_I$ [a]	19.63 (4.43)
R$_{sym}$ (%) [a,b]	5.5 (39.3)
Refinement Statistics	
Working set / Test set Reflections	57034 / 3026
R$_{crys}$/ R$_{free}$ [c,d]	0.190 / 0.236
R.m.s. Deviations	
Bond lengths (Å)	0.015
Bond angles (deg.)	1.494
Averaged B-factors (Å^2)	
protein	24.0
solvent	38.8
ligand	23.2
Wilson B-factor (Å^2)	31.5
Ramachandran plot[e]	
Favored	98.9
Allowed	100
Disallowed	0
No. protein atoms	4669
No. water molecules	453
Protein Data Bank code	Unpublished

Table 4.1 MeaB•GDP(+AlF$_4^-$) Structure and Refinement Statistics. Statistics for the highest resolution shell are enclosed in parentheses. [b] R$_{sym}$ = $\sum |I - <I>|/\sum I$, where I = observed intensity, and $<I>$ = average intensity obtained from multiple measurements. [c] R$_{cryst}$ = $\sum ||F_{obs}| - |F_{calc}||/\sum |F_{obs}|$, where F$_{calc}$ and F$_{obs}$ are the calculated and observed structure factor amplitudes, respectively. [d] R$_{free}$, R-factor based on 5% of the data excluded from refinement. [e] RMSD, root mean square deviation.
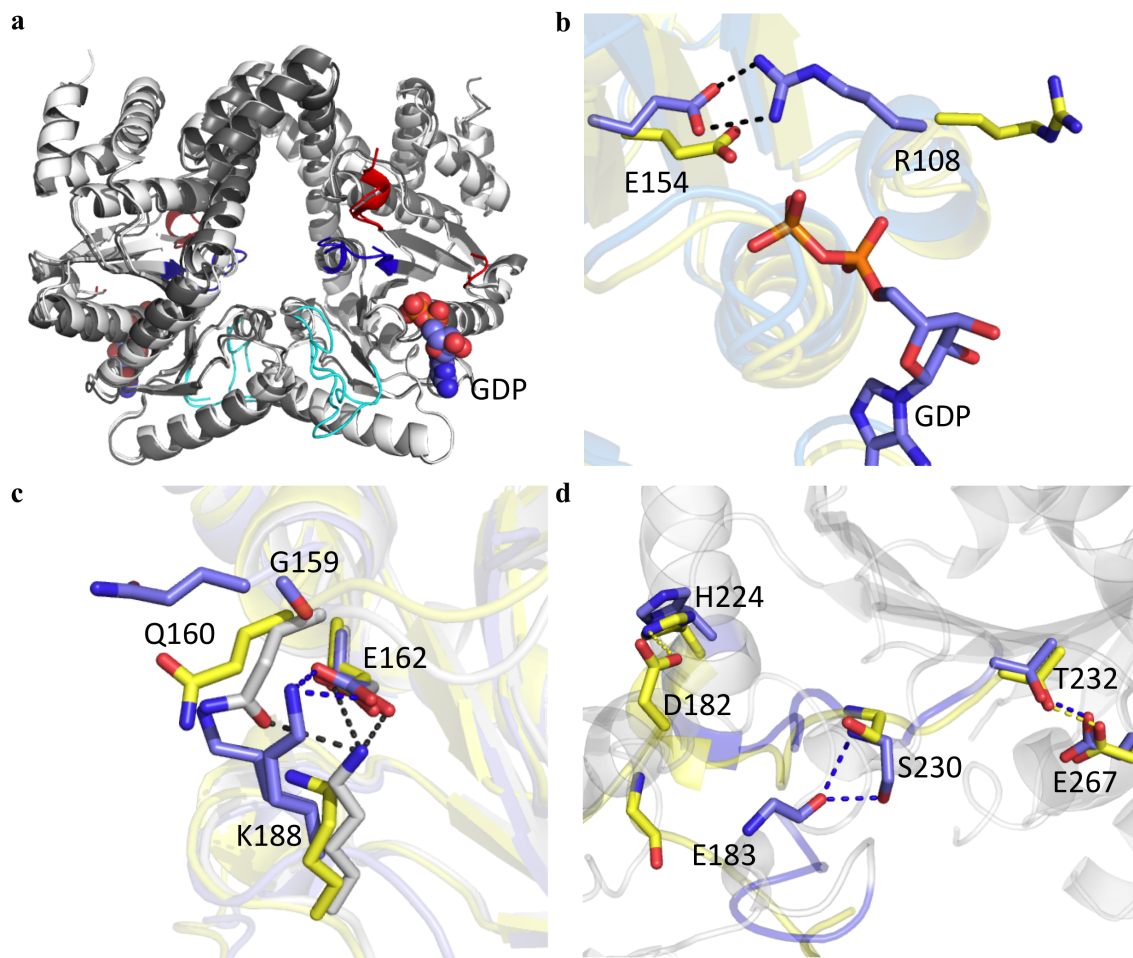
Figure 4.2. **Comparison of the MeaB•GDP(+AlF$_4^-$), MeaB•GDP, and MeaB•GMPPNP structures.** a) Structural superposition of the MeaB•GDP(+AlF$_4^-$) (dark grey, unpublished) and MeaB•GDP (light grey, PDB 2QM7) structures. GDP from the MeaB•GDP(AlF$_4^-$) structure is shown in sphere representation in dark blue. Switch motifs I, II, and III are colored blue, red, and cyan, respectively. b) Comparison of the l orientations and interactions of switch I and II in the structures of MeaB•GDP(+AlF$_4^-$) (blue) and MeaB•GDP (yellow). GDP and amino acid residues are shown in sticks representation and dashed lines represent hydrogen bonding or ionic interactions. c) Comparison of the interactions between switch II and switch III in the structures of MeaB•GDP(+AlF$_4^-$) (blue), MeaB•GDP (yellow), and MeaB•GMPPNP (grey, PDB 4JYC). K188 in the MeaB•GDP(+AlF$_4^-$) is shown in two conformations based on the electron density. d) Superposition of MeaB•GDP(+AlF$_4^-$) (blue) and MeaB•GDP (yellow) and a close-up of the interactions of switch III residues with the flexible loop on the adjacent subunit (224-232).

Additional differences between the MeaB•GDP(+AlF$_4^-$) and MeaB•GDP structures are observed in the Switch III region (residues 178-188) and its interaction with conserved residues Q160 and E162 in switch II (Fig. 4.2c). In the structure of MeaB•GDP(+AlF$_4^-$), the side chain of Q160 is swung ~25° from its position in the MeaB•GDP structure (Fig. 4.2c, blue). The electron density for the side chain of K188 allows it to be modeled in two configurations. In one configuration, K188 contacts switch II via an ionic interaction with the carboxylate of E162 and a single hydrogen bond with the carbonyl oxygen of G159. In the other configuration, the interactions between K188 and switch II are disrupted. In contrast, hydrogen bond contacts between K188 of switch III and E162, or any other part of switch II, are not observed in the MeaB•GDP structure (Fig. 4.2c, yellow). The contacts formed between switch II and III in the MeaB•GDP(+AlF$_4^-$) structure are also distinct from those captured in the structure of MeaB•GMPPNP. In the MeaB•GMPPNP structure, the side chain of K188 is ion paired to the carboxylate of E162 and engaged in a hydrogen bonding contact with the amide side chain of Q160 (Fig. 4.2c, grey).

The MeaB•GDP(+AlF$_4^-$) and MeaB•GDP structures also differ in the interaction of the Switch III region with a flexible loop from the adjacent monomer extending between residues 224-232. In one of the monomers of the MeaB•GDP(+AlF$_4^-$) structure, the backbone carbonyl oxygen of E183 is hydrogen bonded to S230 (Fig. 4.2d, blue). In contrast, the conformation of switch III in the MeaB•GDP structure precludes E183 from contacting the 224-232 loop (Fig. 4.2d, yellow). The only contact formed between Switch III and the 224-232 loop in the MeaB•GDP structure is a single hydrogen bond between the side chain of H224 and the carboxylate of residue D182. At the same subunit interface of the MeaB•GDP(+AlF$_4^-$) structure, D182 is disordered. D182 in the opposing subunit interface of MeaB•GDP(+AlF$_4^-$) structure

does not engage in hydrogen bonding with the 224-232 loop, and is displaced ~9 Å compared to the position of D182 at the same subunit interface in the MeaB•GDP structure. In both MeaB•GDP and MeaB•GDP(+AlF$_4$) structures, T232 is hydrogen bonded to the carboxylate of E267 in helix α11 within the same subunit.

4.4.2 Effect of switch II mutations on MCM:MeaB complex formation

ITC analysis of the binding affinities between MCM and MeaB mutants E154A, T155A, and Q160A revealed that the switch II mutants bind MCM similarly to wild-type MeaB (data not shown). Alternatively, complex formation between MCM and these MeaB mutants, as well as the S161, E162A, and Q160A/E162A MeaB, was also established by gel filtration chromatography. Reconstituting the MCM and wild-type or mutant MeaB complex by combining a 1:1 molar ratio of each protein in the presence of a molar excess of GDP and AdoCbl demonstrated that each MeaB mutant formed a complex with MCM. Wild-type and mutant MeaBs and MCM migrated with molecular masses of 68 and 142 kDa, respectively consistent with their calculated masses. With each MeaB mutant, formation of an MCM:MeaB complex with a molecular mass of 243 kDa was observed, consistent with the formation of a 1:1 complex between the two proteins (data not shown).

4.4.3 GMPPNP binding to switch II MeaB mutants

The MeaB homodimer binds nucleotides with negative cooperativity (Table 4.2). GMPPNP binds to sites 1 and 2 with K$_D$ values of 0.8 ± 0.4 μM and 9.5 ± 1.9 μM, respectively. The K$_D$ values for GMPPNP binding at site 1 range from 0.16 ± 0.01 to 1.29 ± 0.31 μM and from 0.48 ± 0.07 to 9.6 ± 1.4 μM at site 2. Overall, the switch II mutations do not have a substantial impact on GMPPNP binding, with the exception of the E162A and Q160A/E162A double mutants in

which the affinity for the nucleotide increases ~20-fold. GMPPNP binds to each switch II mutant with negative cooperativity.

4.4.4 GTPase activity of switch II mutants

The intrinsic and GAP-stimulated GTPase activities of the single and double switch II mutants were compared to wild-type MeaB (Table 4.3). Surprisingly, the E154A and Q160A mutants exhibited an ~10-fold activation of the intrinsic GTPase activity compared to wild-type MeaB. Furthermore, compared to the ~100-fold rate enhancement observed with wild-type MeaB, the GAP function of MCM was less in the MCM:MeaB complex formed by either of the E154A or Q160A mutants. The T155A, S161A, E162A, and Q160A/E162A mutations had a modest impact on the intrinsic GTPase rate and two (T155A and S161A) exhibited mild impairment GAP activation.

Enzyme	K_D (μM)	
	Site 1	Site 2
Wild-type[a]	0.81 ± 0.50	9.53 ± 1.91
E154A	1.29 ± 0.31	9.60 ± 1.42
T155A	0.47 ± 0.17	3.66 ± 0.46
Q160A	0.73 ± 0.11	3.32 ± 0.58
S161A	1.11 ± 0.29	3.88 ± 0.77
E162A	0.04 ± 0.02	0.60 ± 0.12
Q160A/E162A	0.16 ± 0.01	0.48 ± 0.07

Table 4.2. Thermodynamic data for GMMPNP-binding to MeaB. [a]Determined previously (46).

Enzyme	k_{cat} (min^{-1})		Fold GAP-Activation
	- MCM	+ MCM	
Wild-type[a]	0.039 ± 0.003	4.08 ± 0.20	102.0
E154A	0.335 ± 0.018	0.52 ± 0.11	1.6
T155A	0.091 ± 0.014	2.84 ± 0.31	31.1
Q160A	0.470 ± 0.013	0.54 ± 0.06	1.2
S161A	0.027 ± 0.006	2.35 ± 0.20	87.0
E162A	0.017 ± 0.006	1.07 ± 0.09	62.9
Q160A/E162A	0.018 ± 0.002	0.12 ± 0.02	6.7

Table 4.3 Kinetic parameters for GTP hydrolysis by MeaB mutants. [a]As determined previously (2).

4.4.5 Switch II mutations affect the rate of oxidative inactivation of MCM

In the presence of wild-type apo-MeaB, the rate of oxidative inactivation of MCM is 8.8 x 10^{-3} min^{-1} (Fig. 4.3a, trace 1). Addition of GMPPNP or GDP to the wild-type MCM:MeaB complex decreases the inactivation rate nearly 30-fold (3.0 x 10^{-4} min^{-1}, trace 2) (2). While the Q160A (2.8 x 10^{-4} min^{-1}, trace 3) and E162A (2.8 x 10^{-4} min^{-1}, trace 4) mutants do not appreciably impact the rate of MCM inactivation, E154A (2.0 x 10^{-4} min^{-1}, trace 5) and Q160A/E162A (2.1 x 10^{-4} min^{-1}, trace 6) lead to enhanced protection. The S161A (4.4 x 10^{-4} min^{-1}, trace 7) and T155A (6.8 x 10^{-4} min^{-1}, trace 8) mutations exhibit 1.5- and 2.3-fold higher rates of inactivation than wild-type MeaB.

4.4.6 Impaired GTPase-dependent AdoCbl transfer from ATR to MCM by switch II mutants

The *M. extorquens* ATR binds two equivalents of AdoCbl per homotrimer and binding of ATP to the vacant site initiates the transfer of a single equivalent of AdoCbl to the MCM:MeaB complex (3). In the presence of GMPPNP, transfer of AdoCbl to the wild-type MCM:MeaB complex is blocked. Instead, one equivalent of the cofactor is released from ATR into solution (Fig. 4.3b). With GMPPNP bound to the MCM:E154A MeaB mutant complex, AdoCbl transfer becomes modestly uncoupled from nucleotide hydrolysis (0.82 equivalents released and 0.18 equivalents transferred). Cofactor transfer is more significantly impaired to the complexes of MCM and T155A, Q160A, S161A, or E162A MeaB with GMPPNP bound (0.46–0.52 equivalents of AdoCbl transferred). The Q160A/E162A double severely impacted GTPase gating of AdoCbl transfer and 0.9 equivalents of the cofactor were transferred instead of being released into solution.

4.4.7 Rescue of MCM by switch II mutants

Our previous studies have shown that MeaB promotes expulsion of cob(II)alamin that has become uncoupled from 5′-deoxyadenosine during turnover in MCM (3). Here, we have examined the role of switch II in exerting this MeaB function of MeaB. In the presence of stoichiometric cob(II)alamin (with respect to MCM) and an excess of each switch II mutant MeaB, cob(II)alamin remains bound to MCM. Following addition of an excess of GMPPNP to the wild-type MeaB:MCM•cob(II)alamin complex, ~97% of the inactive cob(II)alamin is detected in the filtrate, indicating that the inactive cofactor was ejected from the MCM active site (Fig. 4.3c). In contrast, in the presence of the MeaB mutants E154A, T155A, Q160A or S161A, only ~35-45% of cob(II)alamin was ejected while the remainder was associated with MCM. In the complex of MCM:MeaB harboring the E162A single or the Q160A/E162A double mutations, ~80% of cob(II)alamin remained bound to MCM following addition of GMPPNP.

4.5 Discussion

While the roles of switch motifs in the catalytic and signaling mechanisms of many G-protein have been studied quite extensively (13,19,20,47,48), their role in cofactor delivery is not as well characterized.. Unlike the structures of CooC and NifH, the crystal structures of MeaB in the apo-, Pi, GMPPNP, and GDP (crystallized in the presence and absence of AlF_4^-) have failed to capture a catalytically active GTPase conformation. This is paralleled by the absence of Mg^{2+} in the active site of all available MeaB crystal structures, raising questions about the possible significance of the inactive conformation to MeaB function. In this study, we have examined the role of the conserved switch II residues in suppressing the intrinsic GTPase activity MeaB in the absence of MCM.

In HypB and other G3E GTPases, the general base is a conserved aspartate residue (D69 in HypB, Fig. 4.1b) positioned N-terminal to switch I following the second β- sheet (25). The structure of HypB•GTPγS shows D69 positioned ~5-6 Å from the γ-phosphinothioyl group of GTPγS and interacting with water molecules, one of which serves presumably serves as the nucleophile. The residue corresponding to D69 in HypB is D92 in MeaB. The MeaB structures containing GDP(+AlF$_4^-$) or GMPPNP, demonstrate how the hydrophobic side chains Val156 and Val158 impede access of D92 to the nucleotide (Figs. 4.4a-c). We speculate that the interaction between E154 and R108 is important for maintaining an auto-inhibitory conformation in MeaB that is alleviated in the MCM:MeaB complex. This model is consistent with the ~10-fold increase in the intrinsic GTPase activity of the E154A mutant and its relative insensitivity to GAP activity of MCM. E154A might be important for Mg^{2+} binding in the MCM:MeaB complex.

The similar effect of the E154A and Q160A mutants on the intrinsic and GAP-stimulated GTPase activities is surprising (Table 4.3). Q160 is not positioned near the active site in any of the MeaB structures and is not conserved in other G3E GTPases and is not predicted to directly participate in catalysis. Q160 engages in various hydrogen bonding interactions with residues in switch II, switch III and a conserved threonine immediately C-terminal to switch II in different MeaB structures (Fig. 4.5). Q160 forms a direct or water-mediated hydrogen bond with E161, E162 T163 or K188. In contrast, Q160 is not engaged in hydrogen bonding interactions in a couple of MeaB structures e.g. MeaB•GDP and in apo-MeaB. Hence, while our kinetic data suggest that Q160 is important for auto-inhibition, the structures of MeaB do not provide insights into a possible mechanism. The inability of the S161 and E162 mutations to mirror the Q160

phenotype suggests that the individual disruption of their interaction with Q160 is insufficient to disrupt the auto-inhibited conformation of MeaB.

The switch II residues T155, S161, and E162, are not conserved among G3E GTPases. Furthermore, obvious roles for T155, S161 and E162 in GTP binding or in the GTPase reaction are not apparent from the various MeaB structures. Both the T155A and S161A mutations result in a modest perturbations to the GTPase activity of isolated MeaB and in the MCM:MeaB complex (Table 4.3). These data indicate that neither T155 nor S161 plays an important role in auto-inhibition. In contrast, E162 significantly decreases the affinity of isolated MeaB for GTP at both sites 1 and 2 (Table 4.2). E162 might exert its effect on auto-inhibition of the intrinsic GTPase activity via reduced affinity for the substrate, GTP.

Many G-proteins use an octahedrally coordinated Mg^{2+} to stabilize the transition state and a general base to activate the nucleophilic water (23,25). In HypB from *Methanocaldococcus jannaschii*, E120 in the ExxG switch II motif directly ligates the active site Mg^{2+}. The corresponding residue in MeaB is E154. In all MeaB structures with the exception of MeaB•GDP (PDB 2QM7), E154 interacts with neighboring residues e.g. K68 from the P-loop and R108 in switch I (Figs. 4.4a and 4.4c). Some/all of these interactions are expected to be disrupted if E154 serves as a Mg ligand in the MCM:MeaB complex.
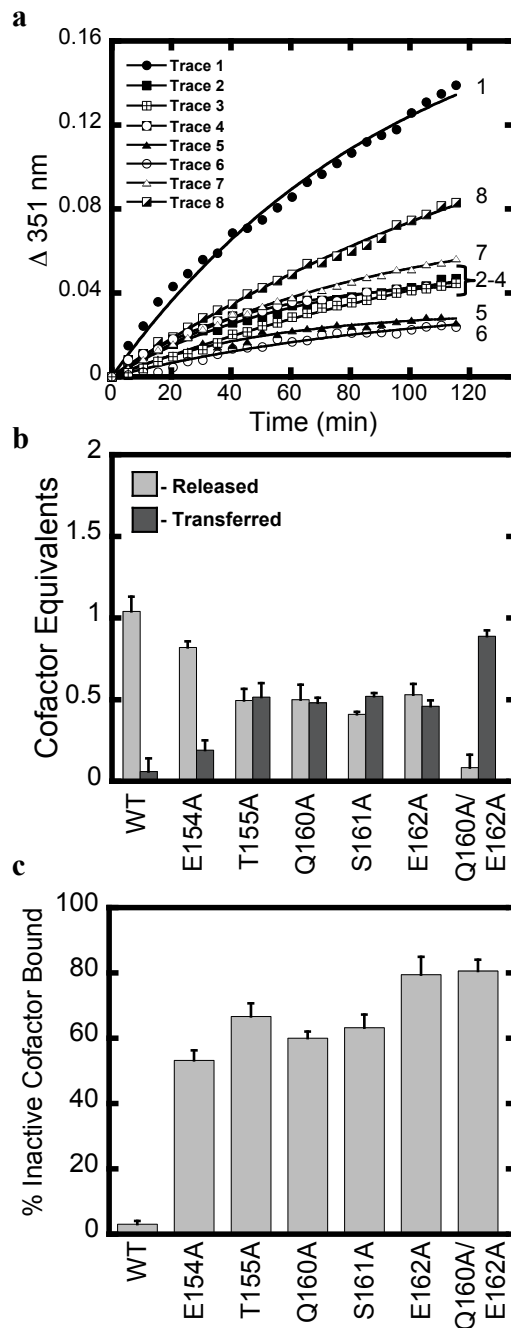
Figure 4.3. **Impact of switch II mutations on the chaperone functions of MeaB.** a) Time-dependent inactivation of MCM in complex with wild-type mutant MeaB•GMPPNP. The data presented here are representative of ≥2 experiments and were fit to a single exponential equation described under Experimental Procedures. b) ATP-dependent AdoCbl release or transfer from holo-ATR to the MCM:MeaB complex (containing wild-type or switch II mutant MeaBs) in the presence of GMPPNP. The data were averaged from ≥2 independent experiments. c) Displacement of cob(II)alamin from MCM•cob(II)alamin:MeaB (wild-type or switch II mutants) following addition of GMPPNP under anaerobic conditions. The data were averaged from ≥2 independent experiments.
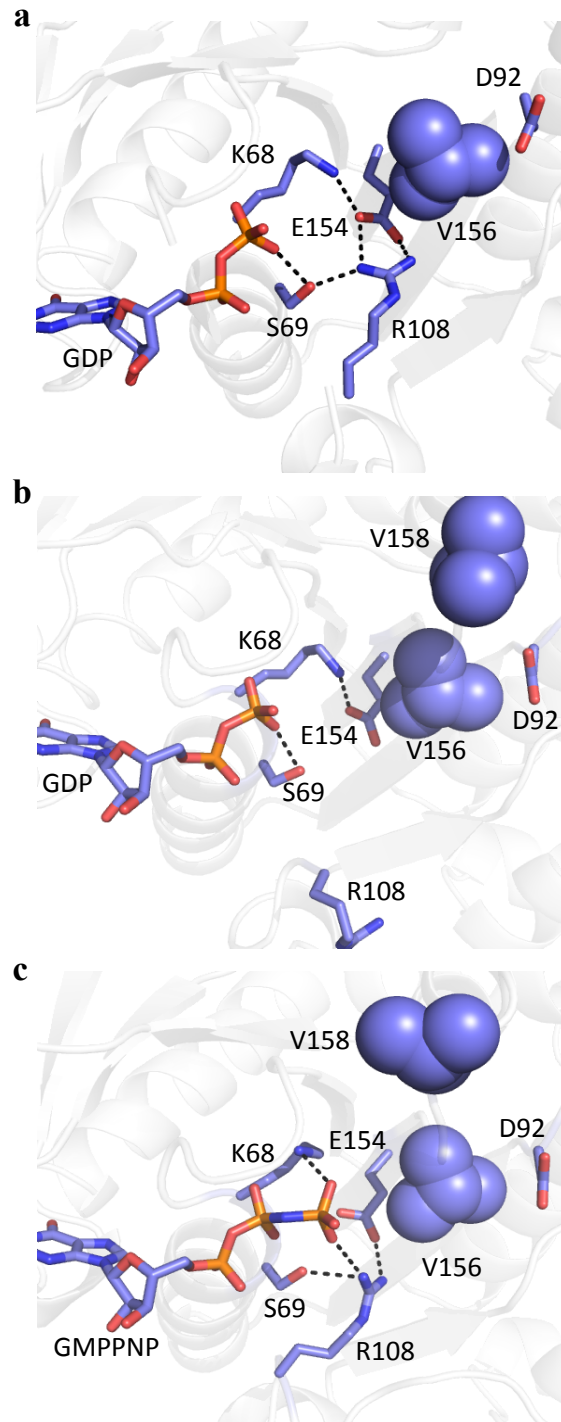
Figure 4.4. **Comparison of MeaB•nucleotide structures**. a) MeaB•GDP(+AlF$_4^-$), b) MeaB•GDP, and c) MeaB•GMPPNP. Bound nucleotide and amino acid side chains are shown in blue stick representation. The hydrophobic residues V156 and V158 are shown as spheres.

We have speculated that switches II and III communicate during bidirectional signal transmission between MeaB and MCM. K188 in switch III and E162 and Q160 in switch II might be important for relaying information about nucleotide identity and hydrolysis between these switch motifs (Fig. 4.2b). A mutation in CblA corresponding to the K188 residue in MeaB is pathogenic (49). We have shown that mutation of K188 has pleiotropic consequences including loss of regulated GTPase depdendent AdoCbl loading into MCM and impaired repair of inactive MCM. In this study, we demonstrate that mutation of the interacting residues Q160 and E162 partially uncouples cofactor docking in MCM from GTP hydrolysis in MeaB (Fig. 4.3b) and ejection of inactive cofactor from MCM (Fig. 4.3c). The Q160A/E162A double mutant is more impaired than either single mutant and more closely resembles the phenotype of the K188 mutant. Similar perturbations in MeaB function, albeit of of varying magnitude, are also observed with other switch II mutants, consistent with a role for motif in signaling between MeaB and MCM via switch III.

G-proteins are engaged in a diverse array of regulatory processes (21,50,51). They are among the most common and ancient regulatory proteins in Nature (13). An increasing body of evidence is demonstrating significant variations in the mechanisms of and factors employed for GTP hydrolysis and signal transduction, which are not readily predicted by sequence and structural homology (52). For instance, MeaB appears to deploy a its putative catalytic motifs, switch I and II, for catalysis in the MCM:MeaB complex and for auto-inhibition of GTPase activity in isolated MeaB. This finding provides the first insight into the mechanism for GAP activation in a G3E metallochaperone.
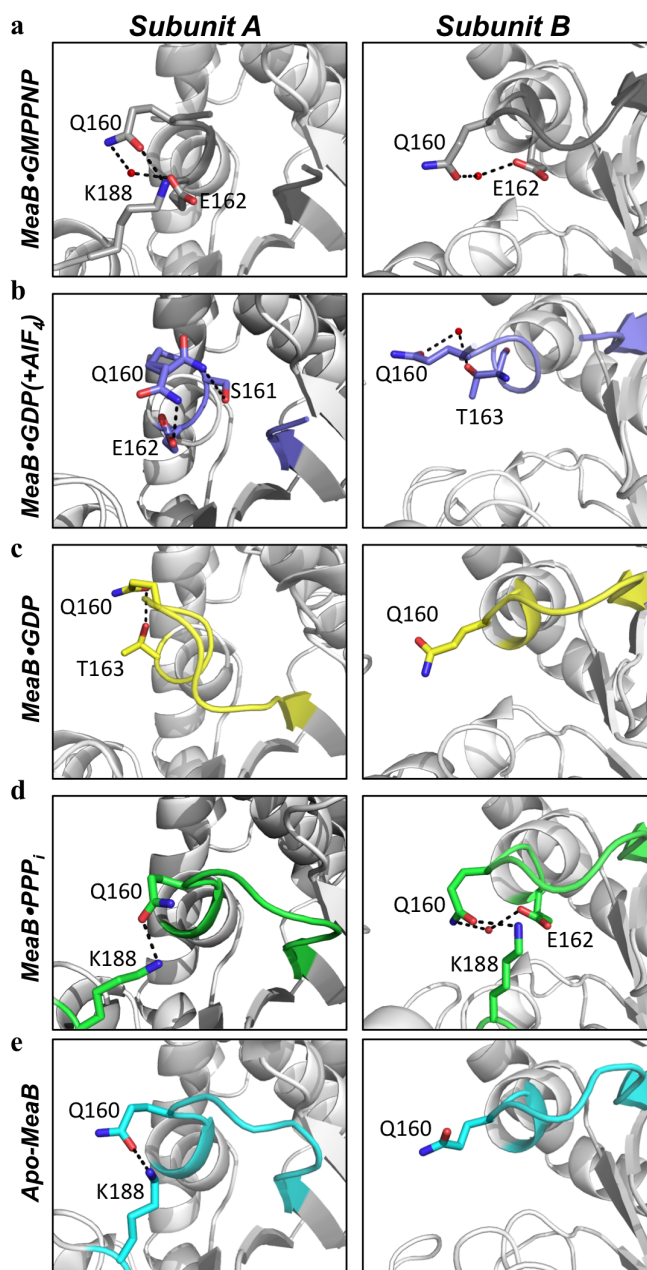
Figure 4.5. **Conformations of Q160 in MeaB structures.** The structures of (a) MeaB•GMPPNP (grey), (b) MeaB•GDP(AlF₄⁻) (blue), (c) MeaB•GDP (yellow), (d)MeaB•PPPᵢ (green), and (e) apo-MeaB (cyan) are shown and were generated from PDB files 4JYB, unpublished (MeaB•GDP(AlF₄⁻), 2QM8, and 4JYC, respectively. Adjacent subunits of the MeaB homodimers from individual crystal structures are shown for comparison. Individual residues are shown as sticks. Hydrogen bonds are shown as black dashes.

4.6 References

1. Korotkova, N., and Lidstrom, M. E. (2004) MeaB is a component of the methylmalonyl-CoA mutase complex required for protection of the enzyme from inactivation. *J Biol Chem* **279**, 13652-13658

2. Padovani, D., and Banerjee, R. (2006) Assembly and protection of the radical enzyme, methylmalonyl-CoA mutase, by its chaperone. *Biochemistry* **45**, 9300-9306

3. Padovani, D., and Banerjee, R. (2009) A G-protein editor gates coenzyme B_{12} loading and is corrupted in methylmalonic aciduria. *Proc Natl Acad Sci U S A* **106**, 21567-21572

4. Padovani, D., Labunska, T., and Banerjee, R. (2006) Energetics of interaction between the G-protein chaperone, MeaB and B_{12}-dependent methylmalonyl-CoA mutase. *J. Biol. Chem.* **281**, 17838-17844

5. Banerjee, R. (2003) Radical carbon skeleton rearrangements: catalysis by coenzyme B_{12}-dependent mutases. *Chem Rev* **103**, 2083-2094

6. Banerjee, R. (2006) B_{12} trafficking in mammals: A for coenzyme escort service. *ACS Chem Biol* **1**, 149-159

7. Banerjee, R., Gherasim, C., and Padovani, D. (2009) The Tinker, Tailor, Soldier in intracellular B_{12} Trafficking. *Cur Op Chem Biol* **13**, 484-491

8. Gherasim, C., Lofgren, M., and Banerjee, R. (2013) Navigating the B_{12} road: assimilation, delivery, and disorders of cobalamin. *J Biol Chem* **288**, 13186-13193

9. Leal, N. A., Olteanu, H., Banerjee, R., and Bobik, T. A. (2004) Human ATP: Cob(I)alamin adenosyltransferase and its interaction with methionine synthase reductase. *J Biol Chem* **279**, 47536-47542

10. Dobson, C. M., Wai, T., Leclerc, D., Kadir, H., Narang, M., Lerner-Ellis, J. P., Hudson, T. J., Rosenblatt, D. S., and Gravel, R. A. (2002) Identification of the gene responsible for the *cbl*B complementation group of vitamin B_{12}-dependent methylmalonic aciduria. *Hum Mol Genet* **11**, 3361-3369

11. Dobson, C. M., Wai, T., Leclerc, D., Wilson, A., Wu, X., Dore, C., Hudson, T., Rosenblatt, D. S., and Gravel, R. A. (2002) Identification of the gene responsible for the *cbl*A complementation group of vitamin B_{12}-responsive methylmalonic acidemia based on analysis of prokaryotic gene arrangements. *Proc Natl Acad Sci U S A* **99**, 15554-15559

12. Ledley, F. D., Lumetta, M., Nguyen, P. N., Kolhouse, J. F., and Allen, R. H. (1988) Molecular Cloning of L-Methylmalonyl CoA Mutase: Gene Transfer and Analysis of mut Mell Lines. *Proc. Natl. Acad. Sci. U.S.A* **85**, 3518-3521

13. Leipe, D. D., Wolf, Y. I., Koonin, E. V., and Aravind, L. (2002) Classification and evolution of P-loop GTPases and related ATPases. *J Mol Biol* **317**, 41-72

14. Jeon, W. B., Cheng, J., and Ludden, P. W. (2001) Purification and characterization of membrane-associated CooC protein and its functional role in the insertion of nickel into carbon monoxide dehydrogenase from Rhodospirillum rubrum. *J Biol Chem* **276**, 38602-38609

15. Zambelli, B., Stola, M., Musiani, F., De Vriendt, K., Samyn, B., Devreese, B., Van Beeumen, J., Turano, P., Dikiy, A., Bryant, D. A., and Ciurli, S. (2005) UreG, a chaperone in the urease assembly process, is an intrinsically unstructured GTPase that specifically binds Zn^{2+}. *J Biol Chem* **280**, 4684-4695

16. Rey, L., Imperial, J., Palacios, J. M., and Ruiz-Argueso, T. (1994) Purification of Rhizobium leguminosarum HypB, a nickel-binding protein required for hydrogenase synthesis. *J Bacteriol* **176**, 6066-6073

17. Milburn, M. V., Tong, L., deVos, A. M., Brunger, A., Yamaizumi, Z., Nishimura, S., and Kim, S. H. (1990) Molecular switch for signal transduction: structural differences between active and inactive forms of protooncogenic ras proteins. *Science* **247**, 939-945

18. Stouten, P. F., Sander, C., Wittinghofer, A., and Valencia, A. (1993) How does the switch II region of G-domains work? *FEBS Lett* **320**, 1-6

19. Sprang, S. R. (1997) G protein mechanisms: insights from structural analysis. *Annu Rev Biochem* **66**, 639-678

20. Vetter, I. R., and Wittinghofer, A. (2001) The guanine nucleotide-binding switch in three dimensions. *Science* **294**, 1299-1304

21. Wittinghofer, A., and Vetter, I. R. (2011) Structure-function relationships of the G domain, a canonical switch motif. *Annu Rev Biochem* **80**, 943-971

22. Scheffzek, K., Ahmadian, M. R., Kabsch, W., Wiesmuller, L., Lautwein, A., Schmitz, F., and Wittinghofer, A. (1997) The Ras-RasGAP complex: structural basis for GTPase activation and its loss in oncogenic Ras mutants. *Science* **277**, 333-338

23. Egea, P. F., Shan, S. O., Napetschnig, J., Savage, D. F., Walter, P., and Stroud, R. M. (2004) Substrate twinning activates the signal recognition particle and its receptor. *Nature* **427**, 215-221

24. Lanzilotta, W. N., Fisher, K., and Seefeldt, L. C. (1997) Evidence for electron transfer-dependent formation of a nitrogenase iron protein-molybdenum-iron protein tight complex. The role of aspartate 39. *J Biol Chem* **272**, 4157-4165

25. Gasper, R., Scrima, A., and Wittinghofer, A. (2006) Structural insights into HypB, a GTP-binding protein that regulates metal binding. *J Biol Chem* **281**, 27492-27502

26. Hubbard, P. A., Padovani, D., Labunska, T., Mahlstedt, S. A., Banerjee, R., and Drennan, C. L. (2007) Crystal structure and mutagenesis of the metallochaperone MeaB: insight into the causes of methylmalonic aciduria. *J Biol Chem* **282**, 31308-31316

27. Froese, D. S., Kochan, G., Muniz, J. R., Wu, X., Gileadi, C., Ugochukwu, E., Krysztofinska, E., Gravel, R. A., Oppermann, U., and Yue, W. W. (2010) Structures of the human GTPase MMAA and vitamin B_{12}-dependent methylmalonyl-CoA mutase and insight into their complex formation. *J Biol Chem* **285**, 38204-38213

28. Chan, K. H., Li, T., Wong, C. O., and Wong, K. B. (2012) Structural basis for GTP-dependent dimerization of hydrogenase maturation factor HypB. *PLoS One* **7**, e30547

29. Lofgren, M., Padovani, D., Koutmos, M., and Banerjee, R. (2013) A Switch III Motif Relays Signaling between a B_{12} Enzyme and its G-protein Chaperone. *Nat Chem Biol*, accepted for publication

30. Li, Q., and Cerione, R. A. (1997) Communication between switch II and switch III of the transducin alpha subunit is essential for target activation. *J Biol Chem* **272**, 21673-21676

31. Warner, D. R., Gejman, P. V., Collins, R. M., and Weinstein, L. S. (1997) A novel mutation adjacent to the switch III domain of G(S alpha) in a patient with pseudohypoparathyroidism. *Mol Endocrinol* **11**, 1718-1727

32. Natochin, M., Gasimov, K. G., and Artemyev, N. O. (2002) A GPR-protein interaction surface of Gi(alpha): implications for the mechanism of GDP-release inhibition. *Biochemistry* **41**, 258-265

33. Day, P. W., Tesmer, J. J., Sterne-Marr, R., Freeman, L. C., Benovic, J. L., and Wedegaertner, P. B. (2004) Characterization of the GRK2 binding site of Galphaq. *J Biol Chem* **279**, 53643-53652

34. Scrima, A., Thomas, C., Deaconescu, D., and Wittinghofer, A. (2008) The Rap-RapGAP complex: GTP hydrolysis without catalytic glutamine and arginine residues. *EMBO J* **27**, 1145-1153

35. Seewald, M. J., Korner, C., Wittinghofer, A., and Vetter, I. R. (2002) RanGAP mediates GTP hydrolysis without an arginine finger. *Nature* **415**, 662-666

36. Takahashi-Iniguez, T., Garcia-Arellano, H., Trujillo-Roldan, M. A., and Flores, M. E. (2011) Protection and reactivation of human methylmalonyl-CoA mutase by MMAA protein. *Biochem Biophys Res Commun* **404**, 443-447

37. Padovani, D., and Banerjee, R. (2006) Alternative pathways for radical dissipation in an active site mutant of B_{12}-dependent methylmalonyl-CoA mutase. *Biochemistry* **45**, 2951-2959

38. Lofgren, M., and Banerjee, R. (2011) Loss of allostery and coenzyme B_{12} delivery by a pathogenic mutation in adenosyltransferase. *Biochemistry* **50**, 5790-5798

39. Kabsch, W. (2010) Xds. *Acta Crystallogr D* **66**, 125-132

40. Kissinger, C. R., Gehlhaar, D. K., and Fogel, D. B. (1999) Rapid automated molecular replacement by evolutionary search. *Acta Crystallogr D* **55**, 484-491

41. Murshudov, G. N., Vagin, A. A., and Dodson, E. J. (1997) Refinement of macromolecular structures by the maximum-likelihood method. *Acta Crystallogr D Biol Crystallogr* **53**, 240-255

42. (1994) The CCP4 suite: programs for protein crystallography. *Acta crystallographica. Section D, Biological crystallography* **50**, 760-763

43. Emsley, P., and Cowtan, K. (2004) Coot: model-building tools for molecular graphics. *Acta Crystallogr D Biol Crystallogr* **60**, 2126-2132

44. Davis, I. W., Leaver-Fay, A., Chen, V. B., Block, J. N., Kapral, G. J., Wang, X., Murray, L. W., Arendall, W. B., 3rd, Snoeyink, J., Richardson, J. S., and Richardson, D. C. (2007) MolProbity: all-atom contacts and structure validation for proteins and nucleic acids. *Nucleic Acids Res* **35**, W375-383

45. Schrodinger, LLC. (2010) The PyMOL Molecular Graphics System, Version 1.3r1.

46. Padovani, D., Labunska, T., and Banerjee, R. (2006) Energetics of interaction between the G-protein chaperone, MeaB, and B12-dependent methylmalonyl-CoA mutase. *J Biol Chem* **281**, 17838-17844

47. Wittinghofer, A. (1998) Signal transduction via Ras. *Biol Chem* **379**, 933-937

48. Chen, Y., Yoo, B., Lee, J. B., Weng, G., and Iyengar, R. (2001) The signal transfer regions of G alpha(s). *J Biol Chem* **276**, 45751-45754

49. Dempsey-Nunez, L., Illson, M. L., Kent, J., Huang, Q., Brebner, A., Watkins, D., Gilfix, B. M., Wittwer, C. T., and Rosenblatt, D. S. (2012) High resolution melting analysis of the MMAA gene in patients with cblA and in those with undiagnosed methylmalonic aciduria. *Mol Genet Metab* **107**, 363-367

50. Bohm, A., Gaudet, R., and Sigler, P. B. (1997) Structural aspects of heterotrimeric G-protein signaling. *Curr Opin Biotechnol* **8**, 480-487

51. Wittinghofer, F. (1998) Ras signalling. Caught in the act of the switch-on. *Nature* **394**, 317, 319-320

52. Anand, B., Majumdar, S., and Prakash, B. (2013) Structural basis unifying diverse GTP hydrolysis mechanisms. *Biochemistry* **52**, 1122-1130

CHAPTER 5

SIGNAL TRANSDUCTION AND CATALYSIS VIA SWITCH I, A CANONICAL SIGNALING MOTIF IN MEAB[9,10]

5.1 Abstract

MeaB and its human ortholog CblA, are G-proteins that function as chaperones for docking AdoCbl into the active site of B_{12}-dependent MCM. Both proteins also safeguard their cognate MCMs against inactivation. In addition, MeaB functions as a reactivase for MCM by eliciting the ejection of inactivated cofactor generated adventitiously during turnover. Conserved motifs known as switch I and II are present in both MeaB and CblA and are predicted to communicate with MCM via conformational changes in response to nucleotide binding and hydrolysis. Both proteins possess an additional motif, switch III, whose involvement in bidirectional signaling between the MCM and MeaB active sites supports the GAP function of MCM and the chaperone function of MeaB. In this study, we have used alanine-substitution mutagenesis of conserved residues in switch I to gain insight into the function of this canonical signaling motif in catalysis and signal transduction. Our results suggest that the chemical mechanism of GTP hydrolysis by

MeaB alone might differ from that utilized in the activated MCM:MeaB complex. We also provide evidence that a single switch I arginine residue is essential for nucleotide binding by MeaB. Finally, we demonstrate that mutations at conserved positions in the switch I sequence of MeaB disrupts the chaperone functions of MeaB, as well as the GAP functions of MCM. Our results reveal that switch I, II and III motifs of MeaB are each involved in multiple chaperone functions, with switch I and II likely involved in controlling and catalyzing the GTPase reaction.

5.2 Introduction

MeaB from *Methylobacterium extorquens* is a member of the SIMIBI [signal recognition particle (SRP), MinD, and BioD-related] class of G-proteins and functions as a chaperone for MCM (1-4). The latter belongs to the family of B_{12}-dependent isomerases that use AdoCbl as a cofactor (5,6). MCM is a mitochondrial protein in humans and participates in the catabolism of branched-chain amino acids, odd-chained fatty acids, and cholesterol by catalyzing a 1,2-carbon skeleton isomerization reaction. The tissue concentration of cobalamins is low in mammals and formation of the MCM holoenzyme is reliant upon an auxiliary pathway for assimilation and post-translational insertion of AdoCbl (7-9). In humans, mutations in auxiliary proteins in the assimilation and in AdoCbl trafficking pathways result in diminished MCM activity and lead to methylmalonic acidemia (10-14). Since catalysis by MCM involves homolysis and geminal recombination of the cobalt-carbon bond in AdoCbl, inadvertent dissociation of deoxyadenosine from the active site during turnover is another source of impairment of MCM activity. Current evidence suggests that MeaB and CblA control the loading of AdoCbl into the MCM active site, and protect MCM from inactivation during steady-state turnover (3,4,15-17).

Other SIMIBI metallochaperones include UreG, CooC and HypB (1) that catalyze the insertion of Ni^{2+} into urease (UreG), CO dehydrogenase (CooC), and [Ni-Fe]-hydrogenase

(HypB), respectively (19-24). CooC and HypB undergo NTP-dependent dimerization, which is required for their control over the transfer of Ni^{2+} to their respective client proteins (24-27). In contrast, MeaB exists as dimer, binds MCM tightly, and does not bind AdoCbl directly. Rather, ATR synthesizes and delivers AdoCbl to MCM via a mechanism that is proposed to be allosterically gated by binding of ATP to ATR and by GTP hydrolysis by MeaB (Fig. 5.1) (3).

G-proteins are identified by a minimum of four sequence elements known as G binding motifs (G1-G4) (18). The G1 motif is commonly known as Walker A or the phosphate-binding loop (P-loop) and recognizes the triphosphate handle of GTP. In MeaB, the P-loop spans residues 62-70 and has a GxxGxGKST consensus sequence (28). The G2 and G3 elements are the switch I and II motifs, respectively. In most G-proteins, switch I and II are involved in catalysis and signaling to downstream effector proteins (1,18,29). Residues in switch I and II provide some of the ligands to the Mg^{2+} ion and undergo conformational rearrangements in response to nucleotide binding, exchange and hydrolysis. In this "loaded spring" mechanism, direct, H_2O-mediated or Mg^{2+}-mediated contacts between switch motif residues and the γ-phosphate of GTP are made upon its binding and are disrupted upon its hydrolysis (30). However, the signaling and catalytic conformations of switch I and II in MeaB await elucidation, as residues in switch I and II that are predicted to be critical for nucleotide binding and catalysis are significantly retracted from the predicted active site in the various MeaB structures. Hence, based on the crystal structures of HypB•GTPγS, crystallographic studies of MeaB with bound nucleotides appear to have failed to capture switch I and II in an active conformation (24). Additionally, the structures of MeaB with bound nucleotides demonstrate that the active site lacks residues predicted to be important in catalysis. Finally, a base-specificity loop (G4), whose consensus sequence is NKxD in MeaB, selectively recognizes the guanine nucleobase.

Most isolated G-proteins are innately slow at catalyzing GTP hydrolysis (18). The cognate mutases of MeaB and CblA, the human ortholog of MeaB, function as GAPs and accelerate the rate of GTP hydrolysis (4,16). Typically, proteins with GAP functions elicit G-protein activation by interfacing with the partner G-protein to provide residues that complete the active site. In many GTPases, an active site aspartate, glutamine, asparagine, or histidine residue, often provided by switch I or II, is required for stabilization or polarization of an active site water molecule for nucleophilic attack of the γ-phosphate (24, 31-33). Typically, an active site arginine residue referred to as an arginine "finger" neutralizes the developing negative charge in the transition state (34-36). In principle, the residues involved in polarization of water in the active site to increase its nucleophilicity and charge stabilization in the transition state can be derived from the G-protein or from its GAP. The α subunits (Gα) of heterotrimeric G-proteins contain catalytic arginine and asparagine residues that are provided by the G-protein (37,38). In contrast, the active site of the Ras:Ras-GAP complex contains an asparagine from Ras and an arginine from Ras-Gap (36). In Rab33, the asparagine from the G-protein is replaced by an asparagine residue (an asparagine "thumb") from Rab-GAP, which also supplies the catalytic arginine residue (39). Thus, GAPs function by providing their G-proteins with active site residue*s* or by stabilizing the catalytic machinery that is provided by the G-protein. One or both of these strategies may be employed by MCM proteins for acceleration of the GTP hydrolysis in CblA and MeaB.
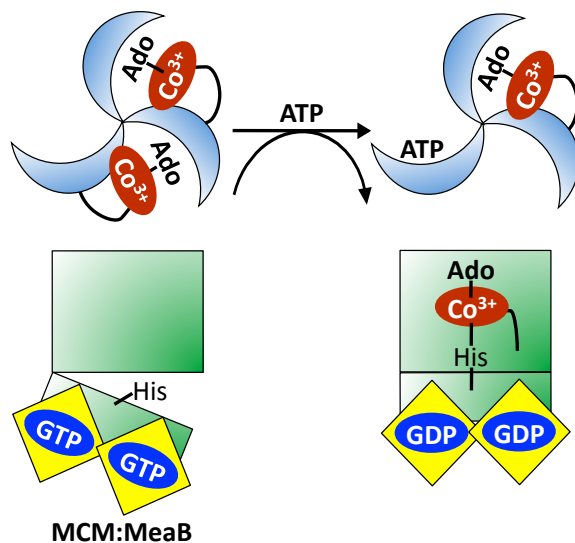
Figure 5.1. **Cartoon representation of the nucleotide-dependent control of AdoCbl transfer from ATR (blue) to MCM (green) in the MCM:MeaB (yellow) complex.** MeaB with bound nucleotides are shown in yellow. Cobalamin is shown as a red oval. The transfer of AdoCbl from ATR to MCM occurs upon binding of ATP to ATR and requires hydrolysis of GTP to GDP on MeaB. AdoCbl switches from a 5-coordinate "base-off" conformation in ATR to a 6-coordinate "base-off/His-on" conformation in MCM.

The minimal consensus sequence in the switch II region of MeaB and other G3E proteins is ExxG (where x denotes any amino acid) (1). Based on the structure of HypB•GTPγS, the leading glutamate residue in the MeaB switch II sequence is E154 and therefore, it is predicted to ligate Mg^{2+} directly (Fig. 5.2) (24,28). However, Mg^{2+} is not present in any of the currently available crystal structures of MeaB. Recent biochemical evidence supports a role for E154 in the stabilization of an auto-inhibited conformation of MeaB, perhaps via its interaction with a conserved R108 residue in switch I. In Ras G-proteins, a conserved glutamine residue immediately following the ExxG sequence, polarizes a catalytic water molecule for nucleophilic attack on the γ-phosphate of GTP (32,40). In most G3E GTPases, a hydrophobic residue substitutes for glutamine (1) and a strongly conserved aspartate residue (Asp^{cat}) at the N-terminus of the switch I motif is proposed to serve as the general base for activation of water (24,41,42). Based on the structure of HypB•GTPγS, D92 in MeaB is proposed to be the Asp^{cat}.

However, in the available MeaB crystal structures, D92 is not positioned for catalysis and is blocked from the active site by the switch II loop, particularly the hydrophobic side chain of residue V156.

Motif / Function	HypB	MeaB
Switch I	D_{69}, $D_{75}AER_{78}$	D_{92}, $D_{105}KTR_{108}$
Switch II	$E_{120}NVG$	$E_{154}TVG$
α-, β-, or γ-phosphate group binding	R_{78}, K_{153}	R_{108}
Nucleophilic H_2O activation	D_{69}, $H_{154}{}^a$	D_{92}
Mg^{2+} ligands	T_{47}, D_{75}, E_{120}	S_{69}, D_{105}, E_{154}
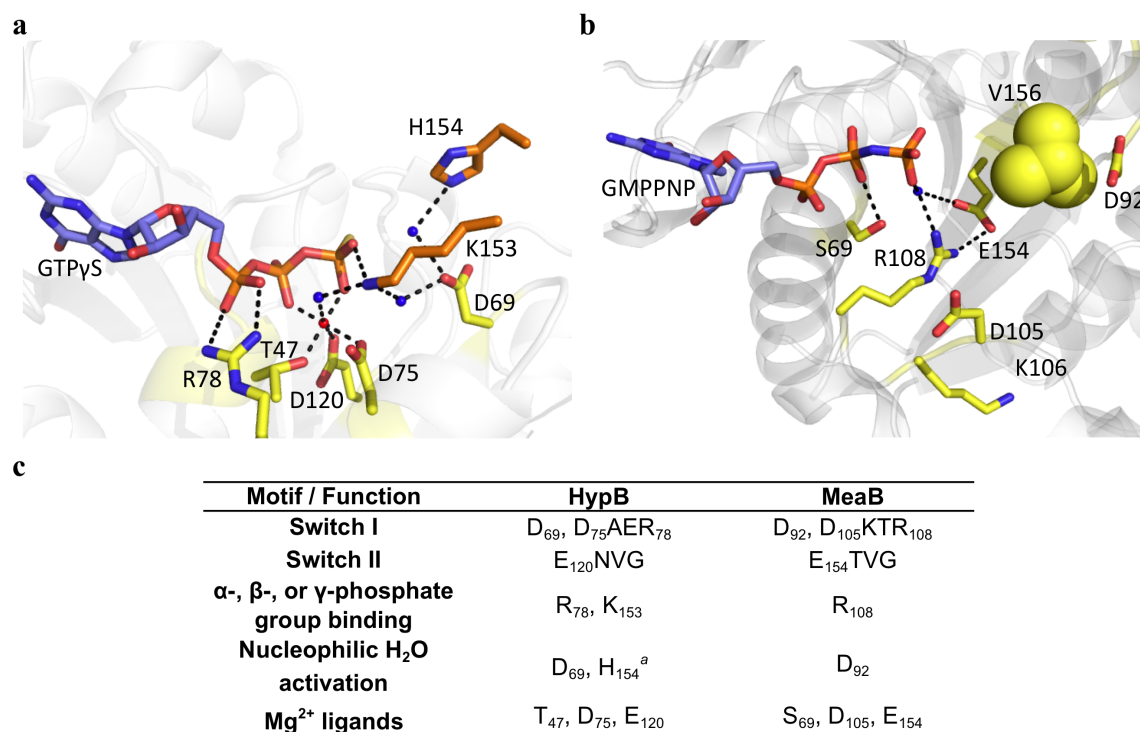
Figure 5.2. Comparison of the enzyme active sites of MeaB and HypB from the crystal structures of a) MeaB•GMPPNP (PDB 4JYC) and of b) HypB•GTPγS (PDB 2HF8). Shown in stick representation are the bound guanosine nucleotides (blue), conserved residues in switch I (yellow), and residues contributed from the adjacent subunit in the structure of HypB•GTPγS (orange). Residue V156 in switch II is shown as Van der waals spheres. C) The table lists the conserved switch I and II sequences in HypB and MeaB, and their proposed functions.

The switch I sequence is conserved between MeaB and its orthologs (12,28,43). Among various families of G-proteins, the boundaries, lengths, and amino acid sequences of the switch I motif varies considerably, and must be empirically defined for each subfamily (1,30). The switch I region in the Ras family of G-proteins has only a single threonine residue that is strongly conserved, and it positions switch I via main-chain hydrogen bond interactions to the γ-

phosphate of GTP (44,45). In HypB•GTPγS, D75, which is strongly conserved in the G3E proteins, replaces that threonine residue and engages in water-mediated and direct interactions with the Mg^{2+} ion (Fig. 5.2) (24). In MeaB and CblA, switch I is on an extended loop with the consensus sequence DPSSxx[S/T]GGShLGDKTR (residues 92–108 in MeaB; x and h represent any and hydrophobic amino acids, respectively) (12,16,28). The residue equivalent to D75 in HypB is D105 in MeaB. However, D105 is not located in the active site in any of the MeaB crystal structures, which has precluded the functional assignment for this conserved residue (28,46). In HypB, K153, is contributed to the active site from the adjacent monomer upon GTP-dependent dimerization and might be crucial for stabilizing the active site (24). While an equivalent residue does not exist in MeaB, either K106 or R108 might play such a role. Alternatively, R108 might be important for GTP binding based on the crystal structure of MeaB•GMPPNP (46).

In the Ras GTPases, nucleotide hydrolysis elicits conformational rearrangements in switch I (also known as the effector recognition motif) that are recognized by downstream target proteins (45,47). Recent evidence suggests that, besides switch II, MeaB uses a rare motif, switch III, for transmission of the chaperone function of MeaB and the GAP function of MCM (46,48). Thus, the role of switch I in transmitting the chaperone functions of MeaB is unknown.

In this study, we examined the role of switch I in supporting MeaB functions. We introduced conservative or alanine substitution mutations at strongly conserved positions in the switch I sequence. We provide evidence that switch I plays a critical role in the GTPase-gated transfer of AdoCbl from ATR to MCM and the displacement of the inactive cob(II) alamin cofactor from MCM. Our study suggests that isolated MeaB might catalyze GTP hydrolysis by a different mechanism than when it is in complex with MCM.

5.3 Experimental Procedures

5.3.1 Materials-AdoCbl, GMPPNP, ATP, GTP, methylmalonic acid, coenzyme-A, and other reagent grade chemicals were purchased from Sigma. Trifluoroacetic acid was purchased from Aldrich. Methylmalonyl-CoA was synthesized using malonyl-CoA synthetase, purified as described previously (49). A μBondapak™ NH2 10 μm, 125 Å 3.9 x 300 mm column was used for the HPLC separation and determination of guanosine nucleotides purchased from Waters.

5.3.2 Construction of site-specific mutants–Plasmids encoding the *M. extorquens* ATR and MCM were generous gifts from Mary E. Lidstrom (University of Washington, Seattle). A synthetic gene encoding *M. extorquens* AM1 MeaB was used for the generation of site-specific mutants of MeaB using a Quickchange kit (Agilent, Santa Clara, CA) according to the manufacturer's protocol. The following forward primers were used to generate the mutations. The reverse primers had the complimentary sequences.

D92A: 5′-GCGGTGCTCGCCGTCGCTCCGTCCTCGACCCGC-3′

D92N: 5′-GCGGTGCTCGCCGTCAATCCGTCCTCGACCCGC-3′

D105A: 5′-CGGTAGCATTCTGGGTGCTAAAACCCGTATGGC-3′

K106A: 5′-GCATTCTGGGTGATGCAACCCGTATGGCACGCC-3′

R108M: 5′-GCTGGGTGATAAAACCATGATGGCACGCCTGGCTATTG-3′

5.3.3 Enzyme Purification–Recombinant *M. extorquens* MeaB, MCM, and ATR were expressed and purified from *E. coli* BL-21 (DE3) as described previously (15,50). The purified enzymes were flash frozen in liquid nitrogen and stored at -80 °C in 50 mM HEPES buffer, pH 8.0, containing 0.3 M KCl, 10 mM $MgCl_2$, 10% glycerol (Buffer A).

5.3.4 Thermodynamics of GMPPNP-binding–Isothermal titration calorimetry (ITC) experiments were performed at 10 °C in Buffer A using a 300 μl injection syringe and a 1.43 ml injection cell. Samples were prepared by filtration through a 0.2 μm filter and then degassed under vacuum at 4 °C using a ThermoVac sample degasser. Each titration was performed at least in duplicate. GMPPNP (10 μl injections of 150-400 μM) was added to 10-25 μM MeaB. The data were analyzed using a two-site binding model using the MicroCal ORIGIN program. Values for the dissociation constant at sites 1 and 2 were then compared to the values obtained from the solution of the Gibbs free energy equation: $\Delta G^o = -RTln(K_A)$.

5.3.5 Enzyme Inactivation Assays with Switch I Mutants–Inactivation of MCM under steady-state turnover conditions was examined by UV/visible spectroscopy by enzyme-monitored conversion of cob(II)alamin to aquocob(III)alamin (OH_2Cbl) at 20 °C in 0.1 M potassium phosphate at pH 7.5 containing 10 mM $MgCl_2$. The reactions and sample preparations were performed in the dark to avert spurious formation of OH_2Cbl by photolysis of AdoCbl. Samples were prepared by the addition of reactions components in the order described below. MCM (25-30 μM) was reconstituted using an equimolar concentration of AdoCbl. A molar excess (35-40 μM) of MeaB was added to the MCM holoenzyme to obtain the MCM:MeaB complex. GMPPNP was then added to the reaction mixture to a final concentration of 1-2 mM and the reaction was initiated by the addition of methylmalonly-CoA to a final concentration of 4.5-5 mM. The rates of inactivation were determined by plotting the change in absorbance at 351 nm, corresponding to OH_2Cbl formation, as a function of time. The kinetic traces were best fit by a single exponential equation: $\Delta A_t = A_o - \Delta A_p e^{(-kt)}$, where ΔA_t is the absorbance at 351 nm as a function of time, A_o is the initial absorbance of cob(II)alamin, ΔA_p is the reaction phase amplitude for OH_2Cbl formation, and k is the observed rate constant for MCM inactivation.

5.3.6 Assay for transfer of AdoCbl from ATR to MCM with Switch I Mutants –The ATP-dependent transfer of AdoCbl from ATR to the MCM:MeaB•GMPPNP complex was performed in the dark at 20 °C and monitored by UV/visible spectroscopy. Two equivalents of AdoCbl were added to one equivalent of ATR to generate holo-ATR in Buffer A. The apo-MCM:MeaB•GMPPNP complex was reconstituted in Buffer A by mixing 40-50 μM MCM with an equimolar concentration of AdoCbl and 50-60 μM MeaB. GMPPNP was added to a final concentration of 1 mM. Holo-ATR (2:1 AdoCbl:ATR) and the MCM:MeaB•GMPPNP complex (40-50 μM) were mixed and incubated for 10 min at 20 °C before addition of ATP to a final concentration of 5 mM. Release/transfer of AdoCbl from ATR was calculated using a $\Delta\varepsilon_{525} = 6.69$ mM^{-1} cm^{-1}. Bound versus free cofactor was separated using an Amicon centrifuge filter (10 kDa cutoff, 20 min, 4 °C, 16,000 x g). The concentration of free AdoCbl in the filtrate was calculated using $\varepsilon_{525} = 8.0$ mM^{-1}cm^{-1}.

5.3.7 Ejection of Cob(II)alamin by Switch I Mutants–MCM (30-40 μM) was mixed with 45-60 μM MeaB (wild-type, D92A, D92N, D105A, or K106A) in Buffer A at 20 °C under strictly anaerobic conditions such that the [MCM]:[MeaB] ratio is 1:1.5. Cob(II)alamin was generated by reduction of OH$_2$Cbl with tris (2-carboxyethyl) phosphine hydrochloride (TCEP) and was added to a final concentration equal to that of the MCM:MeaB wild-type or mutant complex. The reaction mixture was incubated for 10 min at 20 °C. GMPPNP in anaerobic Buffer A was added to a final concentration of 2 mM. The mixture was then incubated for 20 min at 20 °C. Subsequently, the sample was made aerobic by air oxidation for 2 h and then applied to a Centricon YM10 filter (10 kDa cutoff) to separate free from bound OH$_2$Cbl., Cob(II)alamin (but not OH$_2$Cbl) can be released from MCM and is subsequently oxidized to OHCbl, which was quantified using $\varepsilon_{535} = 9.3$ mM^{-1}cm^{-1}.

117

5.3.8 GTPase activity of MeaB–The GTPase activity of MeaB was determined using an HPLC assay as described previously (4).

5.3.9 Size-Exclusion Chromatography–Samples were prepared in the dark in Buffer A containing 0.5 mM GDP and 80-90 μM of wild-type or mutant MeaB ± equimolar MCM and 0.5 mM AdoCbl in a total volume of 150 μL and loaded onto a Superdex-200 HR 10/30 column equilibrated with Buffer A. The protein complexes were eluted in the dark to minimize photolysis of AdoCbl.

5.4 Results

5.4.1 Impact of switch I mutations on formation of the MCM:MeaB Complex

The effect of switch 1 mutations on formation of the MCM:MeaB complex was probed by size-exclusion chromatography (Fig. 5.3). We have previously shown that wild-type MCM (142 kDa, peak a) and MeaB (68 kDa, peak b) elute at a volume consistent with their predicted molecular masses (Fig. 5.3) (48). Reconstitution of the wild-type and mutant MCM:MeaB complexes (65-70 μM) was performed by combining the component proteins in a 1:1 molar ratio in buffer containing a molar excess of GDP and AdoCbl. The wild-type MCM:MeaB complex migrated with a molecular mass of 243 kDa, which is consistent with a complex having 1:1 stoichiometry (Fig. 5.3, peak c). A higher order aggregate of the MCM:MeaB complex migrates with an apparent molecular mass of ~600 kDa (peak d). The individual switch I mutants of MeaB exhibit molecular masses that are comparable to that of the wild-type MeaB homodimer (63-71 kDa) (Fig. 5.3). The R108M and D92A switch I mutations shift the equilibrium away from the 1:1 MCM:MeaB complex and toward the higher order oligomer (peak d). The D92N,

D105A, and K106A have the opposite effect, shifting the equilibrium toward the stoichiometric complex (peak c). The peak eluting at ~24 ml corresponds the free ligands.

5.4.2 Effect of switch I mutations on GMPPNP binding

The active sites of the isolated MeaB homodimer exhibit negative cooperativity for GMPPNP (3,28). The K_D values for GMPPNP binding to sites 1 and 2 in wild-type MeaB are:
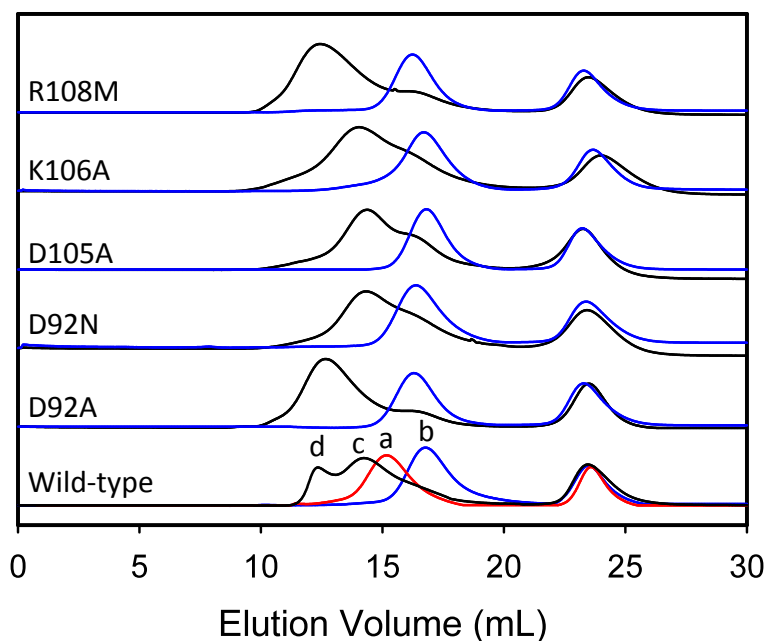
Figure 5.3. Impact of switch I mutations on formation of the MCM:MeaB complex. Size-exclusion chromatographic determination of the molecular masses of isolated wild-type and switch I mutants of MeaB (blue line) with added GDP and of the complexes formed with MCM (black line) in the presence of GDP and AdoCbl. The elution of MCM alone (red line) with added AdoCbl and GDP is shown in the bottom trace. The peak eluting at ~24 ml corresponds to free GDP and AdoCbl. The peaks labeled a-d correspond to molecular masses of 68 kDa (MeaB homodimer), 144 kDa (MCM heterodimer), 243 kDa (a 1:1 MCM:MeaB complex), and 600 kDa (a high order oligomer of MCM:MeaB), respectively.

0.8 ± 0.4 µM and 9.5 ± 1.9 µM, respectively (Table 5.1). In contrast, GMPPNP binding to R108M was not detected. Efforts to examine nucleotide binding to R108A were unsuccessful due to the insolubility of R108A MeaB during over-expression. The impact of the remaining

119

switch I mutations on the K_D for GMPPNP binding at site 1 ranges from 0.05 ± 0.01 µM (D105A) to 1.8 ± 0.2 µM (D92A). The K_D for GMPPNP binding at site 2 of switch I mutants ranges from 1.6 ± 0.2 µM (D105A) to 14.5 ± 4.1 µM (K106A).

5.4.3 GTPase activity of switch I mutants

The D92A, D92N, D105A and K106A mutations, have virtually no impact on the intrinsic GTPase activity compared to wild-type MeaB and exhibit k_{cat} values ranging from 0.031 ± 0.003 min^{-1} to 0.05 ± 0.01 min^{-1} (Table 5.2).

Enzyme	K_D (µM)	
	Site 1	Site 2
Wild-type[a]	0.81 ± 0.50	9.5 ± 1.9
D92A	1.77 ± 0.22	14.3 ± 1.0
D92N	1.06 ± 0.30	12.0 ± 2.1
D105A	0.05 ± 0.01	1.6 ± 0.2
K106A	0.34 ± 0.09	14.5 ± 4.1
R108M	ND[b]	ND[b]

Table 5.1. **Dissociation constants for GMPPNP binding to switch I mutants of MeaB.**
[a]Determined previously (2). [b]Not detectable under assay conditions.

Consistent with its inability to bind GMPPNP, R108M MeaB shows no GTPase activity. Wild-type MeaB exhibits an ~100-fold increase in the k_{cat} for GTP hydrolysis in the MCM:MeaB complex. By comparison, the active switch I mutants are significantly desensitized to the GAP function of MCM. In the presence of a 1.5 molar excess of MCM, the value of k_{cat} is increased by 5- to 7-fold in D92A and D92N MeaB, respectively. The D105A and K106A mutations lead to a smaller diminution in the GAP function of MCM.

| Enzyme | k_{cat} (min^{-1}) | | Fold GAP-Activation |
	- MCM	+ MCM	
Wild-type[a]	0.039 ± 0.003	4.08 ± 0.20	102
D92A	0.039 ± 0.006	0.19 ± 0.04	4.9
D92N	0.036 ± 0.005	0.25 ± 0.04	6.9
D105A	0.031 ± 0.003	0.36 ± 0.03	11.6
K106A	0.051 ± 0.011	1.21 ± 0.20	23.7
R108M	ND[b]	ND[b]	-

Table 5.2. Kinetic parameters for GTP hydrolysis by MeaB mutants. [a]As determined previously (4). [b]Not detected under assay conditions.

5.4.4 Switch I mutations do not impact rate of MCM inactivation

Loss of the 5′-deoxyadenosine group from the active site during steady-state turnover results in gradual inactivation of MCM (3). Addition of MeaB increases the rate of MCM inactivation by ~1.3-fold (Fig. 5.4a). However, inclusion of GDP, GTP, or GMPPNP leads to a 30-fold (3.0×10^{-4} min^{-1}) decrease in the rate of MCM inactivation (Fig. 5.4a). In the presence of GMPPNP, the switch I mutants D92A, D92N, D105A, and K106A, do not appreciably impact the rate of MCM inactivation compared to wild-type MeaB. The rate of MCM inactivation in the complexes formed between MCM and switch I mutants of MeaB ranged from 2.6×10^{-4} (K106A) to 3.4×10^{-4} min^{-1} (D92A).

5.4.5 Effect of switch I mutations on GTPase-gated AdoCbl transfer from ATR to MCM

Binding of ATP to ATR and hydrolysis of GTP in the MCM:MeaB complex result in the transfer of 1 equivalent of AdoCbl from ATR to MCM (50,51). Substitution of GTP with GMPPNP blocks AdoCbl transfer to the MCM:MeaB complex and instead, 0.06 equivalents of AdoCbl are released into solution (Fig. 5.4b). Thus, wild-type MeaB couples GTP hydrolysis to AdoCbl transfer from ATR to MCM. However, mutations at D92, D105 and K106 in MeaB lead to uncoupling of the GTPase activity from AdoCbl transfer. When GMPPNP is bound to the

MCM:MeaB (D92N or K106A) complexes, ~0.42 equivalents of AdoCbl are transferred to MCM while ~0.78 equivalents of AdoCbl are transferred to MCM in the presence of D92A or D105A MeaB.

5.4.6 Reactivation of MCM by switch I mutants

The dissociation of 5′-deoxyadenosine during steady-state turnover leads to the other part of the cofactor, cob(II)alamin, stranded in the MCM active site and consequent accumulation of inactive MCM (4). It has been previously demonstrated that MeaB triggers the GTP-dependent expulsion of inactive cob(II)alamin from MCM during turnover (3). This rescue function of MeaB is specific for expulsion of cob(II)alamin, but not the oxidized product, OH_2Cbl. Addition of GMPPNP to the wild-type MeaB:MCM•cob(II)alamin complex triggers ejection of ~97% cob(II)alamin from MCM under anaerobic conditions (Fig. 5.4c). This displaced cofactor can be separated under aerobic conditions from enzyme-bound cob(II)alamin using a Centricon filter, and the concentration of free OH_2Cbl can be determined from the absorbance at 351 nm. Addition of GMPPNP to the MCM:MeaB complex loaded with cob(II)alamin and MeaB harboring D92A, D92N, D105A, or K106A mutations leads to ejection of only 51-66 % of cob(II)alamin (Fig. 5.4c).

5.5 Discussion

Nearly 40 pathogenic mutations have been described in CblA that are associated with methylmalonic aciduria (12,52-55). MeaB, the closely related bacterial ortholog of CblA, represents the best-studied chaperone of a B_{12}-dependent isomerase and is among the most thoroughly studied NTPase metallochaperone proteins (2-4,15,28). MeaB appears to be novel

among other NTPase metallochaperones by virtue of its deployment of a third switch motif, switch III, for effecting its chaperone functions (46). Recent evidence indicates that conformational changes in switch III are coupled to canonical nucleotide-dependent conformational changes in switch II (46,48). In contrast, the role of switch I in bidirectional signaling had not been assessed prior to this study.

The inability to capture the crystal structures of a switch I motif in a catalytically active conformation containing Mg^{2+} ion has limited our insights into the functional role of switch I in MeaB catalysis (28,46,48). The NTPase activity is highly sensitive to amino acid substitutions at conserved positions in switch I and II in P-loop NTPases (34,40,56). Mutation of the catalytic glutamine in the ExxGQ switch II motif of Ras-related proteins abolishes GTPase activity, activating Ras-proteins toward malignant transformation (32). Similarly, substitution of the putative Asp^{cat} residue in the switch I region of SIMIBI NTPases leads to a substantial decrease in the rate of nucleotide hydrolysis (31). Surprisingly, substitution of the predicted Asp^{cat} in MeaB, D92, and other conserved switch I residues in MeaB has virtually no impact on its intrinsic GTPase activity (Table 2). In contrast, enhancement of GTP hydrolysis in the MCM:MeaB complex is suppressed by mutations in switch I. Based on sequence relationship to HypB and other G3E proteins, the switch I motif of MeaB is predicted to supply the active site with catalytic residues for polarizing a water molecule (D92), ligating Mg^{2+} (D105), and binding the β- and γ-phosphate oxygens of GDP/GTP (R108) (Fig. 5.2) (24,28). The results presented here suggest that at least part of the GAP function of MCM is derived by stabilization of a catalytically active conformation of switch I loop of MeaB, which is predicted to resemble the active site topology observed in the HypB•GTPγS structure (Fig. 5.2b).
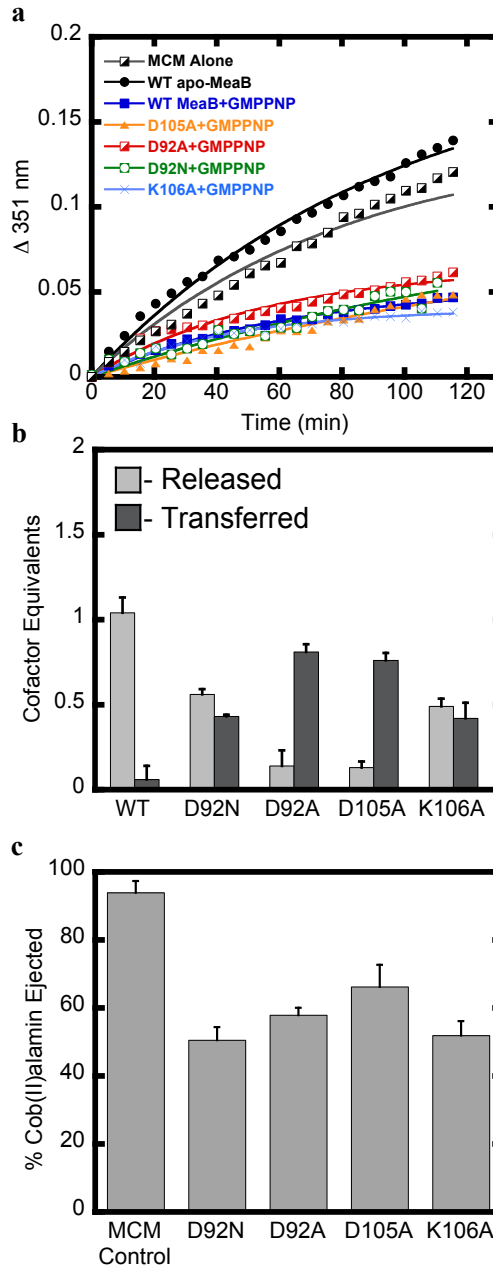
Figure 5.4. **The impact of switch I MeaB mutations on the Chaperone Functions of MeaB**.
a) Time-dependent inactivation of MCM in complex with wild-type or switch I mutants of MeaB
and in the presence of 5 mM methylmalonyl-CoA at pH 7.5, 20 °C. The plot shows the time-
dependent formation of H_2OCbl detected at 351 nm and is representative of at least two
experiments. The data points were fitted using a single exponential equation described under
Experimental Procedures. b) ATP-dependent release or transfer of AdoCbl from ATR to the
MCM:MeaB complex (containing wild-type or switch I mutant MeaBs) in the presence of
GMPPNP. The data represent the average of at least 2 independent experiments. c) Displacement
of cob(II)alamin from MCM•cob(II)alamin:MeaB (wild-type or switch I mutants) following

addition of GMPPNP under anaerobic conditions. The data are the average of at least 2 independent experiments.

Mutations at conserved positions in the switch I motif of MeaB also impair its ability to regulate cobalamin binding to and displacement from MCM. In Gα proteins, GTP hydrolysis triggers a conformational rearrangement in switch I for signaling to downstream effector proteins (18,57). NifH is a SIMIBI class ATPase that, along with the MoFe protein comprises a two-component complex involved in nitrogenase maturation (1). Mutation of the residue in NifH that corresponds to D92 in MeaB severely impairs the ability of NifH to catalyze GTP hydrolysis and to effect the maturation of the MoFe cofactor in nitrogenase (31). Thus, the disruption of GTPase activity among G3E G-proteins disrupts their chaperone function, supporting a role for D92 in catalysis in the MCM:MeaB complex.

The GAP function of MCM might also be conveyed *in trans* via residues from MCM, e.g. by contribution of an arginine "finger" to the MeaB/CblA active site. A pathogenic mutation in human MCM, R616C maps to the surface of MCM from *Propionibacterium shermanii* (58,59). Mimicking the R616C mutation in the *M. extorquens* MCM (R585C) resulted in significantly reduced GAP function by MCM (3). However, in the absence of a crystal structure of the MCM:MeaB complex, the role of the R585 residue in the *M. extorque*ns MCM is uncertain. The strong conservation of R108 in MeaB and its orthologs, and the inability of the R108M mutant to bind GMPPNP and hydrolyze GTP identify R108 as a potential arginine "finger" provided *in cis* by MeaB.

The K106 residue is conserved in the switch 1 motif of MeaB and its orthologs, but not among other G-protein metallochaperones (12,16,28). In the various structures of MeaB, K106 is either positioned on a disordered loop, is solvent exposed, or hydrogen bonded to the carbonyl

groups of L103 in switch I or I120 on the β3 sheet (28,46,48). Thus, the basis for disruption of the GTPase activity in the MCM:MeaB complex of the K106A mutant is not apparent. In the structure of HypB•GTPγS, K153 is supplied to the active site from the surface of the adjacent subunit and is involved in binding the terminal phosphate of GTPγS and the active site Mg^{2+} ion (24). Wittinghofer and colleagues proposed that K153 is a critical factor stabilization of the HypB active site (24). The switch I region of MeaB would have to undergo a significant conformational change in the MCM:MeaB complex for K106 to serve a role equivalent to K153 in HypB.

In this study, we demonstrate that mutations to switch I of MeaB significantly reduce both its gating function for regulating AdoCbl transfer from ATR to MCM and its rescuing function for ejecting inactive cobalamin from MCM (Fig 5.4b and 5.4c). The disruption of these functions suggests that switch I is critical for signaling the GTP-bound conformation of MeaB to MCM. This model is also consistent with the predicted involvement of D105 and D92 in stabilizing the GTP-bound state of the MeaB by ligating Mg^{2+} via D105 and the active site water molecules by D92 (Fig. 5.2b and 5.2c).

The involvement of K106 in signaling the chaperone functions of MeaB to MCM is not apparent from the various crystal structures of MeaB. The surface exposure of K106 and the adverse impact of the K106A mutation on gating AdoCbl binding and stimulating ejection of cob(II)alamin, suggest that this residue might be important for communicating directly with the B_{12}-binding domains of MCM.

G-proteins and ATPases couple the free energy of nucleotide binding, exchange, and phosphodiester hydrolysis to conformational changes in flexible switch regions to effect regulation of diverse functions ranging from DNA replication, protein synthesis and localization,

to cytoskeletal dynamics, and coenzyme trafficking and assimilation (1,18,34,44,47). Recent studies of the vast pool of evolutionarily diverse G-proteins and ATPases have begun to uncover multiple strategies by which these proteins transduce signals. The G3E metallochaperone MeaB, with its atypical active site and an additional switch motif illustrates the diversity of catalytic and signaling strategies within a single G-protein. The results presented in this study demonstrate that MeaB also relies on canonical signaling and catalytic strategies for its chaperone and enzymatic functions.

5.6 Ongoing Research and Future Directions

5.6.1 Background

Isobutyryl-CoA mutase (ICM) is an AdoCbl-dependent isomerase that catalyze the interconversion of isobutyryl-CoA to *n*-butyryl-CoA, a substrate for bacterial polyketide biosynthesis (60). ICM proteins are closely related to methylmalonyl-CoA mutase (MCM) proteins. In mammals, MCM relies upon a cobalamin assimilation and trafficking pathway for the synthesis and delivery of its cofactor, AdoCbl. The fidelity of AdoCbl docking in MCM, as well the propensity of the cofactor to escape from the catalytic cycle, is regulated by an auxiliary pathway G-protein that is CblA in humans and MeaB in *Methylbacterium extorquens* (2-4,7,8,15-17,28). Catalytic turnover in MCM and ICM proteins involves homolysis of the cobalt-carbon bond of AdoCbl. The dissociation of 5'-deoxyadenosine from the active site during catalytic turnover results in inactivation of MCM and ICM. Genetic disruptions to the genes encoding CblA or MeaB result is dyfunctions in MCM activity, reduced AdoCbl, and revealed a role for these auxiliary G-proteins in chaperoning the activity and assembly of MCM proteins (12,52,54,55).

Until recently, it was unclear how ICM averts inactivation of its cofactor during catalysis, whether ICM proteins, like MCM, were protected by dedicated chaperones, and how the fidelity of AdoCbl docking into the ICM active site is achieved. A detailed bioinformatic screen revealed that genes encoding ICM proteins in >70 prokaryotes were incorrectly annotated as MCM (61). It was shown that these genes encoded a fusion between ICM and its G-protein chaperone inserted between the B_{12}- and substrate-binding domains. The "G-domain" has been subsequently designated as MeaI and is a paralog of MeaB, and the fusion protein has been designated as IcmF (ICM-fused) to distinguish it from the stand-alone ICMs.

The MeaI domain of IcmF from *Geobacillus kaustophilus* (*Gk*) mediates the transfer of AdoCbl from *Gk* ATR to *Gk* IcmF (62). As with MeaB, the non-hydrolyzable analog of GTP, GMPPNP, blocks transfer of AdoCbl from ATR to *Gk* IcmF, indicating that cofactor transfer requires GTP hydrolysis. Despite the ability of *Gk* IcmF to bind and hydrolyze ATP, the transfer of AdoCbl from ATR to IcmF is unaffected by AMPPNP, the non-hydrolyzable analog of ATP. Unlike MeaB, the MeaI domain of IcmF does not slow the rate of ICM inactivation and does not stimulate ejection of cob(II)alamin from IcmF that has become uncoupled from 5'-deoxyadenosine. The basis for these differences as still unclear.

The structure of IcmF in complex with AdoCbl and GDP was recently solved in collaboration between our group (Dr. Valentin Cracan and Dr. Ruma Banerjee) and Dr. Catherine Drennan's group (Marco Jost) at MIT. While the full crystal structure remains to be published, preliminary analysis of the structure suggests one mechanism for allosteric communication in which a switch I arginine residue contacts two residues in the adjacent B_{12}-binding domain. The corresponding residues in the *M. extorquens* proteins are D624 and E625 in

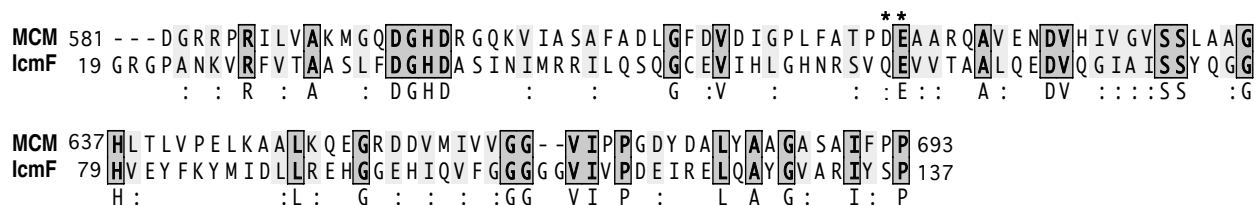the B$_{12}$-binding domain of the α-subunit of MCM and K106 in the switch I region of MeaB (Fig. 5.6).

```
                                                  **
MCM 581 ---DGRRP R ILV A KMGQ DGHD RGQKV IASAFADL G FD V DIGPLFATPD E AARQ A VEN DV HIVGV SS LAA G
IcmF 19 GRGPANKV R FVT A ASLF DGHD ASINIMRRILQSQ G CE V IHLGHNRSVQ E VVTA A LQE DV QGIA I SS YQG G
              :   :  R  :  A   :  DGHD     :        :       G  :V    :      :  :E::   A:   DV  ::::SS    :G

MCM 637 H LTLVPELKAA L KQE G RDDVMIVV GG -- V IP P GDYDAL Y A A GA SA I FP P 693
IcmF 79 H VEYFKYMIDL L REH G GEHIQVFG GG GG V IV P DEIREL Q A Y GV AR I Y S P 137
        H :            :L:      G  :  :  :  :GG      VI  P  :       L    A   G:     I:    P
```

Figure 5.6. Sequence alignment of conserved regions of the B$_{12}$-binding domains of *M. extorquens* MCM and *Geobacillus kaustophilus* IcmF. Identical matches between the aligned sequences are boxed in dark grey and conservative changes are shaded in light grey and marked with a colon.

5.6.2 Current and Future Research

To assess the importance of the D624 and E625 residues in the B$_{12}$-binding domain of the *M. extorquens* MCM, we have introduced the D624A, E625A, and the double D624A/E625A mutations and expressed and purified the single mutants. Expression studies of the D624A/E625A double mutant are underway, and we are optimistic that it too will be expressed in a soluble form.

Following purification of each mutant, we will verify its activity in the MCM assay via enzyme-monitored inactivation by tracking formation of cob(II)alamin. If formation of the cob(II)alamin intermediate or the oxidatively inactivated H$_2$OCbl is not observed, we will analyze the reaction mixtures for product formation using gas chromatography. The thermodynamics of binding MeaB ± nucleotides to the mutant proteins will be quantitatively evaluated by ITC. If formation of the MeaB:MCM mutant complexes is not apparent from ITC (e.g., if the heat release is low), analytical size-exclusion chromatography will be used to characterize the ability of the MCM mutants to bind MeaB as described previously (48).

Binding of AdoCbl to MCM and to the MCM:MeaB complex, and the influence of GDP and GMPPNP will also be determined by ITC. The thermodynamics of binding of nucleotides to MeaB in the complex formed between MeaB and MCM mutants will also be investigated by ITC. If formation of the MCM:MeaB complex, the affinity of MCM for AdoCbl in the MCM:MeaB complex, and the affinity of MeaB for nucleotides in the MCM:MeaB complex are not affected by the D624A, E625A and D624A/E625A mutations, the chaperone and GAP function of MeaB and MCM, respectively, will be assessed as described under Materials and Methods. If any of the alanine-substituted MCM variants exhibit disrupted cofactor or nucleotide binding, enzyme activity, or the formation of the MCM:MeaB complexes, conservative mutations (D625N and E625Q) will be introduced and examined as described above.

5.7 Final Remarks

The body of work presented in this doctoral dissertation has significantly increased our understanding of the mechanism of allosteric communication that guides AdoCbl docking to, protection in, and release from MCM (7,50). Our studies have helped elucidate the complicated mechanism by which MeaB and, most likely, its orthologs, signal nucleotide binding and hydrolysis to orchestrate its chaperone functions. However, an important gap that remains is structural insight into the active site rearrangement of MeaB that is predicted to occur in the MCM:MeaB complex. To that end, we are using both crystallographic and small-angle X-ray scattering approaches to obtain insights into the structure of the MCM:MeaB complex. However, to date, these efforts have not been successful due to the very high solubility and heterogeneity of the MCM: MEaB complex. Analytical gel filtration analysis reveals that the stoichiometry of the MCM:MeaB complex is sensitive to point mutations with the equilibrium shifting in some

instances almost completely to the 1:1 complex. This incrased homogeneity might bode well for future structural studies of the complex. The primary technique that we have chosen to study the mechanism of allostery in the chaperone and GAP functions of MeaB and MCM, respectively, has been site-directed mutagenesis followed by the biochemical characterization of these mutants. To this end, I have created twenty-six unique mutant MeaB constructs and six mutant MCM constructs, which provides a resource for crystallographic screening.

5.8 References

1. Leipe, D. D., Wolf, Y. I., Koonin, E. V., and Aravind, L. (2002) Classification and evolution of P-loop GTPases and related ATPases. *J Mol Biol* **317**, 41-72
2. Padovani, D., Labunska, T., and Banerjee, R. (2006) Energetics of interaction between the G-protein chaperone, MeaB, and B_{12}-dependent methylmalonyl-CoA mutase. *J Biol Chem* **281**, 17838-17844
3. Padovani, D., and Banerjee, R. (2009) A G-protein editor gates coenzyme B_{12} loading and is corrupted in methylmalonic aciduria. *Proc Natl Acad Sci U S A* **106**, 21567-21572
4. Padovani, D., and Banerjee, R. (2006) Assembly and protection of the radical enzyme, methylmalonyl-CoA mutase, by its chaperone. *Biochemistry* **45**, 9300-9306
5. Banerjee, R. (2003) Radical carbon skeleton rearrangements: catalysis by coenzyme B_{12}-dependent mutases. *Chem Rev* **103**, 2083-2094
6. Banerjee, R., Chowdhury, S. (1999) Methylmalonyl-CoA Mutase. (John Wiley & Sons, I. ed.), New York. pp 707-730
7. Gherasim, C., Lofgren, M., and Banerjee, R. (2013) Navigating the B12 road: assimilation, delivery, and disorders of cobalamin. *J Biol Chem* **288**, 13186-13193
8. Banerjee, R., Gherasim, C., and Padovani, D. (2009) The tinker, tailor, soldier in intracellular B_{12} trafficking. *Curr Opin Chem Biol* **13**, 484-491
9. Banerjee, R. (2006) B_{12} trafficking in mammals: A for coenzyme escort service. *ACS Chem Biol* **1**, 149-159
10. Zhang, J., Dobson, C. M., Wu, X., Lerner-Ellis, J., Rosenblatt, D. S., and Gravel, R. A. (2006) Impact of cblB mutations on the function of ATP:cob(I)alamin adenosyltransferase in disorders of vitamin B_{12} metabolism. *Mol Genet Metab* **87**, 315-322
11. Lerner-Ellis, J. P., Gradinger, A. B., Watkins, D., Tirone, J. C., Villeneuve, A., Dobson, C. M., Montpetit, A., Lepage, P., Gravel, R. A., and Rosenblatt, D. S. (2006) Mutation and biochemical analysis of patients belonging to the cblB complementation class of vitamin B_{12}-dependent methylmalonic aciduria. *Mol Genet Metab* **87**, 219-225
12. Dobson, C. M., Wai, T., Leclerc, D., Wilson, A., Wu, X., Dore, C., Hudson, T., Rosenblatt, D. S., and Gravel, R. A. (2002) Identification of the gene responsible for the cblA complementation group of vitamin B_{12}-responsive methylmalonic acidemia based on analysis of prokaryotic gene arrangements. *Proc Natl Acad Sci U S A* **99**, 15554-15559
13. Dobson, C. M., Wai, T., Leclerc, D., Kadir, H., Narang, M., Lerner-Ellis, J. P., Hudson, T. J., Rosenblatt, D. S., and Gravel, R. A. (2002) Identification of the gene responsible for the cblB complementation group of vitamin B_{12}-dependent methylmalonic aciduria. *Hum Mol Genet* **11**, 3361-3369
14. Tanpaiboon, P. (2005) Methylmalonic acidemia (MMA). *Mol Genet Metab* **85**, 2-6
15. Korotkova, N., and Lidstrom, M. E. (2004) MeaB is a component of the methylmalonyl-CoA mutase complex required for protection of the enzyme from inactivation. *J Biol Chem* **279**, 13652-13658
16. Froese, D. S., Kochan, G., Muniz, J. R., Wu, X., Gileadi, C., Ugochukwu, E., Krysztofinska, E., Gravel, R. A., Oppermann, U., and Yue, W. W. (2010) Structures of

the human GTPase MMAA and vitamin B_{12}-dependent methylmalonyl-CoA mutase and insight into their complex formation. *J Biol Chem* **285**, 38204-38213

17. Takahashi-Iniguez, T., Garcia-Arellano, H., Trujillo-Roldan, M. A., and Flores, M. E. (2011) Protection and reactivation of human methylmalonyl-CoA mutase by MMAA protein. *Biochem Biophys Res Commun* **404**, 443-447

18. Wittinghofer, A., and Vetter, I. R. (2011) Structure-function relationships of the G domain, a canonical switch motif. *Annu Rev Biochem* **80**, 943-971

19. Jeoung, J. H., Giese, T., Grunwald, M., and Dobbek, H. (2010) Crystal structure of the ATP-dependent maturation factor of Ni,Fe-containing carbon monoxide dehydrogenases. *J Mol Biol* **396**, 1165-1179

20. Jeoung, J. H., Giese, T., Grunwald, M., and Dobbek, H. (2009) CooC1 from Carboxydothermus hydrogenoformans is a nickel-binding ATPase. *Biochemistry* **48**, 11505-11513

21. Zambelli, B., Stola, M., Musiani, F., De Vriendt, K., Samyn, B., Devreese, B., Van Beeumen, J., Turano, P., Dikiy, A., Bryant, D. A., and Ciurli, S. (2005) UreG, a chaperone in the urease assembly process, is an intrinsically unstructured GTPase that specifically binds Zn2+. *J Biol Chem* **280**, 4684-4695

22. Xia, W., Li, H., Yang, X., Wong, K. B., and Sun, H. (2012) Metallo-GTPase HypB from Helicobacter pylori and its interaction with nickel chaperone protein HypA. *J Biol Chem* **287**, 6753-6763

23. Rey, L., Imperial, J., Palacios, J. M., and Ruiz-Argueso, T. (1994) Purification of Rhizobium leguminosarum HypB, a nickel-binding protein required for hydrogenase synthesis. *J Bacteriol* **176**, 6066-6073

24. Gasper, R., Scrima, A., and Wittinghofer, A. (2006) Structural insights into HypB, a GTP-binding protein that regulates metal binding. *J Biol Chem* **281**, 27492-27502

25. Scrima, A., and Wittinghofer, A. (2006) Dimerisation-dependent GTPase reaction of MnmE: how potassium acts as GTPase-activating element. *EMBO J* **25**, 2940-2951

26. Chan, K. H., Li, T., Wong, C. O., and Wong, K. B. (2012) Structural basis for GTP-dependent dimerization of hydrogenase maturation factor HypB. *PLoS One* **7**, e30547

27. Gasper, R., Meyer, S., Gotthardt, K., Sirajuddin, M., and Wittinghofer, A. (2009) It takes two to tango: regulation of G proteins by dimerization. *Nat Rev Mol Cell Biol* **10**, 423-429

28. Hubbard, P. A., Padovani, D., Labunska, T., Mahlstedt, S. A., Banerjee, R., and Drennan, C. L. (2007) Crystal structure and mutagenesis of the metallochaperone MeaB: insight into the causes of methylmalonic aciduria. *J Biol Chem* **282**, 31308-31316

29. Stouten, P. F., Sander, C., Wittinghofer, A., and Valencia, A. (1993) How does the switch II region of G-domains work? *FEBS Lett* **320**, 1-6

30. Vetter, I. R., and Wittinghofer, A. (2001) The guanine nucleotide-binding switch in three dimensions. *Science* **294**, 1299-1304

31. Lanzilotta, W. N., Fisher, K., and Seefeldt, L. C. (1997) Evidence for electron transfer-dependent formation of a nitrogenase iron protein-molybdenum-iron protein tight complex. The role of aspartate 39. *J Biol Chem* **272**, 4157-4165

32. Wittinghofer, A., and Pai, E. F. (1991) The structure of Ras protein: a model for a universal molecular switch. *Trends Biochem Sci* **16**, 382-387

33. Scarano, G., Krab, I. M., Bocchini, V., and Parmeggiani, A. (1995) Relevance of histidine-84 in the elongation factor Tu GTPase activity and in poly(Phe) synthesis: its substitution by glutamine and alanine. *FEBS Lett* **365**, 214-218

34. Anand, B., Majumdar, S., and Prakash, B. (2013) Structural basis unifying diverse GTP hydrolysis mechanisms. *Biochemistry* **52**, 1122-1130

35. Seewald, M. J., Korner, C., Wittinghofer, A., and Vetter, I. R. (2002) RanGAP mediates GTP hydrolysis without an arginine finger. *Nature* **415**, 662-666

36. Ahmadian, M. R., Stege, P., Scheffzek, K., and Wittinghofer, A. (1997) Confirmation of the arginine-finger hypothesis for the GAP-stimulated GTP-hydrolysis reaction of Ras. *Nat Struct Biol* **4**, 686-689

37. Sondek, J., Lambright, D. G., Noel, J. P., Hamm, H. E., and Sigler, P. B. (1994) GTPase mechanism of Gproteins from the 1.7-A crystal structure of transducin alpha-GDP-AIF-4. *Nature* **372**, 276-279

38. Coleman, D. E., Berghuis, A. M., Lee, E., Linder, M. E., Gilman, A. G., and Sprang, S. R. (1994) Structures of active conformations of Gi alpha 1 and the mechanism of GTP hydrolysis. *Science* **265**, 1405-1412

39. Pan, X., Eathiraj, S., Munson, M., and Lambright, D. G. (2006) TBC-domain GAPs for Rab GTPases accelerate GTP hydrolysis by a dual-finger mechanism. *Nature* **442**, 303-306

40. Valencia, A., Chardin, P., Wittinghofer, A., and Sander, C. (1991) The ras protein family: evolutionary tree and role of conserved amino acids. *Biochemistry* **30**, 4637-4648

41. Egea, P. F., Shan, S. O., Napetschnig, J., Savage, D. F., Walter, P., and Stroud, R. M. (2004) Substrate twinning activates the signal recognition particle and its receptor. *Nature* **427**, 215-221

42. Leonard, T. A., Butler, P. J., and Lowe, J. (2005) Bacterial chromosome segregation: structure and DNA binding of the Soj dimer--a conserved biological switch. *EMBO J* **24**, 270-282

43. Froese, D. S., Dobson, C. M., White, A. P., Wu, X., Padovani, D., Banerjee, R., Haller, T., Gerlt, J. A., Surette, M. G., and Gravel, R. A. (2009) Sleeping beauty mutase (sbm) is expressed and interacts with ygfd in Escherichia coli. *Microbiol Res* **164**, 1-8

44. Wittinghofer, F. (1998) Ras signalling. Caught in the act of the switch-on. *Nature* **394**, 317, 319-320

45. Wittinghofer, A. (1998) Signal transduction via Ras. *Biol Chem* **379**, 933-937

46. Lofgren, M., Padovani, D., Koutmos, M., Banerjee, R. (2013) A Switch III Motif Relays Signaling Between a B_{12} Enzyme and its G-protein Chaperone. Accepted at. *Nature Chemical Biology*

47. Sprang, S. R. (1997) G protein mechanisms: insights from structural analysis. *Annu Rev Biochem* **66**, 639-678

48. Lofgren, M., Padovani, D., Koutmos, M., Banerjee, R. (2013) Roles of a Swtich II Loop in Signaling and Catalysis in the B_{12} Chaperone, MeaB. *Prepared for Submission*

49. Padovani, D., and Banerjee, R. (2006) Alternative pathways for radical dissipation in an active site mutant of B_{12}-dependent methylmalonyl-CoA mutase. *Biochemistry* **45**, 2951-2959

50. Lofgren, M., and Banerjee, R. (2011) Loss of allostery and coenzyme B_{12} delivery by a pathogenic mutation in adenosyltransferase. *Biochemistry* **50**, 5790-5798

51. Padovani, D., Labunska, T., Palfey, B. A., Ballou, D. P., and Banerjee, R. (2008) Adenosyltransferase tailors and delivers coenzyme B_{12}. *Nat Chem Biol* **4**, 194-196

52. Yang, X., Sakamoto, O., Matsubara, Y., Kure, S., Suzuki, Y., Aoki, Y., Sakura, N., Takayanagi, M., Iinuma, K., and Ohura, T. (2004) Mutation analysis of the MMAA and MMAB genes in Japanese patients with vitamin B(12)-responsive methylmalonic acidemia: identification of a prevalent MMAA mutation. *Mol Genet Metab* **82**, 329-333

53. Martinez, M. A., Rincon, A., Desviat, L. R., Merinero, B., Ugarte, M., and Perez, B. (2005) Genetic analysis of three genes causing isolated methylmalonic acidemia: identification of 21 novel allelic variants. *Mol Genet Metab* **84**, 317-325

54. Lerner-Ellis, J. P., Dobson, C. M., Wai, T., Watkins, D., Tirone, J. C., Leclerc, D., Dore, C., Lepage, P., Gravel, R. A., and Rosenblatt, D. S. (2004) Mutations in the MMAA gene in patients with the cblA disorder of vitamin B_{12} metabolism. *Hum Mutat* **24**, 509-516

55. Dempsey-Nunez, L., Illson, M. L., Kent, J., Huang, Q., Brebner, A., Watkins, D., Gilfix, B. M., Wittwer, C. T., and Rosenblatt, D. S. (2012) High resolution melting analysis of the MMAA gene in patients with cblA and in those with undiagnosed methylmalonic aciduria. *Mol Genet Metab* **107**, 363-367

56. Pai, E. F., Kabsch, W., Krengel, U., Holmes, K. C., John, J., and Wittinghofer, A. (1989) Structure of the guanine-nucleotide-binding domain of the Ha-ras oncogene product p21 in the triphosphate conformation. *Nature* **341**, 209-214

57. Chen, Y., Yoo, B., Lee, J. B., Weng, G., and Iyengar, R. (2001) The signal transfer regions of G alpha(s). *J Biol Chem* **276**, 45751-45754

58. Mancia, F., Keep, N. H., Nakagawa, A., Leadlay, P. F., McSweeney, S., Rasmussen, B., Bosecke, P., Diat, O., and Evans, P. R. (1996) How coenzyme B_{12} radicals are generated: the crystal structure of methylmalonyl-coenzyme A mutase at 2 A resolution. *Structure* **4**, 339-350

59. Worgan, L. C., Niles, K., Tirone, J. C., Hofmann, A., Verner, A., Sammak, A., Kucic, T., Lepage, P., and Rosenblatt, D. S. (2006) Spectrum of mutations in mut methylmalonic acidemia and identification of a common Hispanic mutation and haplotype. *Hum Mutat* **27**, 31-43

60. Cracan, V., and Banerjee, R. (2012) Novel B(12)-dependent acyl-CoA mutases and their biotechnological potential. *Biochemistry* **51**, 6039-6046

61. Cracan, V., Padovani, D., and Banerjee, R. (2010) IcmF is a fusion between the radical B_{12} enzyme isobutyryl-CoA mutase and its G-protein chaperone. *J Biol Chem* **285**, 655-666

62. Cracan, V. (2012) Structure, Function and Metabolic Roles of IcmF-a Fusion Between the Radical B_{12} Enzyme and its G-protein Chaperone. in *Department of Biological Chemistry*, University of Michigan, Ann Arbor, MI